

AD-A054 160

MASSACHUSETTS INST OF TECH LEXINGTON LINCOLN LAB
BANDWIDTH LIMITATIONS ON ACHIEVABLE CANCELLATION FOR ADAPTIVE N--ETC(U)
FEB 78 J T MAYHAN

F/G 9/5

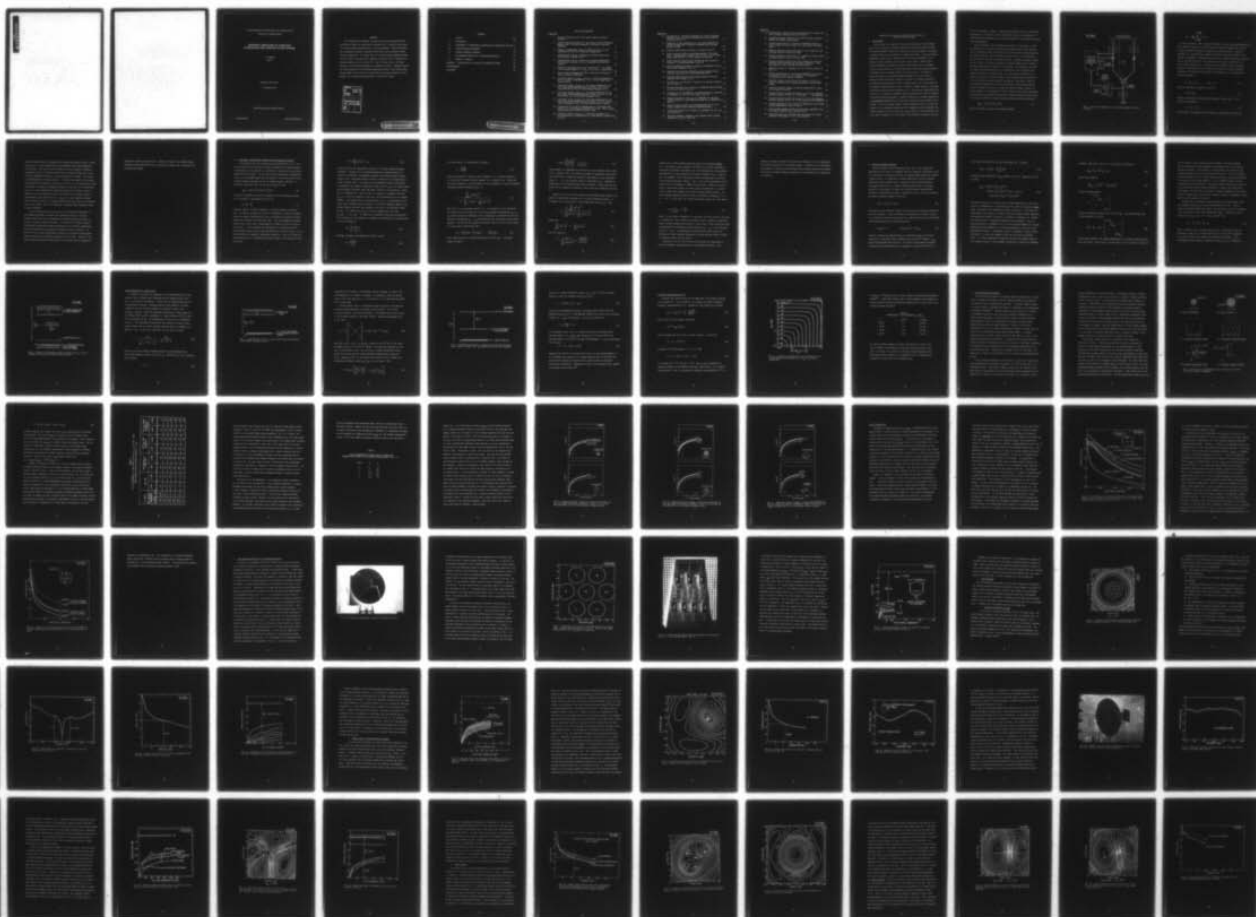
UNCLASSIFIED

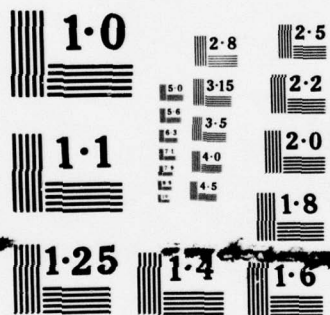
TN-1978-1

ESD-TR-78-25

NL

1 OF 2
ADA
054160





NATIONAL BUREAU OF STANDARDS

AD A 054160

MASSACHUSETTS INSTITUTE OF TECHNOLOGY
LINCOLN LABORATORY

BANDWIDTH LIMITATIONS ON ACHIEVABLE
CANCELLATION FOR ADAPTIVE NULLING SYSTEMS

J. T. MAYHAN

Group 61

TECHNICAL NOTE 1978-1

17 FEBRUARY 1978

Approved for public release; distribution unlimited.

LEXINGTON

MASSACHUSETTS

ABSTRACT

This technical note examines in detail the various limitations which influence the amount of cancellation achievable for a closed-loop type adaptive nulling system operating over a non-zero bandwidth. These limitations are categorized according to antenna limitations, and post-antenna channel tracking limitations. The former tend to be RF percentage bandwidth limited and the latter on the achievable component tolerances used to implement the channel (whether at RF or a lower IF). Both of these factors, and their influence on the nulling bandwidth, are examined in detail. Measured results are also presented for a seven-beam paraboloid-reflector type multiple-beam antenna (MBA), and the effects of feed-reflector multipath inherent in this geometry on the cancellation bandwidth is evaluated in detail.

ACCESSION for	
NTIS	Write Section <input checked="" type="checkbox"/>
DDC	Buff Section <input type="checkbox"/>
UNANNOUNCED	<input type="checkbox"/>
JUSTIFICATION.....	
BY.....	
DISTRIBUTION/AVAILABILITY CODES	
Dist.	AVAIL. and/or SPECIAL
A	

CONTENTS

Abstract	111
I. Introduction	1
II. Development -- Interference Cancellation and Eigenvalue Spectrum	9
III. Channel Tracking Tolerances	15
IV. Antenna Frequency Variations	30
V. Some Measured Results for a Seven-Beam Paraboloid	51
VI. Summary of Results	94
Appendix I - Cancellation as a Function of Eigenvalue Spread	96
Acknowledgments	98
References	99

LIST OF ILLUSTRATIONS

Figure No.

1. General configuration for an N-channel adaptive nulling processor.	3
2. Typical eigenvalue spread for J interference sources separated greater than a half-power beamwidth, and having a non-zero bandwidth.	6
3. Effects of independent channel tracking errors σ_k^2 on the eigenspectrum of \underline{M} for an arbitrary antenna type.	21
4. Eigenspectrum of \underline{M} for a planar array having statistically equal channel tracking errors σ_k^2 .	23
5. Eigenspectrum of \underline{M} for a planar array having statistically equal channel tracking error, σ_k^2 , dominates over the other channels.	25
6. Parametric representation of the tracking error σ^2 vs. amplitude and phase mismatch, $20 \log_{10} (1+\sigma_a)$ and σ_ϕ , respectively.	28
7. Basic antenna configurations used to evaluate the effects of antenna frequency dispersion.	32
8. Eigenvalue spread, S_2/S_{MAX} , in dB vs. fractional bandwidth for the six antenna configurations of Fig. 7 and a single interference source.	34
9. Eigenvalue spread, S_2/S_{MAX} , vs. fractional bandwidth for the four single interference locations of Table 3 for (a) the seven-beam MBA and (b) the seven-element hexagonal array.	40
10. Eigenvalue spread, S_2/S_{MAX} , vs. fractional bandwidth for the four single interference locations of Table 3 for (a) the 19-beam MBA and (b) the 19-element hexagonal array.	41
11. Eigenvalue spread, S_2/S_{MAX} , vs. fractional bandwidth for the four single interference locations of Table 3 for (a) the six-element pentagon and (b) the seven-element double triangle.	42
12. Cancellation in the earth coverage mode vs. fractional bandwidth for the six antenna configurations of Fig. 7 and a single interference source located at $\theta_j=8^\circ$, $\phi=90^\circ$.	45
13. Eigenvalue spread, S_5/S_{MAX} , vs. fractional bandwidth for a four-interference source scenario for each antenna configuration of Fig. 7.	47

Figure No.

14. Cancellation vs. fractional bandwidth for an earth coverage quiescent vector for the four-interference source scenario considered in Fig. 13.	48
15. Comparison of the cancellation vs. fractional bandwidth for the MBA antennas when a separate broadband earth coverage antenna is used.	49
16. Reflector-feed antenna structure at L-band ($D/\lambda=10.7$).	52
17. Three dB contour levels of each beam relative to its peak value. Measured gain of beam 2,2 is 25.5 dB. Gain of other beams varies from 0 to -0.7 dB relative to beam 2,2.	54
18. Weight-combiner network used in evaluating the nulling performance of the seven-beam MBA of Fig. 16.	55
19. Measured eigenvalue spread as a function of bandwidth for the seven weight channels of Fig. 18.	57
20. Quiescent earth coverage radiation pattern obtained using a composite excitation of the seven MBA beam ports.	59
21. Measured composite beam earth coverage pattern with zero-bandwidth null formed at (4,2).	61
22. Cancellation as a function of frequency for the null formed at (4,2) in Fig. 21.	63
23. Average cancellation as a function of bandwidth about 1550 MHz for the (4,2) null of Fig. 21.	64
24. Eigenspectrum of the measured correlation matrix as a function of bandwidth for the (4,2) null case of Fig. 21.	65
25. Measured results for (S_2/S_{MAX}) vs. bandwidth for the four single interference source locations used in the simulation of Fig. 9a.	67
26. Measured contour pattern with zero-bandwidth null at (4,2) using a separate earth coverage reference antenna.	69
27. Average cancellation as a function of bandwidth for the (4,2) null of Fig. 26.	70
28. Amplitude frequency response of the separate earth coverage antenna for the (4,2) null case.	71

Figure No.

29. Feed/reflector structure with ground plane used to isolate the earth coverage reference from the reflector.	73
30. Amplitude frequency response of the earth coverage reference channel with ground plane present.	74
31. Average cancellation as a function of bandwidth using the earth coverage reference antenna with and without the ground plane.	75
32. Measured radiation contour with null at (4,2) using the earth coverage reference with ground plane.	76
33. Measured eigenvalue spread S_2/S_1 vs. bandwidth with and without the ground plane for the (4,2) null case.	78
34. Measured radiation contour with nulls produced at three 120° separated triad positions and the center beam peak. Seven-beam composite earth coverage quiescent pattern.	79
35. Eigenvalue spread vs. bandwidth for the four-null scenario of Fig. 34.	80
36. Average cancellation as a function of bandwidth for the four-null scenario of Fig. 34, as a function of technique of realizing the earth coverage reference.	82
37. Radiation contour with nulls for the scenario of Fig. 34 using the separate earth coverage reference (without ground plane).	83
38. Quiescent radiation pattern allocating maximum gain to users at the center of the FOV.	84
39. Measured radiation pattern having null at (2,0) for quiescent radiation pattern of Fig. 38. 8 MHz weight setting bandwidth.	86
40. Measured radiation pattern having null at (2,0) for quiescent radiation pattern of Fig. 38. 44 MHz weight setting bandwidth.	87
41. Average cancellation as a function of bandwidth for the weight setting bandwidths of Figs. 39 and 40.	88
42. Reflector-feed antenna structure using "space qualified" type feed support modeled after satellite ATS-6.	92
43. Eigenvalue spread vs. bandwidth with and without the "space qualified" feed support. (4,2) null position.	93

Bandwidth Limitations on Achievable Cancellation for Adaptive Nulling Systems

I. Introduction

In this report we consider the factors determining over what bandwidth one is able to achieve a specified interference cancellation using an adaptive antenna having a single set of adaptively controlled weights (as opposed to using multiple sets of weights on a tapped delay line). This cancellation bandwidth is often loosely referred to as the "nulling bandwidth" of the system, and this convention will be used in this report. Heuristically, achieving wideband cancellation requires a precise match in the frequency transfer characteristics of N signal-flow paths, which when properly weighted and summed result in minimum output at the sum junction. The degree to which these paths can be matched depends strongly on two basic factors: Antenna frequency variations (hereafter referred to as antenna dispersion), including any multipath and RF mutual coupling present, and post-antenna output channel tracking, which we refer to simply as channel tracking. Frequency variations resulting from the antenna are to a certain degree unavoidable, and at best one can choose an "optimum" antenna configuration in order to minimize the inherent dispersion present. Antenna limitations are largely dependent on the percentage bandwidth about the RF center frequency used for signal transmission. On the other hand, channel tracking limitations tend to be more dependent on the achievable tolerances for the components used to implement the channel (whether at RF or a lower IF), and the degree to which amplifiers, filters, mixers, weights, etc. can be made to have identical frequency character-

istics from channel to channel. Channel tracking effects are to a first order independent of the direction of the interference and can, in principle, be minimized greatly depending on the resources available to the particular system under consideration.

Before developing a more quantitative description of the effects of channel dispersion, it is useful to digress and consider briefly some characteristics of adaptive nulling and how each of the two factors, antenna dispersion and channel tracking, can be evaluated, and point out in a very qualitative way what effects they have on the depth of null. Consider the general configuration of Fig. 1, in which we illustrate N signal channels with an adaptive processor controlling the weights in each channel. For generality we assume the adaptive processor operates over a bandwidth BW , and the desired user signals are packed in a bandwidth BW_s . For some types of processors it is useful to choose $BW \gg BW_s$ (for example, when the interference is spread out over a much larger spectrum than BW_s , choosing $BW \gg BW_s$ offers a means of identifying the interference sources on the basis of received power alone), so that the weights are set over a wider band than that which contains the desired signals. The consequences of such a choice of BW , and the limitations on how wide one can actually choose BW are of primary interest in this report. To this end, we define the average channel covariance matrix \underline{R} according to

$$\underline{R}_{k,q} \equiv \langle E_k(\omega) E_q^*(\omega) \rangle + \underline{M}_N \quad (1)$$

where the brackets $\langle . \rangle$ denote the frequency average

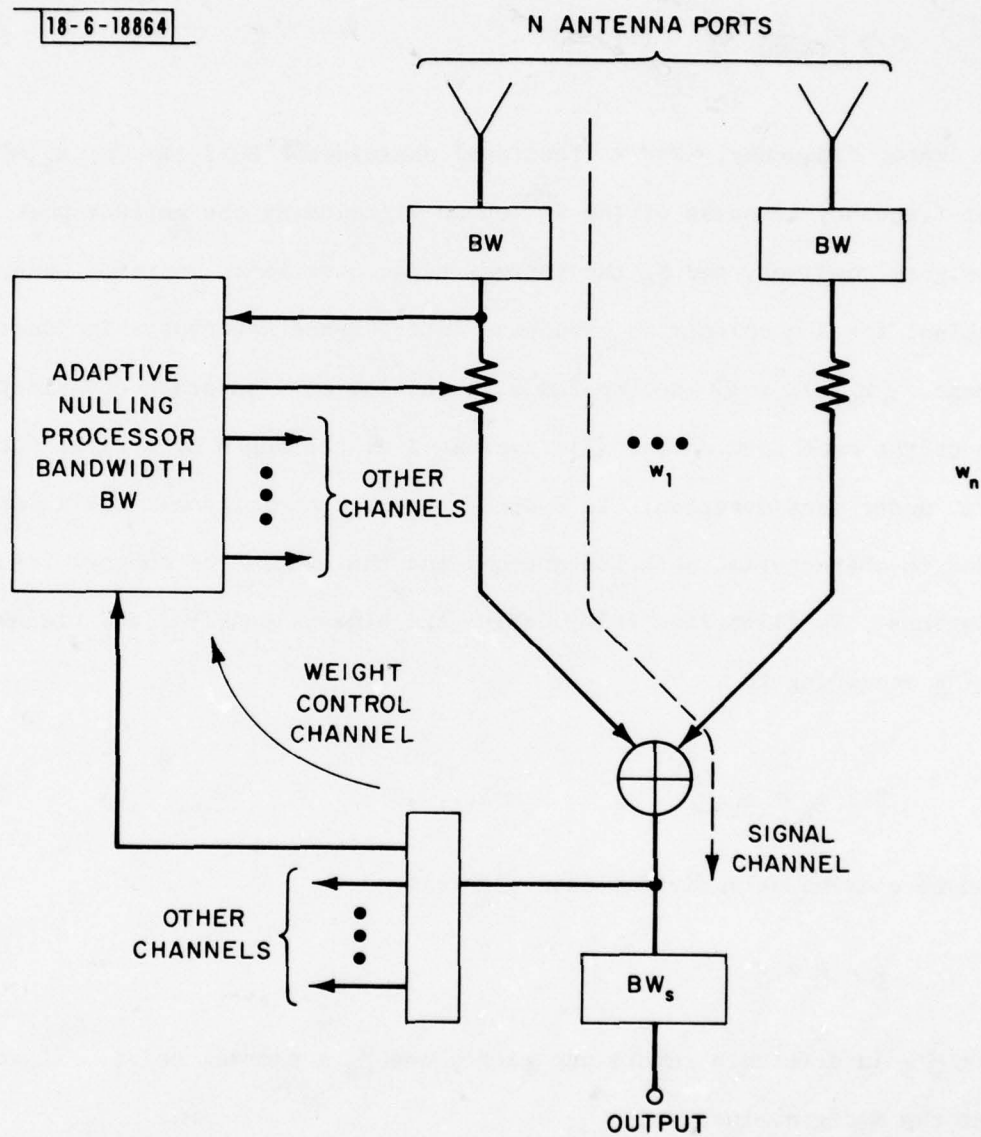


Fig. 1. General configuration for an N-channel adaptive nulling processor.

$$\langle \cdot \rangle \equiv \frac{1}{\text{FBW}} \int_{1 - \frac{\text{FBW}}{2}}^{1 + \frac{\text{FBW}}{2}} (\cdot) dW, \quad (2)$$

$\omega_0 \equiv$ center frequency, $\text{FBW} = \text{fractional bandwidth} \equiv \text{BW}/f_0$, $W \equiv \omega/\omega_0$, $E_k(\omega)$ denotes the total frequency response of the k^{th} channel including the antenna port through the signal combiner, and \underline{M}_N the thermal noise covariance matrix. Generally speaking, for J uncorrelated broadband interference wavefronts incident on the antenna, $\langle E_k(\omega) E_q^*(\omega) \rangle$ decomposes into the sum of J separate covariance matrices, each of the same form as Eq. (2), evaluated at the angle of arrival for the source under consideration. In essence, then, \underline{R} contains all the information needed to characterize both the antenna and the effects of channel frequency variations. To illustrate this, define the eigenvalues, s_k , and eigenvectors \underline{e}_k of \underline{R} according to

$$\underline{R} \cdot \underline{e}_k = s_k \underline{e}_k, \quad k=1, \dots, N. \quad (3)$$

\underline{R} can be conveniently divided into the form

$$\underline{R} = \underline{M} + \underline{M}_N, \quad (4)$$

where \underline{M} = interference covariance matrix and \underline{M}_N = thermal noise. If we order the N eigenvalues

$$s_1 > s_2 > \dots > s_N \quad (5)$$

and consider J interference sources incident on the antenna, then the spec-

trum of \underline{R} will generally decompose as illustrated in Fig. 2. (This excludes the case of closely spaced interference sources; if the interference sources are closely spaced, then some eigenvalues may arise in the second grouping due to these proximity effects.) The effects of channel dispersion result in a set of eigenvalues raised above the thermal noise level. Generally speaking these eigenvalues increase in magnitude as the bandwidth is increased. The effect of such an eigenvalue spread can be seen by considering their effects on the weights after adapting to the interference. A properly designed adaptive feedback processor will result in a set of weights (neglecting the dispersion introduced by the processor)

$$\underline{w} = [\underline{I} + \mu \underline{R}]^{-1} \cdot \underline{w}_0 \quad (6)$$

being applied to the signal channels, where \underline{I} is the identity matrix, μ is the effective loop gain and \underline{w}_0 is the steering vector controlling the weights in the absence of interference sources. Generally μ is a function of the dynamic range of the processor. By decomposing \underline{R} into its eigenvalue spectrum, Eq. (6) can be conveniently written

$$\underline{w} = \sum_{k=1}^N \frac{1}{1+\mu s_k} (\underline{e}_k^\dagger \cdot \underline{w}_0) \underline{e}_k \quad (7)$$

Thus the weights are formed from linear combinations of all the eigenvectors of \underline{R} , weighted according to $(1/(1+\mu s_k)) \underline{e}_k^\dagger \cdot \underline{w}_0$, so that eigenvectors corresponding to the larger eigenvalues are excluded from contributing to the weights, which

18-6-18865

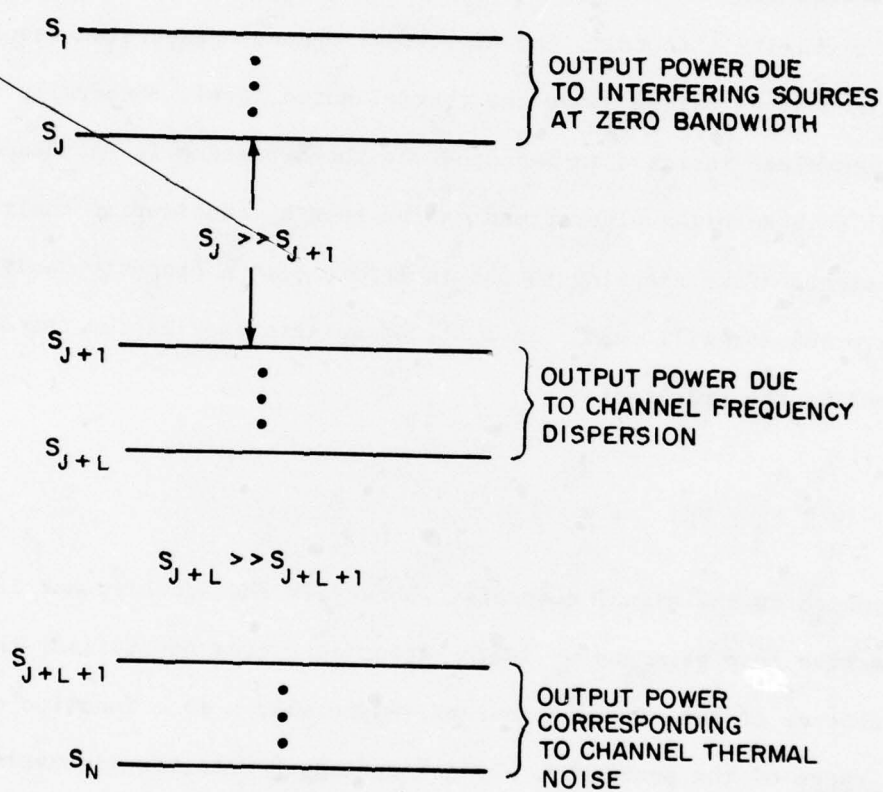


Fig. 2. Typical eigenvalue spread for J interference sources separated greater than a half-power beamwidth, and having a non-zero bandwidth.

gives the desired effect of minimizing the strong interference sources. Assuming $\underline{e}_k^\dagger \cdot \underline{w}_0 \neq 0$, then the magnitude of μs_k determines which eigen-components of \underline{R} are used. The $\{s_k\}$ are often referred to as the "degrees of freedom of the antenna," and it is readily observed that if frequency dispersion is significant, bandwidth effects can use up these degrees of freedom. This effect is disadvantageous for several reasons: It reduces the number of interference sources which can be nulled by the array; if only one or two interference sources are present, it reduces the allowable proximity of any user to an interference source, as a very wideband null (spatially broad) will be formed in order to compensate for the dispersion effects; and finally, if the dynamic range of the processor is not sufficient (i.e., $\mu s_{J+L} \lesssim 1$), these eigenvalues cannot even be nulled and result in a perhaps prohibitively large value of interference power at the output. Thus it is desirable to minimize these bandwidth effects as much as possible.

In the following we will rely heavily on the eigenvalue description of the bandwidth phenomena to quantify the tradeoffs involved in choosing between antenna types and in determining the channel-tracking tolerances required to achieve a desired null depth. In Section II we develop a general relationship relating interference cancellation to the spread in eigenvalues and the steering vector \underline{w}_0 governing the quiescent mode of operation. In Section III we use this relationship to develop the tolerances required when channel matching for a specified cancellation or null depth. Section IV considers frequency dispersion resulting due to the antenna and the fundamental

limitations imposed by aperture size. Finally in Section V we examine antenna dispersion using measured data for one particular antenna type--a reflector-type multiple-beam antenna.

II. Development--Interference Cancellation and Eigenvalue Spectrum

In the general case, the covariance matrix \underline{R} defined in (1) is a complicated function both of antenna frequency dispersion and channel mismatch with frequency, and in general it is difficult to separate out the coupling between these two effects. To see this, consider the general configuration of Fig. 1, and decompose $E_k(\omega)$ into the product of two factors-- $A_k(\omega)$ due to antenna dispersion and $H_k(\omega)$ due to the channel frequency response. In this case, referring to Eqs. (1) and (4), \underline{M} takes the form

$$\underline{M}_{k,q} = \langle A_k(\omega) A_q^*(\omega) H_k(\omega) H_q^*(\omega) \rangle \quad (8)$$

In order to elucidate the effect of bandwidth on the cancellation process, it is convenient to approximate \underline{M} in the form

$$\underline{M} = \underline{M}_0 + \Delta \underline{M} \quad (9)$$

where $\underline{M}_0 \equiv \underline{M}(\omega=\omega_0)$ and $\Delta \underline{M}$ corresponds to a small perturbation of \underline{M} about $\omega=\omega_0$. In order to determine the effects of bandwidth, we assume the weights are set for perfect cancellation at $\omega=\omega_0$, and examine the increase in output power as the frequency is varied about $\omega=\omega_0$. This zero-bandwidth weighting assures that at most, only a single degree of freedom is used per interference source. It also simulates the performance of an adaptive processor having dynamic range (for user power considerations) such that $\mu s_{J+1} \lesssim 1$ (i.e., the system does not respond to eigenvalues beyond s_J). The set of weights \underline{w} which perfectly null J incoherent wavefronts incident on the aperture at $\omega=\omega_0$ is given by

$$\underline{w} = [\underline{I} - \sum_{j=1}^J \underline{e}_j \underline{e}_j^{\circ}] \cdot \underline{w}_0 \quad (10)$$

where the \underline{e}_j° are the eigenvectors of \underline{M}_0 and "+" "denotes complex-conjugate transpose". Consider now the eigenvalue/eigenvector characterization as a function of bandwidth. As bandwidth increases, the second grouping of eigenvalues in Fig. 2 associated with \underline{M} increases, resulting in a corresponding increase in output power. (Of course, as the bandwidth increases indefinitely, the eigenvalue s_{J+1} becomes significantly large so that μs_{J+1} is no longer small, and the adaptive processor would then sense, and null, this eigenvalue, resulting in a wideband null. Since our aim is to design to a bandwidth such that $\mu s_{J+1} \lesssim 1$, the set of weights in (10) are a valid representation of the adapted weights.) The eigenvectors of \underline{M} corresponding to s_1, \dots, s_J essentially do not change (again assuming sources separated \gtrsim a half-power beamwidth (HPBW) of the antenna radiation pattern) when compared to the first J zero-bandwidth eigenvectors. If we denote the set $\{\underline{e}_j\}$ to be the eigenvectors of \underline{M} , then $\underline{e}_1 \sim \underline{e}_1^{\circ}, \dots, \underline{e}_J \sim \underline{e}_J^{\circ}$. To compute the cancellation resulting from applying a set of weights \underline{w} to the channels, we determine the interference to thermal noise ratio I/N according to

$$I/N \equiv \frac{\underline{w}^{\dagger} \cdot \underline{M} \cdot \underline{w}}{\underline{w}^{\dagger} \cdot \underline{M}_N \cdot \underline{w}} \quad (11)$$

Since \underline{M}_N is diagonal and normalized to unity, we have

$$I/N = \frac{\underline{w}^{\dagger} \cdot \underline{M} \cdot \underline{w}}{\underline{w}^{\dagger} \cdot \underline{w}} \quad (12)$$

The cancellation C is then defined according to

$$C \equiv \frac{(I/N)_a}{(I/N)_b} \quad (13)$$

where the subscript "a" denotes "after" adaption (i.e., using the weights of Eq. (10)), and "b" denotes "before" adaption (i.e., using $\underline{w} = \underline{w}_0$). Saving the details for Appendix 1, the cancellation C can be expressed in the form (assuming normalized quiescent weights $\underline{w}_0^\dagger \cdot \underline{w}_0 = 1$)

$$C = \frac{\sum_{k=J+1}^N s_k |\underline{e}_k^\dagger \cdot \underline{w}_0|^2}{[1 - \sum_{j=1}^J |\underline{e}_j^\dagger \cdot \underline{w}_0|^2] \sum_{j=1}^J s_j |\underline{w}_0^\dagger \cdot \underline{e}_j|^2} \quad (14)$$

Note that C is an increasing function of ω . The numerator in (14) represents the increase in output power due to the second grouping of eigenvalues s_{J+1}, \dots, s_N , which increase with bandwidth, and the denominator is dominated by the first grouping of eigenvalues s_1, \dots, s_J which determine the interference output before adaption. For the case of a single interference source, Eq. (14) can be written in a particularly illustrative form:

$$C_{J=1} = \frac{s_2}{s_1} F_2(\underline{w}_0) + \frac{s_3}{s_1} F_3(\underline{w}_0) + \dots + \frac{s_N}{s_1} F_N(\underline{w}_0) \quad (15)$$

which takes the form of a series having terms of order s_k/s_1 . The factor $F_k(\underline{w}_0)$ is given by

$$F_k(\underline{w}_0) = \left| \frac{\underline{e}_k^\dagger \cdot \underline{w}_0}{\underline{e}_1^\dagger \cdot \underline{w}_0} \right|^2 \frac{1}{1 - |\underline{e}_1^\dagger \cdot \underline{w}_0|^2} \quad (16)$$

and determines the dependence of cancellation on the quiescent mode of operation. Otherwise said, even though s_2/s_1 might be large, which could lead to poor cancellation, a significant amount of cancellation is still possible if $F_2(\underline{w}_0) \ll 1$, i.e., the quiescent weight is orthogonal to \underline{e}_2 . Although the achievement of this condition might seem fortuitous, in some cases the condition can be reasoned out physically, and we shall give examples in Section IV.

Equation (14) can be used to obtain some interesting upper bounds on the amount of cancellation achievable for a resultant eigenvalue spread. To accomplish this, we bound the $N-J$ lower eigenvalues of \underline{M} by s_{J+1} . Thus

$$C \leq \frac{s_{J+1} \sum_{k=J+1}^N |\underline{e}_k^\dagger \cdot \underline{w}_0|^2}{\left[1 - \sum_{j=1}^J |\underline{e}_j^\dagger \cdot \underline{w}_0|^2\right] \sum_{j=1}^J s_j |\underline{w}_0^\dagger \cdot \underline{e}_j|^2} \quad (17)$$

Noting that

$$\sum_{k=J+1}^N |\underline{e}_k^\dagger \cdot \underline{w}_0|^2 = 1 - \sum_{j=1}^J |\underline{e}_j^\dagger \cdot \underline{w}_0|^2, \quad (18)$$

then (17) reduces to

$$C \leq \frac{s_{J+1}}{\sum_{j=1}^J s_j |\underline{w}_0^\dagger \cdot \underline{e}_j|^2} \leq \frac{(s_{J+1}/s_1)}{|\underline{w}_0^\dagger \cdot \underline{e}_1|^2} \quad (19)$$

Equation (19) clearly indicates that the greater the eigenvalue spread (i.e., the smaller s_{J+1}/s_1 becomes), the better the resultant cancellation which will be achieved. Furthermore, Eq. (19) indicates that the achievable cancellation is a strong function of the mode of operation (i.e., choice of \underline{w}_0). For example, if the interference sources are positioned in the nulls of the quiescent patterns, then $|\underline{e}_j^\dagger \cdot \underline{w}_0| \ll 1$ and little cancellation (as defined in (13)) is obtained, or needed for that matter. However two special cases of significant interest are worth special consideration: 1) A planar array for which each element has an earth coverage radiation pattern. An earth-coverage quiescent pattern can then be obtained by choosing $\underline{w}_0^\dagger = [1, 0, \dots, 0]$. In this case, for a single interference source, Eq. (19) reduces to

$$C \leq \frac{s_2}{s_1 |\underline{e}_{10}|^2} = N \left(\frac{s_2}{s_1} \right) \quad (20)$$

where N is the number of elements; 2) A quiescent radiation pattern is directed to a single user. When a single interference source is present, \underline{e}_1 applied as weight allocates maximum directive gain to this source. Hence as the user position approaches the interference source position, $\underline{w}_0^\dagger \cdot \underline{e}_1 \rightarrow 1$, and the upper bound on $C \rightarrow s_2/s_1$. The importance of minimizing the spread (s_2/s_1) for achieving the lowest possible cancellation for these important modes of operation becomes evident from this result.

Returning to (14) or (15), we note that the spread in eigenvalues is the most fundamental characterization of the bandwidth behavior of the

channel, and hence the amount of cancellation achievable, as it is independent of the mode of operation of the antenna system. In Section III we characterize this spread as a function of post-antenna output channel tracking, and consider the effects of antenna frequency dispersion on the distribution of eigenvalues in Section IV.

III. Channel Tracking Tolerances

Having developed a general expression (Eqs. (14), (15)) quantitatively specifying how the effects of bandwidth limit the achievable cancellation level, it is instructive to examine the effects of channel-channel mismatches relative to these results. As contrasted to antenna dispersion, for which frequency mismatches between channels tend to continually increase with deviations in frequency away from $\omega = \omega_0$, channel tracking mismatch tends to be characterized by a fixed amount of ripple over the band having a specified RMS variation in amplitude and in phase. Returning now to Eq. (8), let us express the channel frequency response in the form

$$H_k(\omega) = H_0(\omega)[1 + \Delta_k(\omega)] \quad (21)$$

where $H_0(\omega)$ is some reference transfer function and $\Delta_k(\omega)$ represents deviations from this reference. Since all channels are designed to be ideally the same, it is realistic to model the error $\Delta_k(\omega)$ as a sample function of an uncorrelated random process having the following properties:

$$E\{\Delta_k(\omega)\} = 0 \quad ; \quad E\{\Delta_k(\omega)\Delta_q^*(\omega)\} = \sigma_k^2 \delta_{k,q} \quad (22)$$

where $E\{\cdot\}$ denotes the expected value in a statistical sense, and we have defined σ_k^2 to represent the rms tracking errors for the k^{th} channel. $\delta_{k,q}$ denotes the Kronecker delta function. The choice of the reference transfer function $H_0(\omega)$ follows directly as a consequence of $E\{\Delta_k(\omega)\}=0$ in (22), as

can be seen by solving (21) for $\Delta_k(\omega)$ and using (22). We obtain

$$H_o(\omega) = E\{H_k(\omega)\} \approx \frac{1}{N} \sum_{k=1}^N H_k(\omega) \quad (23)$$

Consider now the expression for $M_{k,q}$ defined in Eq. (8). Using (21) in (8), we obtain

$$\begin{aligned} M_{k,q} = & \langle |H_o(\omega)|^2 A_k(\omega) A_q^*(\omega) \rangle \\ & + \langle A_k(\omega) A_q^*(\omega) |H_o(\omega)|^2 [\Delta_k(\omega) + \Delta_q^*(\omega)] \rangle \\ & + \langle A_k(\omega) A_q^*(\omega) |H_o(\omega)|^2 \Delta_k(\omega) \Delta_q^*(\omega) \rangle \end{aligned} \quad (24)$$

The first term in (24) is affected only by antenna dispersion, as the factor $|H_o(\omega)|^2$ is independent of k, q and hence will not affect the eigenvalue spread of M . This term will be considered in detail in Section IV. The second and third terms of (24) indicate a definite interaction between antenna dispersion and tracking error which is difficult, in general, to separate out. However, two limiting cases of considerable importance can be examined: first, if antenna dispersion is negligible (e.g., for most antenna diameters of interest, percentage nulling bandwidth $\ll .01$ RF center frequency), then $A_k(\omega)$ can be approximated by $A_k(\omega_o)$. Furthermore, $|H_o(\omega)|^2$ is generally a slowly varying function of ω , so that the averages in (24) are only over the functions $\Delta_k(\omega)$. It is also reasonable to assume that the $\Delta_k(\omega)$ are sample functions of an ergodic process, so that ensemble averages may be replaced by frequency

averages. Then $E\{\Delta_k\} = \langle \Delta_k \rangle = 0$. In this case (24) reduces to

$$\underline{M}_{k,q} = \underline{M}_0 + \langle \underline{Z}^\dagger \cdot \underline{M}_0 \cdot \underline{Z} \rangle \quad (25)$$

where we have defined

$$(\underline{M}_0)_{k,q} \equiv |H_0(\omega)|^2 A_k(\omega_0) A_q^*(\omega_0) \quad (26)$$

and \underline{Z} the diagonal matrix

$$\underline{Z} = \begin{bmatrix} \Delta_1(\omega) & & & \\ & \Delta_2(\omega) & & 0 \\ & & \ddots & \\ 0 & & & \ddots \\ & & & & \Delta_N(\omega) \end{bmatrix} \quad (27)$$

Noting the properties assumed in Eq. (22), $\langle \underline{Z}^\dagger \cdot \underline{M}_0 \cdot \underline{Z} \rangle$ becomes diagonal and can be expressed in the form

$$\langle \underline{Z}^\dagger \cdot \underline{M}_0 \cdot \underline{Z} \rangle = \begin{bmatrix} \sigma_1^2 M_{11} & & & \\ & \sigma_2^2 M_{22} & & 0 \\ & & \ddots & \\ 0 & & & \ddots \\ & & & & \sigma_N^2 M_{NN} \end{bmatrix} \quad (28)$$

which clearly indicates the assumed independence of the channel matching errors.

Note also that Eq. (25) is now in the same form as Eq. (9) defined in Section II

and the results of this section can now be applied. The second limiting case occurs when the nulling bandwidth is sufficiently wide so that antenna dispersion dominates. This regime is a strong function of antenna size and operating frequency, and will be discussed in Section IV. We note in passing that the limiting case of no antenna dispersion provides a good practical means for checking out the channel behavior; i.e., if broadband signals of equal amplitude are fed into each port of the weight channel, the result is identical to an interference source incident broadside to a planar array connected to the channels. For this case, the antenna is ideally broadband, and the cancellation is limited only by the effects of channel tracking. Measurements to this effect will be presented in Section V.

Consider now the eigenvalue spread generated by the perturbation of the zero bandwidth matrix \underline{M}_0 by the matrix $\Delta \underline{M}$ defined in Eq. (28). Since we assume the perturbed matrix $\Delta \underline{M}$ is small, the eigenvalues of \underline{M} can be estimated using the results of first order perturbation theory. Denoting the eigenspectrum of \underline{M} as s_k , $k=1, \dots, N$, it can be shown⁽¹⁾ that

$$s_k = s_k^0 + \underline{e}_k^\dagger \cdot \Delta \underline{M} \cdot \underline{e}_k \quad (29)$$

where, as before, we have assumed that the first J eigenvectors of \underline{M}_0 are essentially those of \underline{M} . Of prime interest in (29) is the $J+1^{\text{st}}$ eigenvalue, s_{J+1} , which, from Eq. (14) governs the achievable cancellation. Since the diagonal values of $\Delta \underline{M}$ are in general not equal, s_{J+1} is a complicated

function of the interference scenario. However, a useful upper bound on s_{J+1} can readily be obtained, and we now derive this bound. The special case of a planar array will then be considered.

First observe that $s_{J+1}^0 \approx 0$. Hence

$$s_{J+1} = \max_{\{\underline{e}\}} \{\underline{e}^\dagger \cdot \underline{\Delta M} \cdot \underline{e}\} \quad (30)$$

where the maximization in (30) is performed over all orthonormal vectors \underline{e} such that $\underline{e}_j^\dagger \cdot \underline{e} = 0$, $j=1, \dots, J$. Note then that $\underline{e}^\dagger \cdot \underline{M}_0 = 0$, so that, using (28) for $\underline{\Delta M}$ in (30), we obtain

$$s_{J+1} = \max_{\{\underline{e}\}} \{\underline{e}^\dagger \cdot \langle \underline{Z}^\dagger \cdot \underline{M}_0 \cdot \underline{Z} \rangle \cdot \underline{e}\} \quad (31)$$

Using Eq. (28) in (31), we have

$$s_{J+1} = \max_{\{\underline{e}\}} \sum_{k=1}^N |e_k|^2 \sigma_k^2 M_{kk} \quad (32)$$

where e_k denotes the k^{th} component of the vector \underline{e} . The dependence of s_{J+1} on the antenna type (i.e., MBA or array) is exhibited via the presence of the factor $M_{k,k}$, and the dependence on channel tracking errors by way of σ_k^2 . Since \underline{e} is orthonormal, it follows that

$$s_{J+1} \leq \max (\sigma_k^2 M_{k,k}) \sum_{k=1}^N |e_k|^2 = \max (\sigma_k^2 M_{k,k}) \quad (33)$$

Hence the predominant eigenvalue s_{J+1} resulting from the various channel tracking errors is bounded by the worst case tracking error over all the channels. To estimate the spread s_{J+1}/s_1 , we estimate s_1 by noting that

$$Js_1 \geq s_1 + s_2 + \dots + s_J \approx \text{trace } (\underline{\underline{M}}) \quad (34)$$

Hence

$$s_1 \geq \frac{1}{J} \sum_{k=1}^N M_{k,k} \quad (35)$$

Using (33) and (35) the spread in eigenvalues resulting from channel tracking errors can be bounded by

$$\frac{s_{J+1}}{s_1} \leq J \frac{\text{MAX } (\sigma_k^2 M_{kk})}{\sum_{k=1}^N M_{k,k}} \quad (36)$$

The spectrum of $\underline{\underline{M}}$ must then generally appear as illustrated in Fig. 3.

Noting Eq. (19), Eq. (36) then yields a direct upper bound on the achievable interference cancellation

$$C \leq J \frac{\text{MAX } (\sigma_k^2 M_{k,k})}{|\underline{e}_1 + \underline{w}_0|^2 \sum_{k=1}^N M_{k,k}} \quad (37)$$

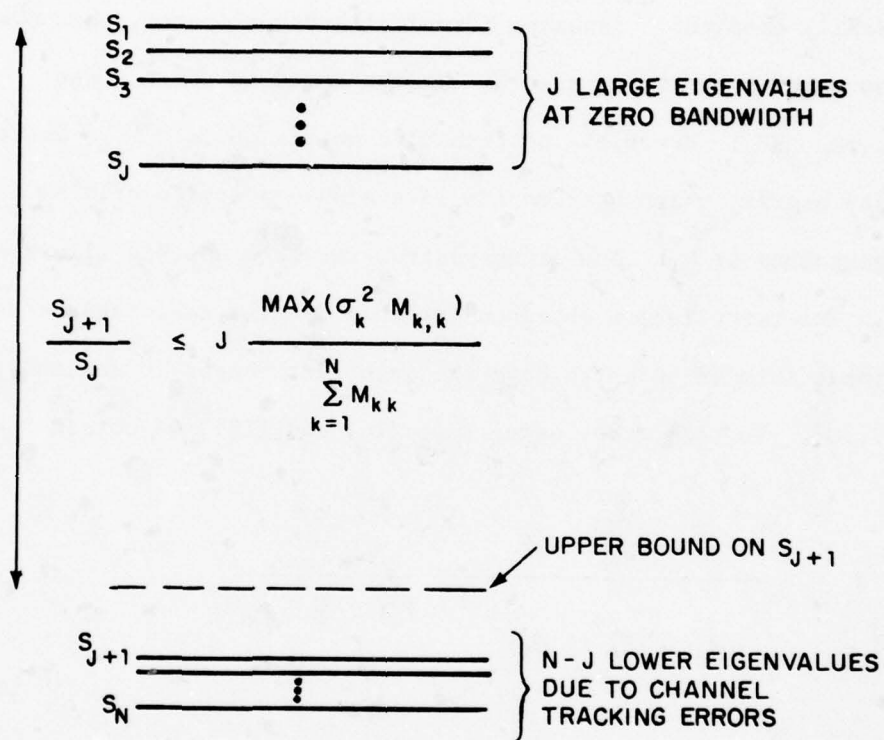


Fig. 3. Effects of independent channel tracking errors σ_k^2 on the eigenspectrum of \underline{M} for an arbitrary antenna type.

Exact Computations -- Planar Array

In order to illustrate the tightness of the bounds derived above, the special case of a planar array configuration with channels having $\sigma_k^2 = \sigma^2$, $k=1, \dots, N$ will now be considered. In this case the eigenspectrum of $\underline{\underline{M}}$ can be analytically obtained. Assuming identical array elements, the power received by each of the array elements is the same, in which case $M_{11} = M_{22} = \dots = M_{N,N} = M_o$. Hence the perturbation matrix $\Delta \underline{\underline{M}}$ is $\sigma^2 M_o \underline{\underline{I}}$, where $\underline{\underline{I}}$ is the identity matrix, which corresponds to a simple addition of $\sigma^2 M_o$ to each of the eigenvalues of $\underline{\underline{M}}_o$. The eigenspectrum for this case is illustrated in Fig. 4. The cancellation obtained for this special case takes a particularly simple form if an earth coverage quiescent vector is assumed; i.e., $\underline{w}_o^\dagger = [1, 0, \dots, 0]$. In this case, using Eqs. (14) and (18), we obtain

$$C = \frac{\sigma^2 M_o}{\sum_{j=1}^J s_j \cdot |\underline{w}_o^\dagger \cdot \underline{e}_j|^2} = \frac{\sigma^2 M_o}{\underline{w}_o^\dagger \cdot \underline{\underline{M}} \cdot \underline{w}_o} \quad (38)$$

where, for an earth coverage radiation pattern, the interference-noise ratio before adaption is equal to $\underline{w}_o^\dagger \cdot \underline{\underline{M}} \cdot \underline{w}_o$. Noting that $\underline{w}_o^\dagger \cdot \underline{\underline{M}} \cdot \underline{w}_o = M_{11} = M_o$, then we obtain

$$C = \sigma^2 \quad (39)$$

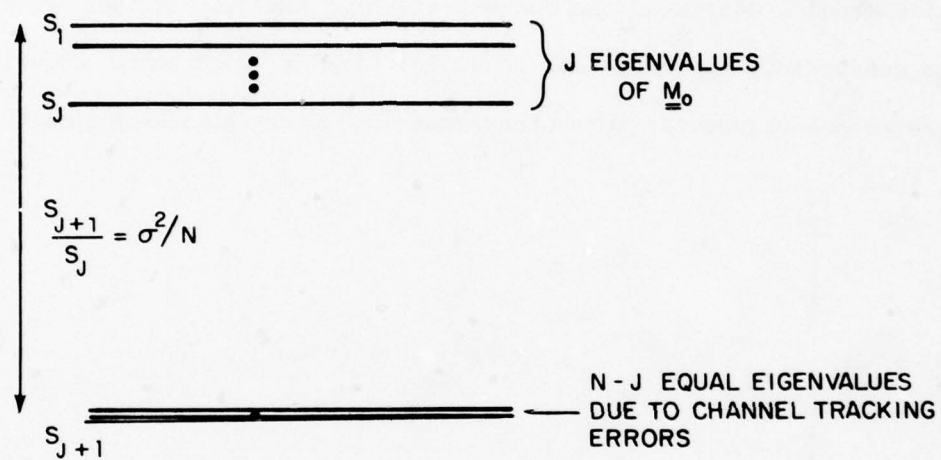


Fig. 4. Eigenspectrum of $\underline{\underline{M}}$ for a planar array having statistically equal channel tracking errors σ^2 .

independent of the number of interference sources (assuming, of course, $J < N$) and independent of the number of channels. By comparison, using the general bound in (37), with $M_{kk} = M_0, k=1, \dots, N$, we obtain $C \leq J \sigma^2$, indicating the tightness of this bound.

A second special case of considerable practical interest occurs when one particular channel dominates the channel tracking errors. For an earth coverage constraint, two cases are possible: the dominant error occurs either in the reference channel or some other channel. Denoting the dominant error as σ_k^2 , then

$$\underline{\underline{M}} = M_0 \begin{bmatrix} \sigma^2 & & & & \\ & \ddots & & & \\ & & \sigma_k^2 & & \\ & & & \ddots & \\ 0 & & & & \sigma^2 \end{bmatrix} = M_0 \sigma^2 \underline{\underline{I}} + (\sigma_k^2 - \sigma^2) \underline{u}_k \underline{u}_k^\dagger \quad (40)$$

where $\underline{u}_k^\dagger = [0, 0, \dots, 1, 0, \dots, 0]$ and the 1 appears in the k^{th} slot of the vector. We assume that $\sigma_k^2 \gg \sigma^2$ for the k^{th} channel. The eigenvalue spectrum for this case is illustrated in Fig. 5 for the case of a single interference source. Notice that in this case the second eigenvalue dominates and is given by σ_k^2/N . Assuming $\sigma_k^2 \gg \sigma^2$, we can use the first term in (15) to estimate the cancellation achieved as long as $\underline{e}_2^\dagger \cdot \underline{w}_0$ is not too small. Thus

$$C \approx (s_2/s_1) \left[\frac{|\underline{e}_2^\dagger \cdot \underline{w}_0|^2}{|\underline{e}_1^\dagger \cdot \underline{w}_1|^2} \cdot \frac{1}{1 - |\underline{e}_1^\dagger \cdot \underline{w}_0|^2} \right] \quad (41)$$

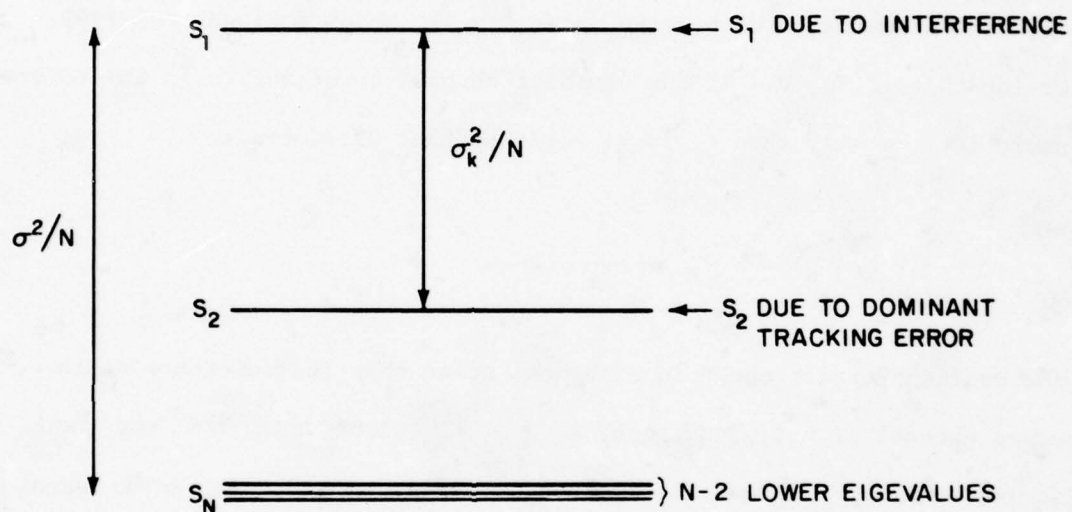


Fig. 5. Eigenspectrum of $\underline{\underline{M}}$ for a planar array having statistically equal channel tracking error, σ_k^2 , dominates over the other channels.

However for a single interference source, $|\underline{e}_1^\dagger \cdot \underline{w}_0|^2 = 1/N$ for the array antenna, so that (41) becomes, using $s_2/s_1 = \sigma_k^2/N$

$$C \approx \sigma_k^2 (N/N-1) |\underline{e}_2^\dagger \cdot \underline{w}_0|^2 \quad (42)$$

Now \underline{e}_2 can be approximated by $\underline{e}_2 = \underline{u}_k - (\underline{e}_1^\dagger \cdot \underline{u}_k) \underline{e}_1$ which follows from (40), observing that $\underline{e}_2^\dagger \cdot \underline{e}_1 = 0$. If the dominant channel error occurs in the reference channel, i.e., $\underline{w}_0 = \underline{u}_k$, then $\underline{e}_2^\dagger \cdot \underline{w}_0 = 1 - 1/N$ so that C reduces to

$$C \approx \sigma_k^2 \left(\frac{N-1}{N}\right) \approx \sigma_k^2 \quad (43)$$

If the dominant errors occur in a channel other than the reference earth coverage channel, i.e., $\underline{w}_0 = \underline{u}_q$, $q \neq k$, then $\underline{e}_2^\dagger \cdot \underline{w}_0$ is of order $1/N^2$ and the remaining terms of (15) must be included in estimating C . It can be shown that, for this case

$$C \approx \sigma^2 (1 - 1/N^2) + \sigma_k^2 / N^2 \quad (44)$$

Comparing (43) and (44), it becomes clear that it is very disadvantageous to use a dominant error channel as a reference channel, since in this case the rms deviation between this channel and the others limits the attainable interference cancellation. Otherwise the effect of this dominant error channel is decreased by the factor $1/N^2$.

Parametric Representation of σ^2

Equation (39) clearly points out the importance of the channel tracking error parameter σ^2 . For this reason, it is useful to present a graphical, parametric representation of σ^2 . Consider Eq. (22), where σ_k^2 is defined

$$\sigma_k^2 \equiv \langle |\Delta_k(\omega)|^2 \rangle = \left\langle \left| 1 - \frac{H_k(\omega)}{H_o(\omega)} \right|^2 \right\rangle \quad (45)$$

Denote $\sigma^2 = \sigma_k^2$ for the present, and define

$$re^{+j\phi} = H_k(\omega)/H_o(\omega) \quad (46)$$

where we assume that $|\phi| \ll 1$ and r is close to unity. In this case,

$$\sigma^2 = \langle |1 - re^{+j\phi}|^2 \rangle \quad (47)$$

We expand $r \approx 1 + \epsilon$ and assume $\langle \epsilon \rangle = \langle \phi \rangle = 0$. Then

$$\sigma^2 = \langle |\epsilon + j\phi|^2 \rangle = \langle |\epsilon|^2 \rangle + \langle |\phi|^2 \rangle \quad (48)$$

If we define $\sigma_A^2 = \langle |\epsilon|^2 \rangle$ and $\sigma_\phi^2 = \langle |\phi|^2 \rangle$, then σ_A and σ_ϕ represent the standard deviation of the amplitude and phase, respectively, of the channel tracking errors. Fig. (6) illustrates a parametric representation of σ^2 vs.

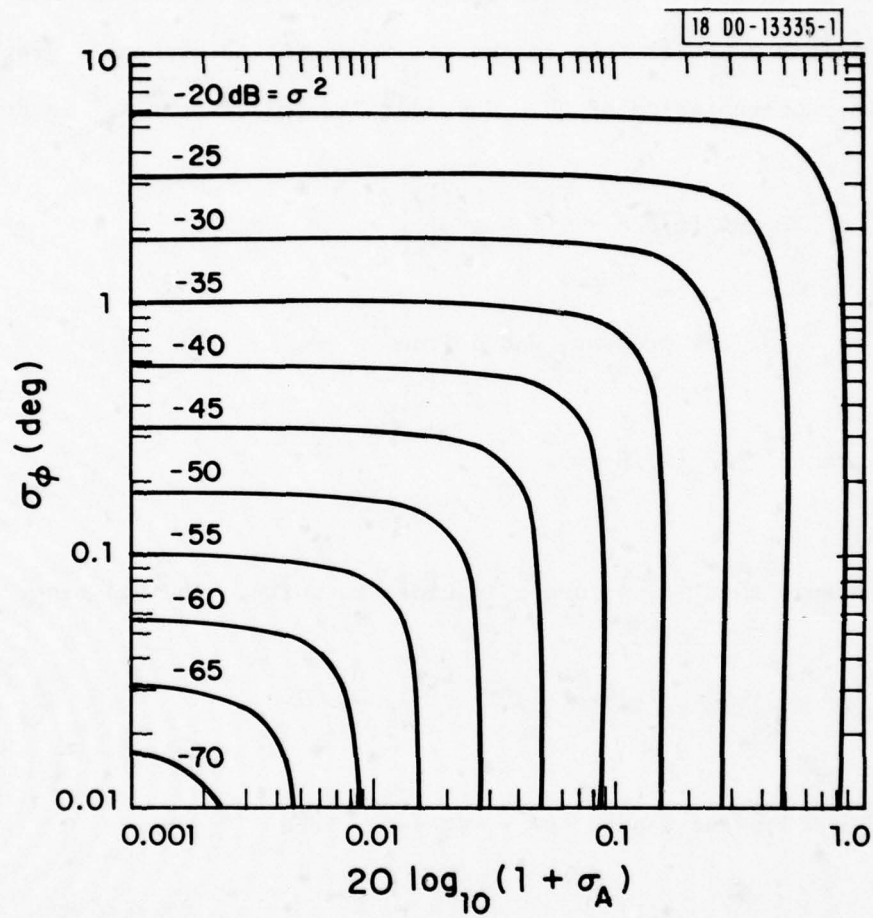


Fig. 6. Parametric representation of the tracking error σ^2 vs amplitude and phase mismatch, $20 \log_{10}(1 + \sigma_A)$ and σ_ϕ , respectively.

$20 \log_{10} r \approx 20 \log_{10} (1 + \sigma_A)$ and σ_ϕ using a graphical presentation developed by Hodsdon⁽²⁾. Using these results, Table 1 below summarizes some matching tolerances required to assure cancellation (assuming $C = \sigma^2$ as in Eq. (39)) to the desired specified null depth.

TABLE 1
CANCELLATION σ^2 AS A FUNCTION OF σ_A AND σ_ϕ

σ^2	σ_ϕ (deg)	$(1 + \sigma_A)$ dB
-20 dB	5.7	0.83 dB
-30 dB	1.8	0.27 dB
-40 dB	0.57	0.09 dB
-50 dB	0.18	0.03 dB

The tight tolerances required to achieve cancellation to below -40 dB clearly indicate the difficulty in achieving cancellation down to this level. Of course, it is possible to introduce channel equalizers into each channel (either adaptive or non-adaptive) to aid in meeting these tolerances, but this will not be considered here.

IV. Antenna Frequency Variations

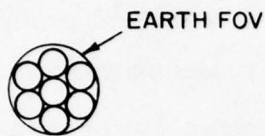
In this section we examine the frequency dispersive properties of various types of antennas which might be used for adaptive nulling in the UHF band in conjunction with a geosynchronous satellite. A detailed tradeoff between the various classes of antennas which might be considered for this application is presented elsewhere⁽³⁾. The main purpose of this section is to evaluate the bandwidth potential of each of the more promising candidates for an antenna system operating in the UHF band and, relative to these dispersion characteristics, some of the consequences of choosing a weight setting bandwidth greater than the signal bandwidth. Because of the UHF band consideration, most of the antenna configurations consist of thinned arrays or reflector type (unfurlable) multiple beam antennas (MBA's). At higher frequencies such as X-band, filled arrays and larger MBA's (in terms of wavelength) become definite possibilities. In order that the antenna types considered here might be extrapolated as much as possible to the higher frequencies, all dimensions will be normalized to D/λ , and percentage bandwidths will be used where appropriate. Element gain is assumed to be 13 dB (as might be obtained from a cluster of four dipoles) for all of the array configurations considered.

In the following development we will attempt to present the tradeoffs between wideband-nulling and spatial resolution to a user located close to an interference source. Some general comments relative to this tradeoff can be made a priori by noting that, for the array antenna, aperture dispersion can be expressed as a function of the product $\omega \sin \theta$; hence, as θ increases, the fre-

quency sensitivity of the array increases. Interpreted conversely, forming a broadband null (fix θ , vary ω) also results in a spatially broader null being formed (fix $\omega=\omega_0$, vary θ). This spatial null broadening also increases as θ increases. These effects can be characterized using the eigenvalue approach discussed previously and will be used throughout the following analysis.

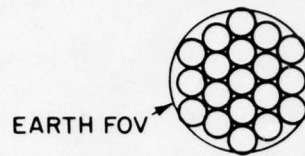
Furthermore, we will attempt to demonstrate how the choice of weight-setting bandwidth affects the overall signal (user) to interference improvement which occurs after nulling. This improvement depends not only on the cancellation achieved, but also the loss in directive gain to the desired user source as a consequence of nulling. Since the adapted gain to the user depends strongly on the steering vector and nulling bandwidth, as well as does the cancellation, it is not clear at this point which factor will, in general, dominate. Some example cases will be treated in detail to examine this effect.

The six basic antenna types to be considered in this section are illustrated in Fig. 7. The MBA types have been included to determine the effects of a time-delayed beam geometry on the nulling bandwidth. Large diameters for the array configurations are considered feasible (neglecting the deployment problem) because of the narrow scan angle required to cover earth field of view (FOV), since for the array, aperture dispersion varies directly as $(\omega D/c)\sin \theta_s$, where θ_s is the angle of the beam maximum. The "ideal" MBA's are modeled in this section in a manner similar to that discussed in Ref. (4). These simulations neglect multipath effects inherent in the antenna geometry (particularly, for the reflector, feed-reflector multipath). These effects will be evaluated using measured data in Section V. The seven and nineteen element arrays were



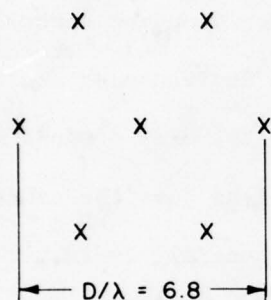
$$D/\lambda = 10.7$$

(a) IDEAL 7-BEAM MBA

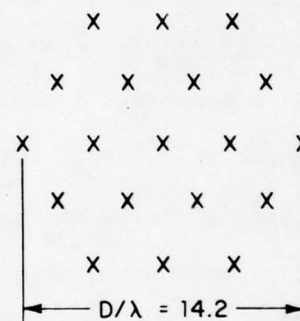


$$D/\lambda = 16.0$$

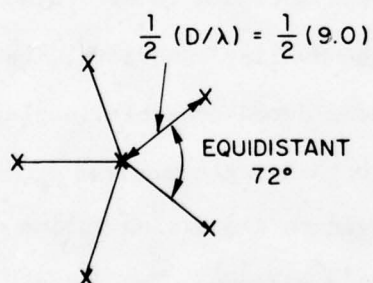
(b) IDEAL 19-BEAM MBA



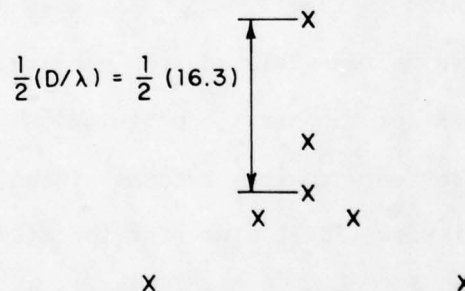
(c) 7-ELEMENT HEXAGONAL ARRAY



(d) 19-ELEMENT HEXAGONAL ARRAY



(e) 6-ELEMENT PENTAGONAL ARRAY



(f) 7-ELEMENT DOUBLE TRIANGLE

Fig. 7. Basic antenna configurations used to evaluate the effects of antenna frequency dispersion.

chosen to have a half-power beamwidth (HPBW) as close as possible to the seven and nineteen beam MBA's, respectively, while constraining all the grating lobes to lie outside the FOV for any scan angle within the FOV. The seven and nineteen element arrays represent regular arrays (array element positioning a subset of a periodic lattice structure) whereas the pentagon and double triangle arrays represent irregular arrays which are sufficiently thinned so that grating lobes are minimized over the FOV. A detailed discussion of the narrow-bandwidth nulling performance characteristics of these antenna types is given in Ref. (3).

Equations (14) and (15) derived in Section II characterize the dependence of cancellation on the frequency dispersion properties of the antenna (via the eigenvalues s_k , $k=J+1, \dots, N$) and on the mode of operation (i.e., the choice of \underline{w}_0). The eigenvalues of interest here are governed by the first term in Eq. (24), where now we assume all $\Delta_k(\omega)=0$; i.e., perfect channel match and ideal weighting. Consider then, for example, a single interference source located at $\theta_j=8^\circ$, $\phi=90^\circ$ as illustrated in the insert of Fig. 8. For each of the antenna configurations of Fig. 7, the eigenvalue spread s_2/s_{MAX} is plotted in Fig. 8 vs. fractional bandwidth, BW/f_0 , where BW =nulling bandwidth and f_0 =center frequency. For the cases considered, s_{MAX} is taken to be the maximum power at the combiner output assuming maximum antenna gain allocated to the interference source. In all cases, the third eigenvalue s_3 is down some 30 dB from s_2 , so that the cancellation predicted by Eq. (15) reduces to

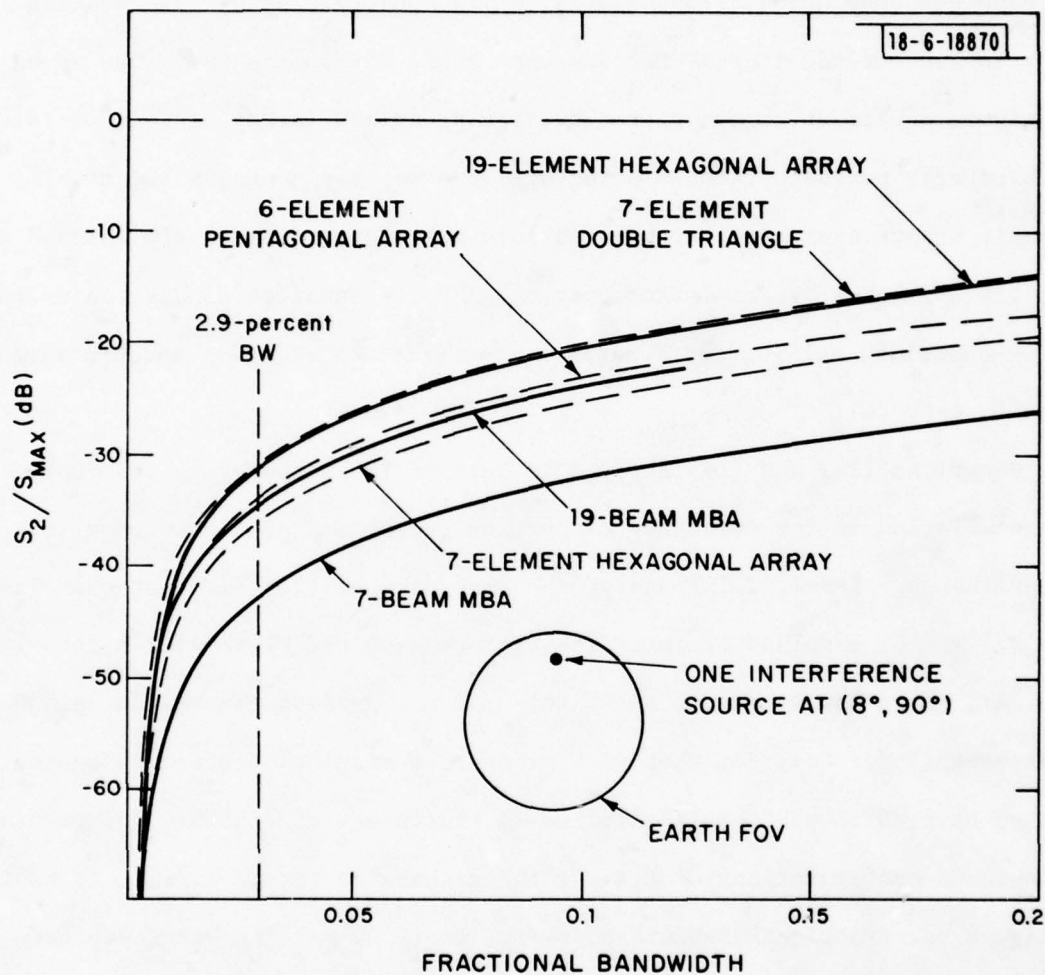


Fig. 8. Eigenvalue spread, S_2/S_{MAX} , in dB vs fractional bandwidth for the six antenna configurations of Fig. 7 and a single interference source.

$$C \approx (s_2/s_1) F_2(\underline{w}_0) + (s_3/s_1) F_3(\underline{w}_0) \quad (49)$$

Assuming $F_2(\underline{w}_0) \neq 0$, then clearly the ratio (s_2/s_1) dominates the interference cancellations. Note that (s_2/s_{MAX}) is largest for the two larger arrays ($D/\lambda \approx 16$) and becomes smaller as the aperture size decreases. Note in particular the low value of s_2/s_{MAX} for the MBA's having time-delayed beams. For all except the 7 beam MBA, a nulling processor having a 40 dB dynamic range operating over a 2.9% bandwidth (approximately 10 MHz bandwidth at 350 MHz) would sense and minimize the second eigenvalue resulting from the wideband operation. (See Eq. (17), where $\mu_{s_{MAX}} \equiv$ dynamic range; then $\mu_{s_2} \equiv \mu_{s_{MAX}}(s_2/s_{MAX}) = 10^{+4}(s_2/s_{MAX}) > 1.$)

In order to illustrate the effects of setting a wideband null, consider an adaptive processor having a 40 dB dynamic range and the single interference source at $(8, 90^\circ)$ in Fig. 8. Table 2 below tabulates, for the seven element double triangle configuration, the loss in directive gain, ΔD_s in the direction of a user (desired) signal as $\theta_s \rightarrow \theta_j$ in the $\phi=90^\circ$ plane, (θ_s is the direction angle to the user, θ_j , to the interference) along with the cancellation and signal to interference, (S/I), improvement from before to after nulling for both a 2 MHz weight setting band (i.e., 0.57% nulling band) and a 10 MHz weight setting band (2.86%) at $f_0=350$ MHz assuming a broadband interference source. For each case, we compute the loss in directive gain in the signal direction, the cancellation and the signal to interference improvement as $\theta_s \rightarrow \theta_j$ in the $\phi=90^\circ$ plane. The cancellation is computed over a 1 MHz signal band centered at 350 MHz.

TABLE 2

(S/I) IMPROVEMENT IN 1 MHz SIGNAL BAND AS θ_S θ_J in $\phi=90^\circ$ PLANE.
SEVEN ELEMENT DOUBLE TRIANGLE (HPBW=3.7°) $\theta_J=8^\circ$.

$\Delta\theta$ (deg)	ΔD_S (dB)		Cancellation in 1 MHz (dB)		(S/I) IMP (dB) Simulation		(S/I) IMP Assum. Cancellation > -40 dB	
	Wt. Setting Bandwidth		2 MHz		2 MHz		2 MHz	
	$\Delta\theta$ /HPBW $\Delta\theta$ deg.		10 MHz		10 MHz		10 MHz	
0.07	0.25	19	19	-50	-42	31	21	21
0.14	0.5	13	15	-51	-49	38	27	25
0.27	1	8	12	-50	-56	42	32	28
0.54	2	3	7	-49	-60	46	37	33
0.81	3	1	4	-48	-59	47	39	36
1.1	4	1	2	-53	-60	52	39	38

Note the greater loss in gain, ΔD_S , as $\theta_S \rightarrow \theta_J$ using the 10 MHz weight setting bandwidth. For $\Delta\theta \equiv |\theta_J - \theta_S| < 1^\circ \approx 0.3^\circ$ HPBW, the improvement in (S/I) is clearly better for the narrower weight setting bandwidth. For $\Delta\theta > 1^\circ$, however, the wider weight setting bandwidth leads to more cancellation over the 1 MHz signal band (i.e., the null is skewed, and actually lower in the signal band) resulting in greater (S/I) improvement for this case. This latter result can be misleading, however, as the cancellation obtained from the simulation is -50 dB or greater, which is, perhaps, unachievable from a channel tracking view point. In reality, the actual cancellation achieved over the nulling band will be limited by the tracking errors between channels in the signal band as discussed in Section III. The last column in Table 2 tabulates the (S/I) improvement assuming the cancellation is limited to -40 dB by channel tracking errors. For this case, the loss in signal gain is clearly the dominating factor, as one would expect, and the narrower nulling bandwidth leads to a better nulling resolution as $\theta_S \rightarrow \theta_J$.

We return now to the dependence of the eigenvalue spread on bandwidth as a function of array configuration. Since frequency dispersion is scenario dependent, particularly for the array configurations, results analogous to Fig. 8 should be obtained for various interference scenarios and also for more than a single interference source. For the array, antenna frequency variations are more directly related to the scan angle of the interference off the array boresight, with near-zero scan angles offering a very broadband behavior. For the MBA, dispersion is most directly related to the positions of the interference sources relative to the beam peak positions, e.g., a triad

location (equispaced from three beam peaks) tends to be broader band than a beam peak location. Reasons for this have been discussed in detail in Ref. (4). In order to illustrate these dependences on bandwidth vs. interference location, we will determine the eigenvalue spread s_2/s_{MAX} for each antenna configuration in Fig. (7) for each single interference location listed in the table below.

TABLE 3

SINGLE INTERFERENCE LOCATIONS USED TO COMPARE THE
BANDWIDTH-LIMITATIONS OF THE ANTENNA CONFIGURATIONS IN FIG. (7)

Case #	θ_J	ϕ_J
1	0	0
2	8°	90°
3	7.3°	90°
4	8.5°	120°
5	4.5°	0°

Figures (9) - (11) illustrate the spread s_2/s_{MAX} for each antenna configuration. Minimum dispersion results in conjunction with the seven beam MBA, and maximum dispersion is obtained for the 19 element hexagonal array when the scan angle is at the edge of the FOV. When the interference source is located at the edge of the FOV, the time-delayed nature of the filled aperture beams tends to yield a broader-band performance when compared to an array configuration having nearly the same HPBW, as can be seen by comparing Fig. (9a) to (9b) and (10a) to (10b). The results of Figs. (11a) and (11b) for the thinned arrays indicate the importance of element positioning. Note that the seven element double triangle, which is enclosed within a diameter of 46', has nearly the same dispersion characteristics as the 19 element hexagonal array filling the same diameter. However, the pentagonal array, which can be enclosed within a 25' diameter (45% smaller) has nearly the same dispersive characteristics as the larger arrays. A more quantitative assessment of these tradeoffs is beyond the scope of this technical note. We simply note that for all the configurations except the seven beam MBA and the small seven element hexagonal array, a weight control processor operating over a 2.9% bandwidth would sense and minimize the second eigenvalue resulting from antenna frequency dispersion, resulting in possible loss of a second degree of freedom, and a broadband (and possibly a broad-angle) null with consequent loss in signal resolution similar to that evaluated in Table 2. Results for more than a single interference source will be considered in the following paragraphs, along with results for a particularly useful mode of operation - earth coverage.

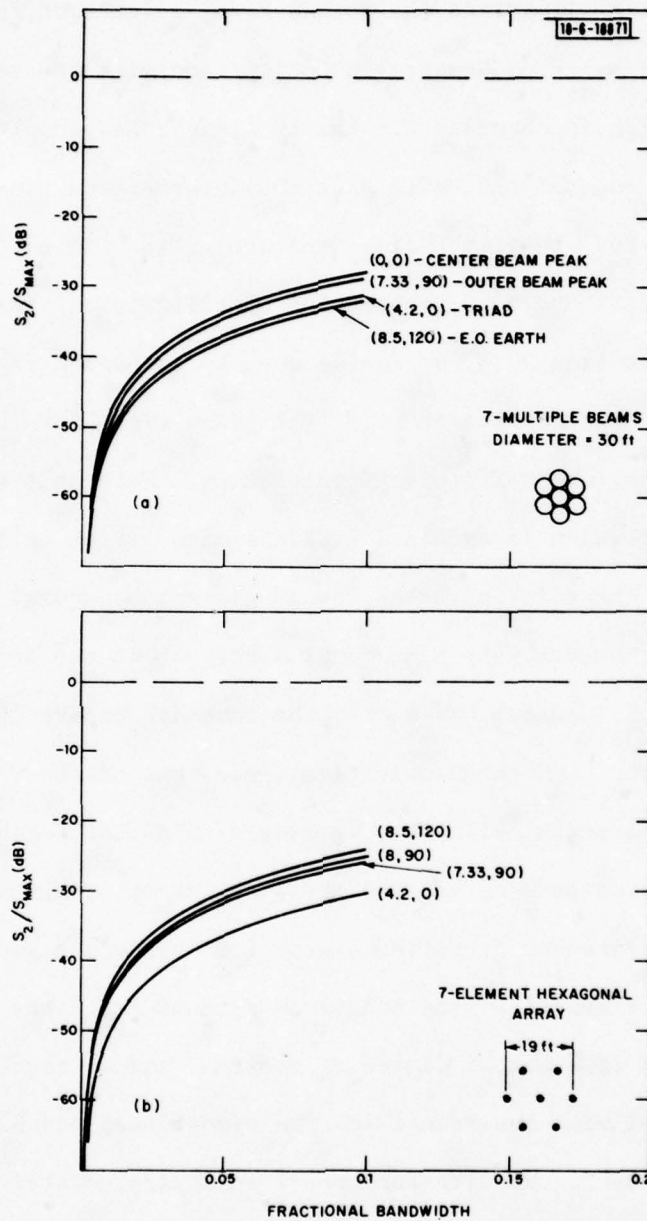


Fig. 9. Eigenvalue spread, S_2/S_{MAX} , vs fractional bandwidth for the four single interference locations of Table 3 for (a) the seven-beam MBA and (b) the seven-element hexagonal array.

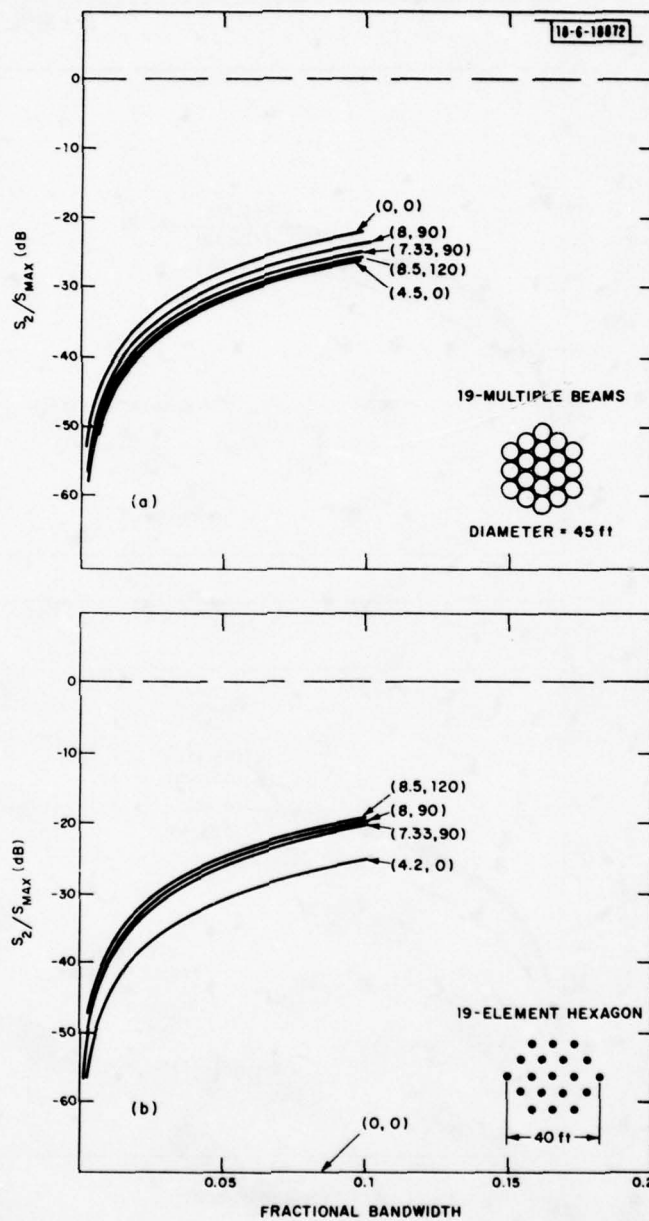


Fig. 10. Eigenvalue spread, S_2/S_{MAX} , vs fractional bandwidth for the four single interference locations of Table 3 for (a) the 19-beam MBA and (b) the 19-element hexagonal array.

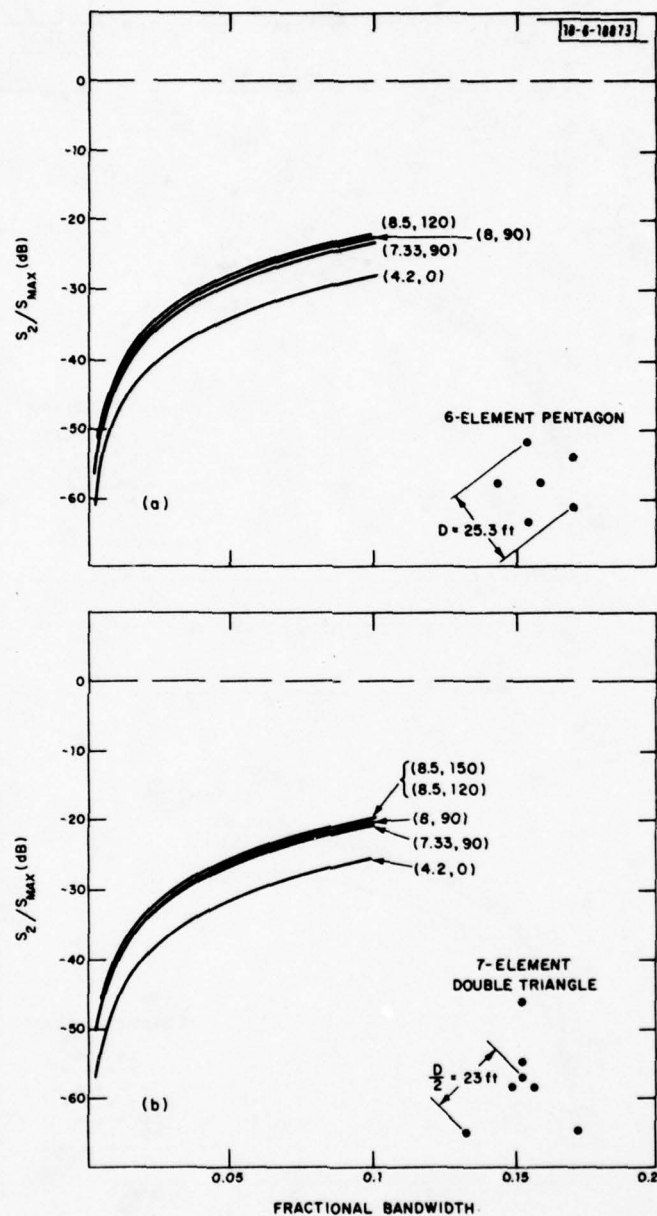


Fig. 11. Eigenvalue spread, S_2/S_{MAX} , vs fractional bandwidth for the four single interference locations of Table 3 for (a) the six-element pentagon and (b) the seven-element double triangle.

Earth Coverage Mode

Although the eigenvalue spread, s_{J+1}/s_{MAX} , vs. bandwidth offers the most general means of characterizing the frequency dependence of the antenna, it is possible under certain circumstances to improve the cancellation for certain modes of operation for which $\underline{e}_{J+1}^\dagger \cdot \underline{w}_0 = 0$. In this case, Eq. (14) predicts a cancellation on the order of s_{J+2}/s_{MAX} , which can be considerably lower. This effect can be interpreted physically by viewing the nulling process as the combinations of two radiation patterns⁽⁵⁾ -- a reference pattern, and a cancelling pattern weighted with the reference pattern so as to cancel in the desired direction. If the reference pattern is relatively frequency insensitive in the direction of cancellation, then the resultant cancellation obtained after zero-bandwidth weighting will be wideband since the scan angle of the cancelling beam varies only slightly with frequency. One particular mode of operation where this occurs is that of earth coverage, and will now be considered.

Assume, for example, an array configuration consisting of identical elements. (Note, the degree to which one can realize this identicalness of elements practically remains to be seen. However, one anticipates that for a thinned array having negligible mutual coupling between elements, one could, with enough time and effort realize this similarity in performance.) If the quiescent vector \underline{w}_0 is chosen to be $\underline{w}_0^\dagger = [1, 0, \dots, 0]$, then the requirements for wideband cancellation discussed above are satisfied. Any absolute variations in frequency for each element become unimportant, since the

radiation pattern can be factored into an element factor and an array factor. The latter affects the cancellation and is independent of absolute element variations. We note that in satisfying these requirements one sometimes trades off resolution, as it can be shown that for a symmetric array where the array center of phase occurs at the reference element, the resultant null formed in this case is necessarily quadratic in angle measured from the null, as opposed to a linear variation in angle for the narrowband cancellation. This phenomenon is illustrated in Fig. 12 where, for the same single interference source treated in Fig. 8, the cancellation C is plotted vs. bandwidth after zero-bandwidth weighting is applied to the channels. For comparison we illustrate the results for the MBA, where the earth-coverage quiescent pattern is obtained by proper weighting of all the beamports, which results in a frequency dependent reference over some regions of the FOV. (This depends on the degree of ripple in this quiescent pattern. A separate, broadband earth coverage antenna could be used in conjunction with the MBA to obtain a broadband cancellation. This possibility will be considered at the end of the section.) For all the array configurations, the results of Fig. 12 indicate a broadband cancellation, even though s_2 is significant (see Fig. 8). For these cases, one finds that $\underline{e}_2^+ \cdot \underline{w}_0 < 1$, so that the second term in (49) dominates the cancellation. For the seven beam MBA the cancellation is quite narrowband due to the frequency sensitive ripple in the earth coverage radiation pattern. For the MBA, the cancellation bandwidth is strongly dependent on the location of the interference source relative to the beam positions and the edge of the FOV, as is evident for the 19 beam case where the MBA appears

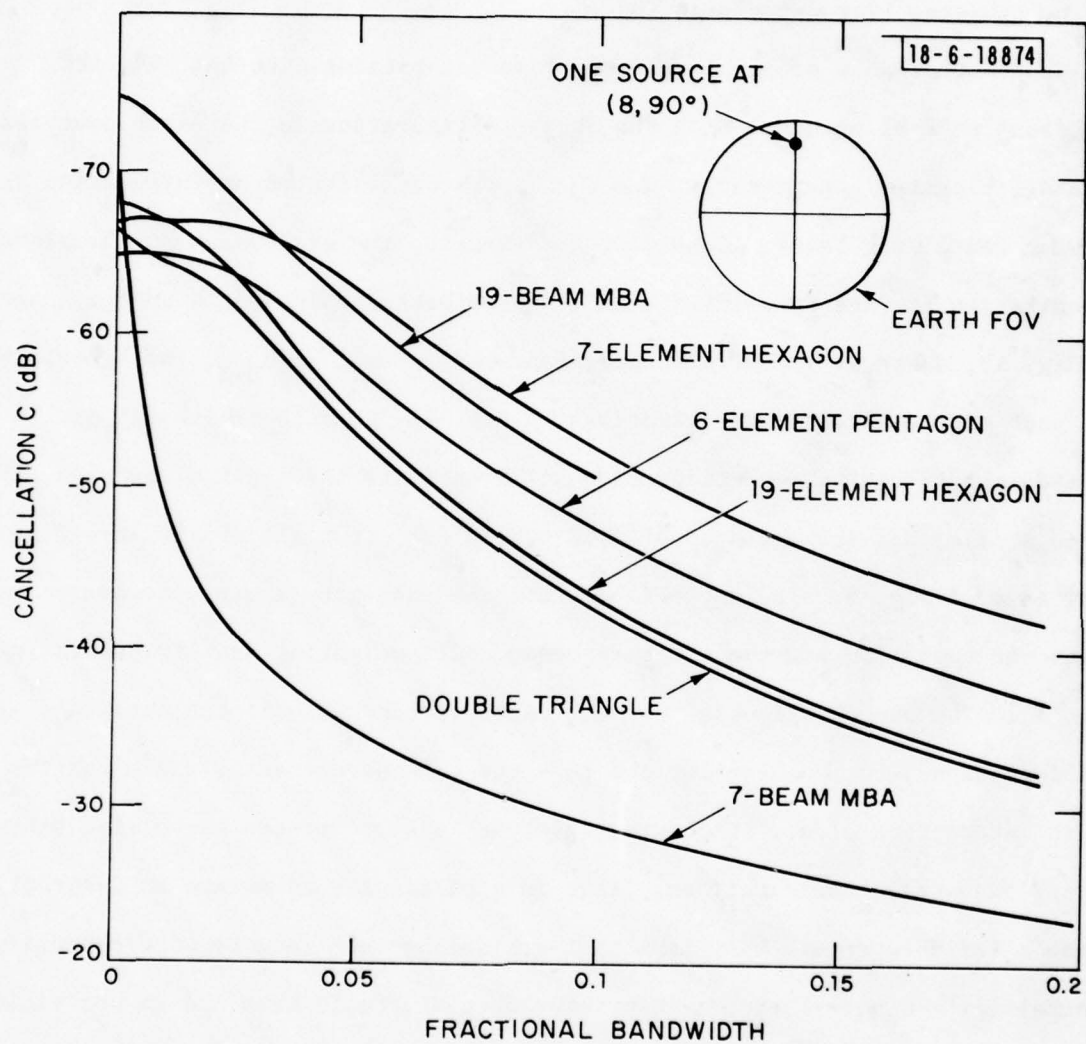


Fig. 12. Cancellation in the earth coverage mode vs fractional bandwidth for the six antenna configurations of Fig. 7 and a single interference source located at $\theta_j = 8^\circ$, $\phi = 90^\circ$.

to be quite broadband in this case. However, for other locations this would not be the case (for example at (0,0)).

For more than a single interference source present over the FOV, the broadband nulling obtained with the array configuration in the earth coverage mode deteriorates considerably, due to the frequency dependent interaction between cancelling beams. Consider, for example, the eigenvalue spectrum and cancellation for the four-interference-source scenario indicated in the insert of Fig. 13, where we illustrate the eigenvalue spread, s_5/s_{MAX} , vs. bandwidth for each of the antenna configurations in Fig. 7. Note that although the time-delayed seven beam configuration still exhibits the least dispersion, the ratio s_5/s_{MAX} has increased about 5 dB over s_2/s_{MAX} for the single interference case of Fig. 8. The cancellation obtained using an earth coverage quiescent radiation pattern after zero-bandwidth weighting is illustrated in Fig. 14. The cancellation is now much narrower-band for all the antenna configurations, but is best for the 19 element hexagonal array which has the least interaction (i.e., the lowest sidelobe levels) between cancelling beams of all the array configurations. This is a particular advantage in favor of using a filled aperture MBA, in that the sidelobe level can be more carefully controlled. We note that the lower sidelobes of the 19 beam MBA do not yield as broadband a result due to the ripple inherent in the MBA earth coverage quiescent pattern. This can be compensated for by employing a separate broadbeam earth coverage antenna having the same center of phase as the MBA (and less frequency sensitivity) as a reference. This case is illustrated in Fig. 15 using a seven and nineteen beam MBA in conjunction with a separate earth coverage antenna having a 3 dB

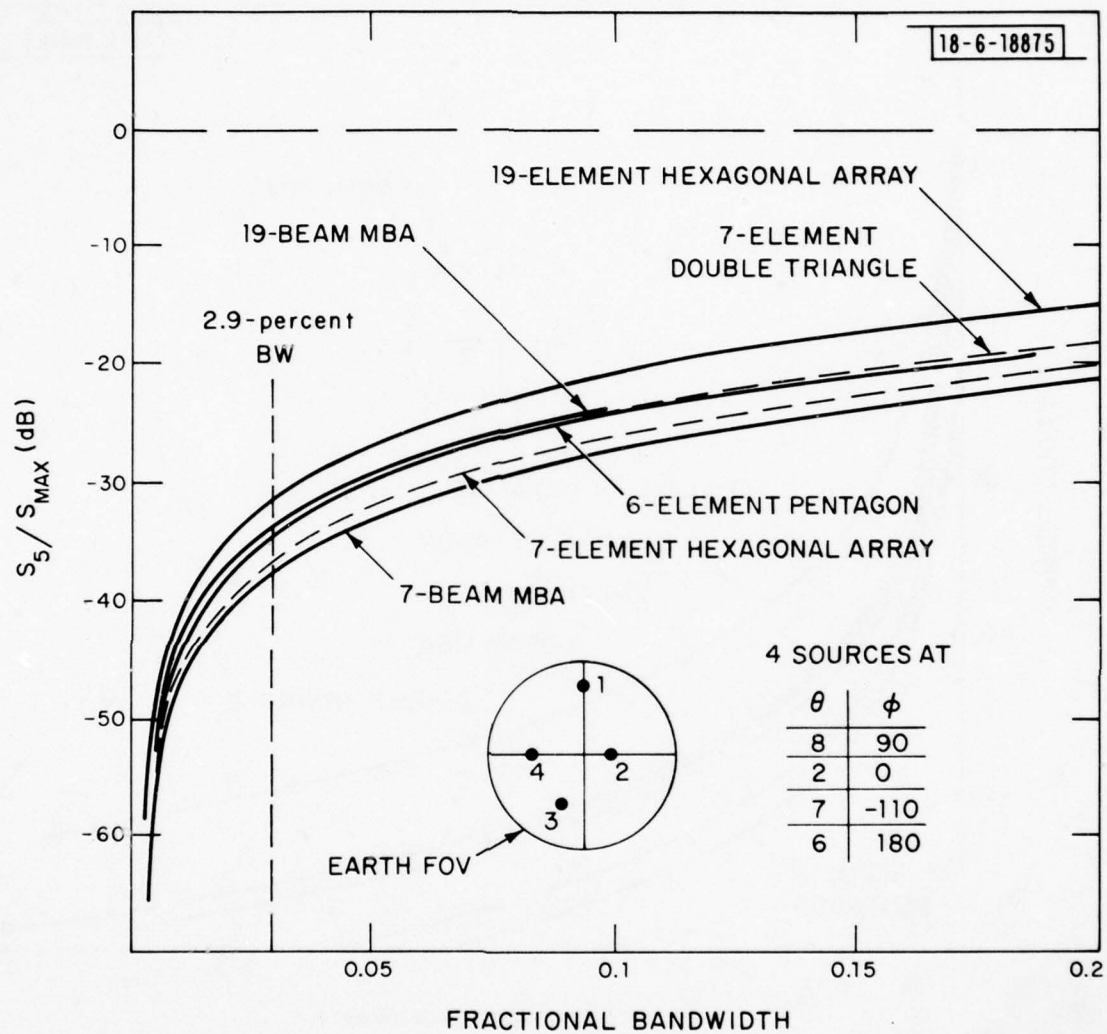


Fig. 13. Eigenvalue spread, S_5/S_{MAX} , vs fractional bandwidth for a four-interference source scenario for each antenna configuration of Fig. 7.

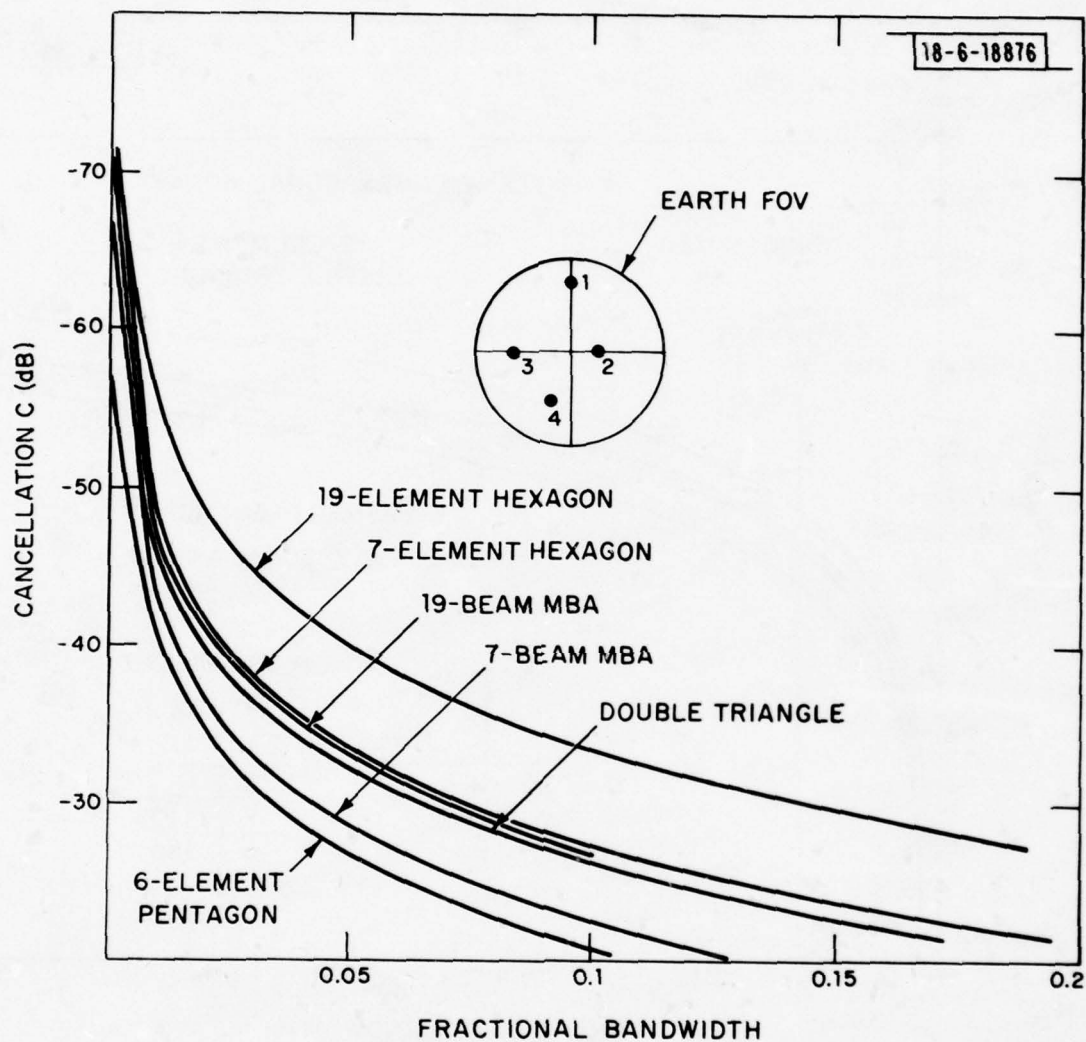


Fig. 14. Cancellation vs fractional bandwidth for an earth coverage quiescent vector for the four-interference source scenario considered in Fig. 13.

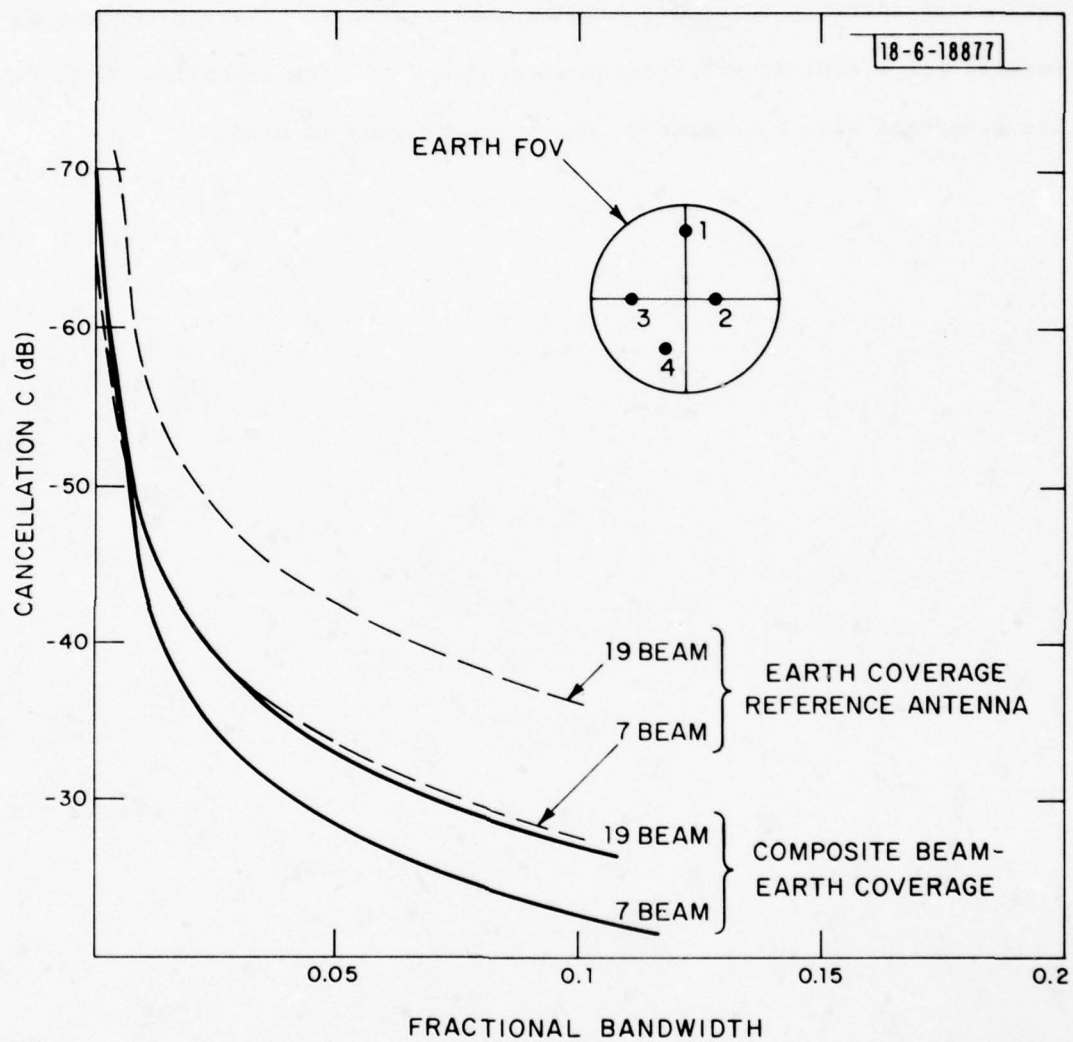


Fig. 15. Comparison of the cancellation vs fractional bandwidth for the MBA antennas when a separate broadband earth coverage antenna is used.

beamwidth of approximately 20° . The cancellation vs. fractional bandwidth (FBW) using either a composite beam or separate earth coverage antenna is compared for a four-interference-source scenario. The cancellation is clearly more broadband when the separate reference antenna is used.

V. Some Measured Results for a Seven-Beam Paraboloid

In order to tie together some of the results of the previous sections, and to assess the accuracy of the estimates of antenna frequency dispersion presented in Section IV, we now consider some measured results. A seven beam, focal-plane-fed paraboloid was designed to operate at UHF (350 MHz) and scaled to L-band (1550 MHz). The nominal 3% bandwidth of interest at UHF then scales to 45 MHz, and will be used throughout the following as the nominal bandwidth of interest. The UHF design parameters are essentially those given in Fig. (7a); i.e., $D/\lambda=10.7$. Simulations on an ideal MBA having these design parameters in conjunction with an adaptive nulling processor have been discussed in considerable detail in Ref. (4). It is the purpose of this section to obtain measured results for a real antenna structure, including the effects of reflector-feed multipath which were not modeled in these simulations, nor in the simulations on the effects of frequency dispersion in Section IV. Each beam was generated by a circularly polarized, broadband crossed dipole of the same type, designed by Lindberg, offset in the focal plane transverse to the focal axis. This dipole is a light-weight version of those designed for experimental satellites LES-8 and -9. A single port, four dipole array was mounted on the back side of the feed structure, facing the earth as viewed from an orbiting position, and was used as an 8th output port which could be used as a separate earth coverage antenna. In this way the comparison of using the composite beams for earth coverage or a separate earth coverage reference could be made (see Fig. 15). A photograph of the paraboloid-feed structure considered is illustrated in Fig. 16. In order to assess the

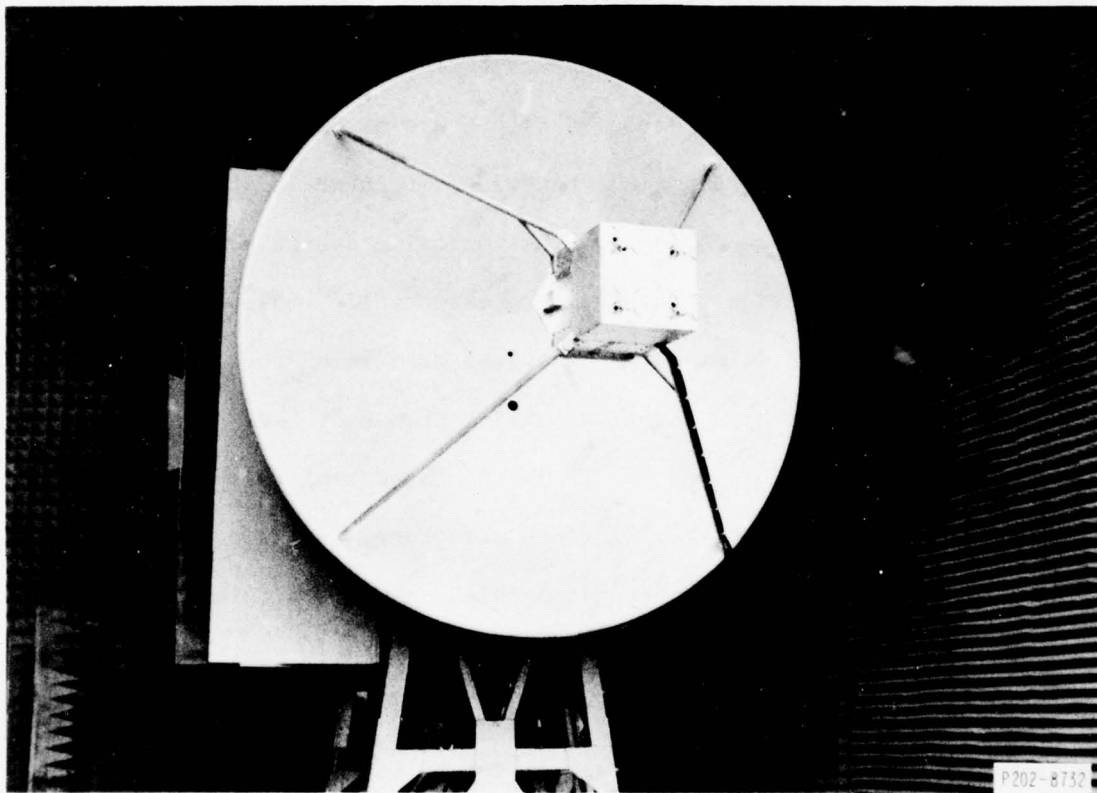


Fig. 16. Reflector-feed antenna structure at L-band ($D/\lambda=10.7$).

performance characteristics of a "clean" paraboloid, the four edge-to-feed struts were used to obtain minimum feed-support multipath. In practice, for an unfurlable paraboloid, such a minimum blockage feed support could probably not be used, and additional effects of feed-support multipath would have to be assessed. However, since this poses a formidable design problem in itself, it was felt that, for lack of an optimum support design, the minimum blockage support would be the most meaningful to evaluate in detail at this time. The effects of a more realistic support structure will be considered at the end of this section. The 3 dB contour levels of each beam relative to its maximum are illustrated in Fig. 17. The measured gain of the center beam was 25.5 dB, and the gain of the other beams varied slightly (from 0 to -0.7 dB) from this value. The measured HPBW was 5.75° (consistent with an approximate 10 dB edge illumination).

As an aid in evaluating the antenna performance characteristics, the weight-combiner network illustrated in Fig. 18 was constructed (Note: an eighth channel was added at a later date). The weight network used a series combination of a variable time delay and attenuator for each weight. The effect of using time delay phase shifters as opposed to broadband frequency independent phase shifters was evaluated and found to be negligible for the percentage bandwidths ($\sim 3\%$) and aperture sizes of interest. In order to evaluate the channel tracking errors present in the weight system, the technique alluded to in Section III was used. Recall the results of Fig. 3: if the output power from a swept frequency source is divided and fed into each of the seven weight-combiner channels (without the antenna), then the result

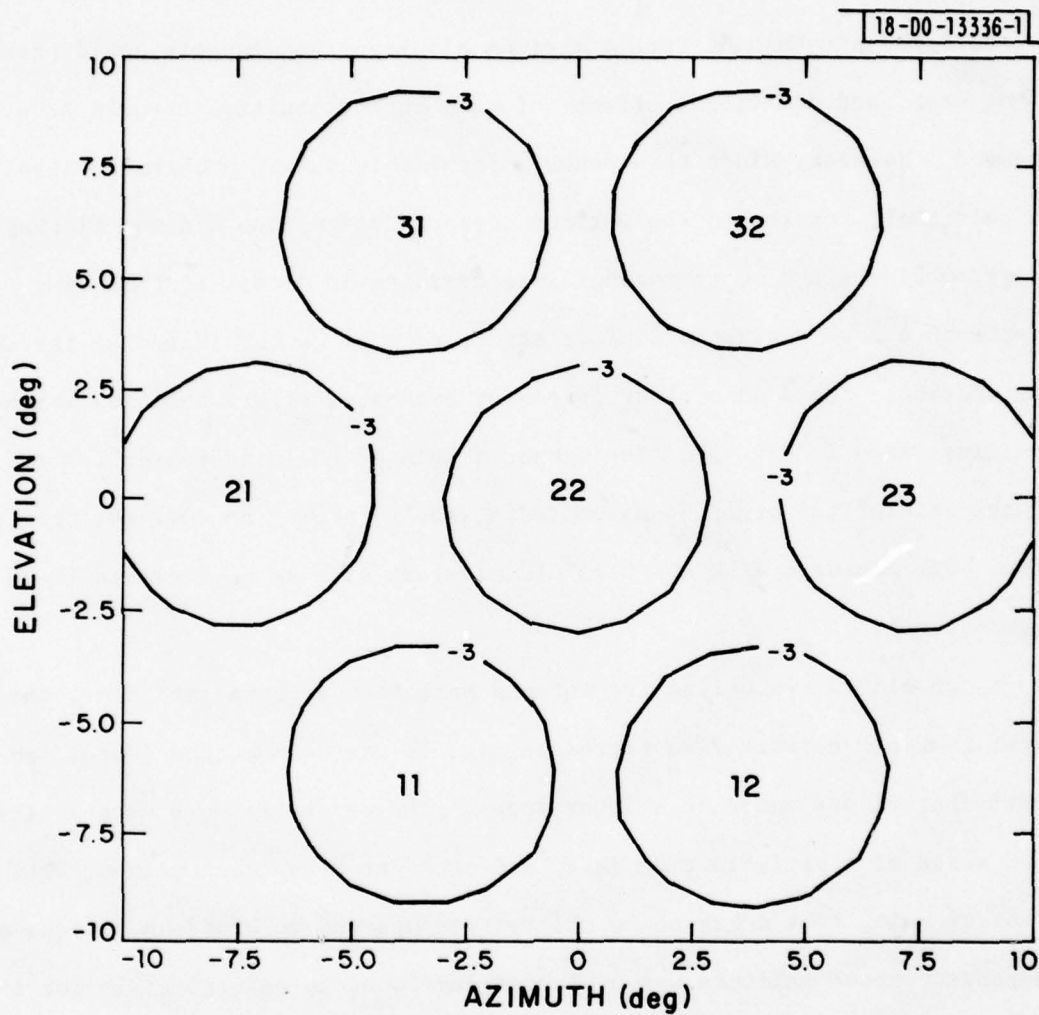
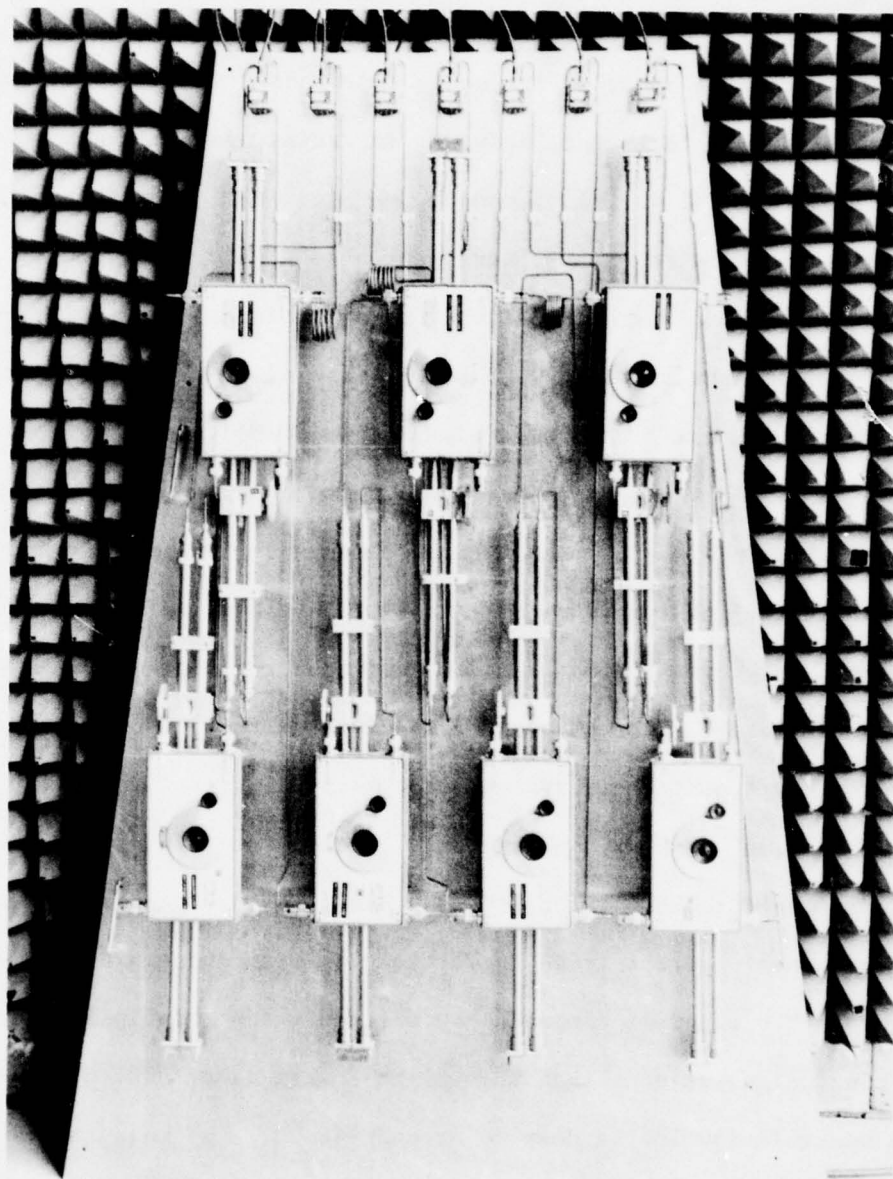


Fig. 17. Three dB contour levels of each beam relative to its peak value. Measured gain of beam 2,2 is 25.5 dB. Gain of other beams varies from 0 to -0.7 dB relative to beam 2,2.



P202-8734

Fig. 18. Weight-combiner network used in evaluating the nulling performance of the seven-beam MBA of Fig. 16.

is identical to what one would expect for a source incident broadside to a planar array. Since the array is frequency independent in this case, any dispersion resulting as the input bandwidth is varied must be due to channel tracking errors. For $J=1$ in Fig. 3, and $M_{11}=M_{22}=\dots=M_{NN}$, then the spread of the second eigenvalue, s_2/s_{MAX} , is bounded by $s_2/s_{MAX} \leq \sigma_{MAX}^2/N$, where σ_{MAX}^2 is the worst case channel matching error. By measuring s_1 and s_2 vs. bandwidth, σ_{MAX}^2 can then be obtained. If the statistics of the channel tracking errors were equal, then all the lower eigenvalues would appear σ^2/N below s_{MAX} as in Fig. 4. If a single channel dominates the error, it would stand out as illustrated in Fig. 5. The measured eigenvalue spread vs. fractional bandwidth for the weight system of Fig. 18 is illustrated in Fig. 19 (the result is shown for seven of the eight channels, as the eighth channel was added at a later date). Note that $\sigma_{MAX}^2/N \approx -47$ dB so that, for $N=7$, $\sigma_{MAX}^2 \approx -38.5$ dB. Furthermore, the eigenvalues tend to be clustered into two groups of three eigenvalues, so that some channels track worse than others. However, even the worst case tracking error is good enough for our purposes. As expected, the tracking error tends to flatten out with increasing bandwidth, indicating that the error is dominated by a fixed amount of ripple over the band. In conclusion, we note that the weight system is of sufficient accuracy to measure cancellation levels down to around -40 dB. Any measured cancellation levels above this level can then be attributed to the antenna structure itself or its measurement environment.

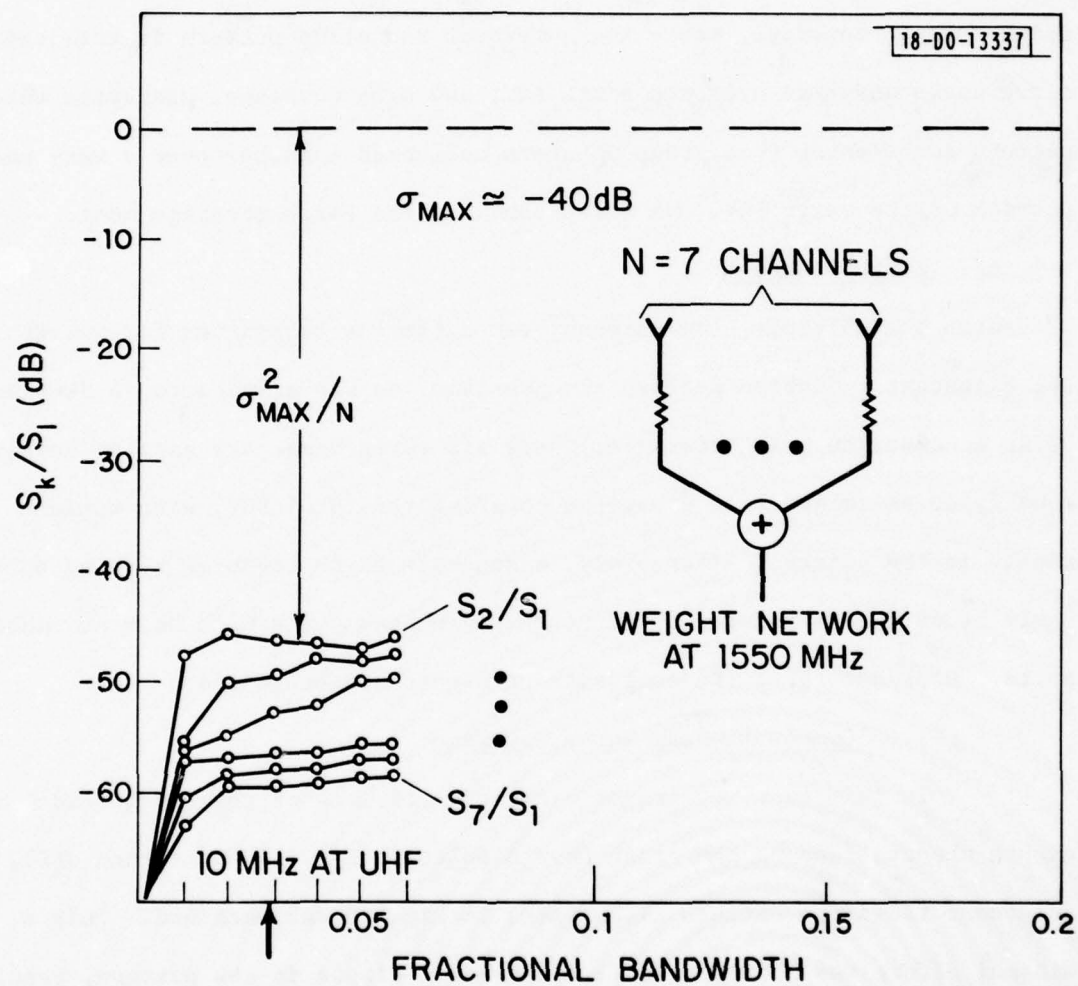


Fig. 19. Measured eigenvalue spread as a function of bandwidth for the seven weight channels of Fig. 18.

Analogous to the results of Section IV, it is convenient to present the measured results relative to the two modes of operation which one might consider: Earth coverage, where the quiescent radiation pattern is tailored to serve users anywhere over the earth FOV; and Area Coverage, where the quiescent pattern corresponds to a group of users collected together over a very small portion of the earth FOV. We first consider the earth coverage mode.

A. Earth Coverage

With the multiple beam antenna, two different techniques for generating the quiescent radiation pattern are possible, as was alluded to in Section IV: Using a composite beam reference, where all seven beams are excited nearly equally so as to generate a pattern covering the total FOV, with minimum ripple in the pattern; alternately, a separate earth coverage receive antenna could be used as a reference, with the seven beam ports used only as cancelling ports. Consider first the composite beam earth coverage mode.

1. Composite Beam Earth Coverage

In this case, by proper excitation of each of the seven feeds, (the eighth channel feeding the front four dipoles in Fig. 16 was turned off), the quiescent radiation pattern illustrated in Fig. 20 was obtained. Only a minimal effort was made to reduce the overall ripple in the pattern, resulting in a 4 dB deviation occurring at the center and at the edge of the FOV. The gain at the pattern maximum is 15.5 dB. For convenience in measurement, the pattern coordinates in Fig. 20 are now designated in terms of azimuth (AZ) and elevation (EL), or simply (AZ,EL).

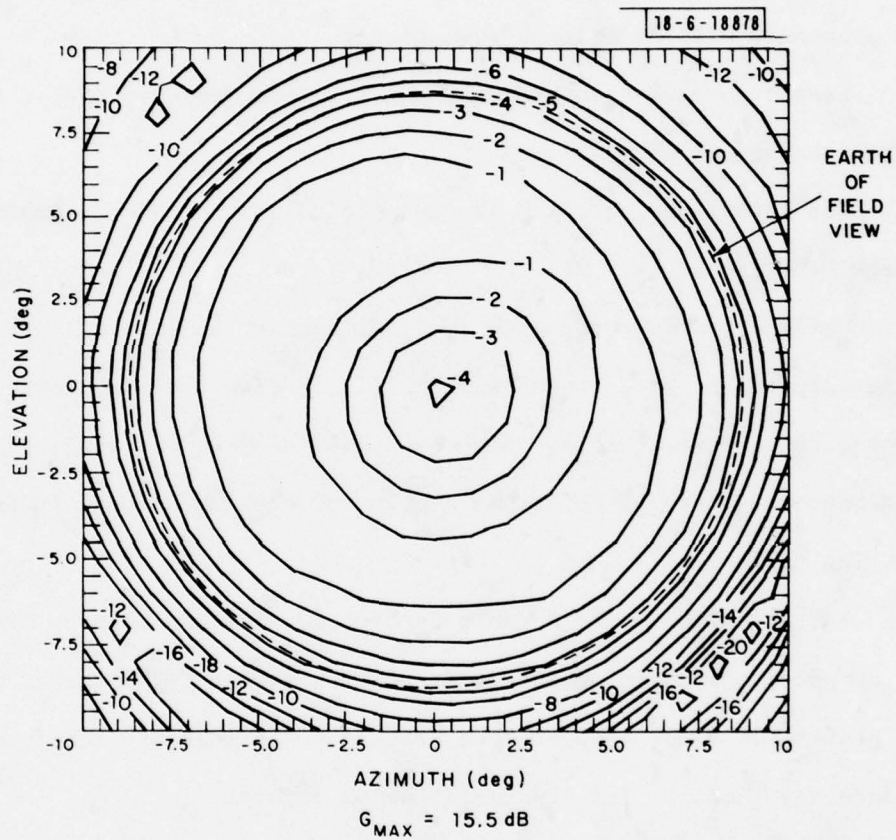


Fig. 20. Quiescent earth coverage radiation pattern obtained using a composite excitation of the seven MBA beam ports.

Consider the formation of a null at, for example, $AZ=4^\circ$, $EL=2^\circ$. For this case, and all of the following data, the techniques developed in Section I and II were used to evaluate the antenna performance. For convenience, the measurement procedure will be briefly summarized:

- a) Each channel response $E_k(\omega)$, $k=1, \dots, N$ is measured over a specified spread bandwidth BW_s .
- b) The covariance matrix \underline{M} is computed as a function of bandwidth BW , where $BW \leq BW_s$.
- c) Using \underline{M}_0 corresponding to $BW=0$, we compute and manually set the weights producing a zero-bandwidth null, as discussed in Section II. This assures that at most, only one degree of freedom is allocated per interference source. We assume a gain threshold of -40 dB (μ in Eq. (6) $= 10^{-4}$).
- d) The cancellation as a function of bandwidth can then be measured, or computed using the measured correlation matrix. The latter method is preferable since an open-loop setting of the weights has inherent inaccuracy problems for low cancellation levels.
- e) Finally, using the measured \underline{M} as a function of BW , the eigenvalues of \underline{M} can be computed vs. BW , leading to an antenna evaluation consistent with that of Section IV.

The zero-bandwidth radiation pattern obtained using the above procedure (the weights are set open-loop to an accuracy of 0.1 dB amplitude, 0.5° phase) having a null at $(4,2)$ is illustrated in Fig. 21. The results are very

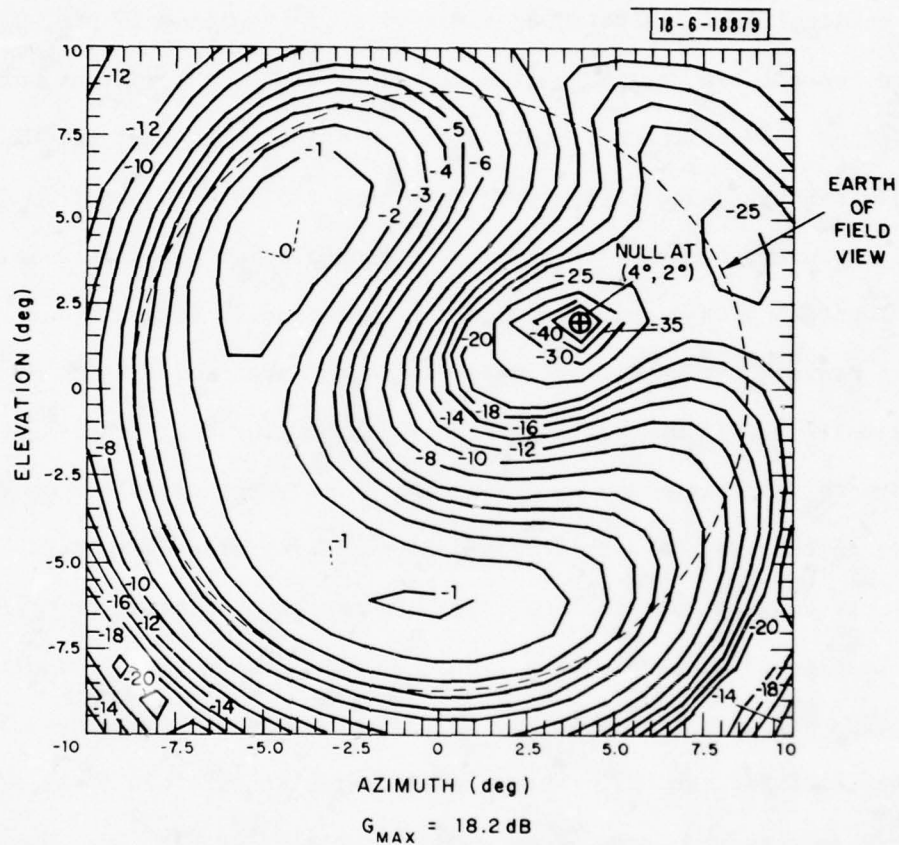


Fig. 21. Measured composite beam earth coverage pattern with zero-bandwidth null formed at $(4, 2)$.

similar to those obtained from a simulation of the seven-beam MBA using ideal beams. Maximum gain has increased to 18.2 dB. The measured cancellation (interference output power after nulling/interference output power before nulling) is illustrated as a function of frequency in Fig. 22. Note the good cancellation at the center frequency (1550 MHz) and the narrow bandwidth of the resulting cancellation. Using the measured cancellation curve, an average cancellation over a 3% band (45 MHz) is about 30 dB. (Recall, however, from Eq. (15) that the cancellation obtainable is a strong function of the quiescent mode of operation.) However, due to the time-lag between the setting of the weights and the cancellation measurement (approximately 10-15 minutes), and the fact that the weights are set open-loop, a more reliable means of evaluating the average cancellation for ultimate use of the antenna with a closed-loop nulling processor would be to compute the average cancellation using the measured correlation matrix. This yields results consistent with a closed loop weight setting. Results of this computation are illustrated in Fig. 23, where we plot the average cancellation in dB vs. bandwidth in MHz. Note that a cancellation of 30 dB at a bandwidth of 45 MHz is obtained, consistent with the results of Fig. 22. However, the better cancellation as $BW \rightarrow 0$ shown in Fig. 23, relative to Fig. 22, indicates the error in the open-loop measurement of cancellation. Finally, in Fig. 24, we illustrate the eigenspectrum of the measured correlation matrix as a function of bandwidth for the interference at (4,2). The dominant eigenvalue dispersion, s_2/s_1 , is -34 dB at 45 MHz. Consequently s_2 would be sensed and minimized by a processor having a 40 dB dynamic range and operating over a 3% bandwidth.

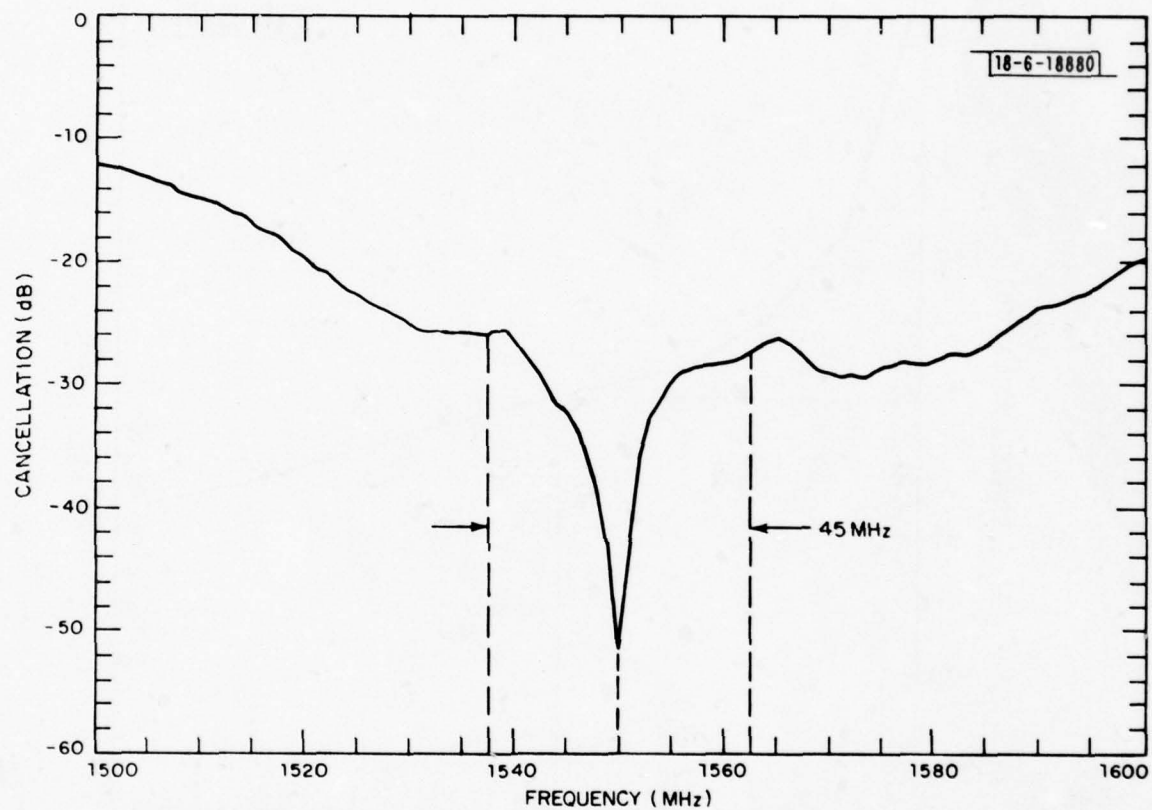


Fig. 22. Cancellation as a function of frequency for the null formed at (4,2) in Fig. 21.

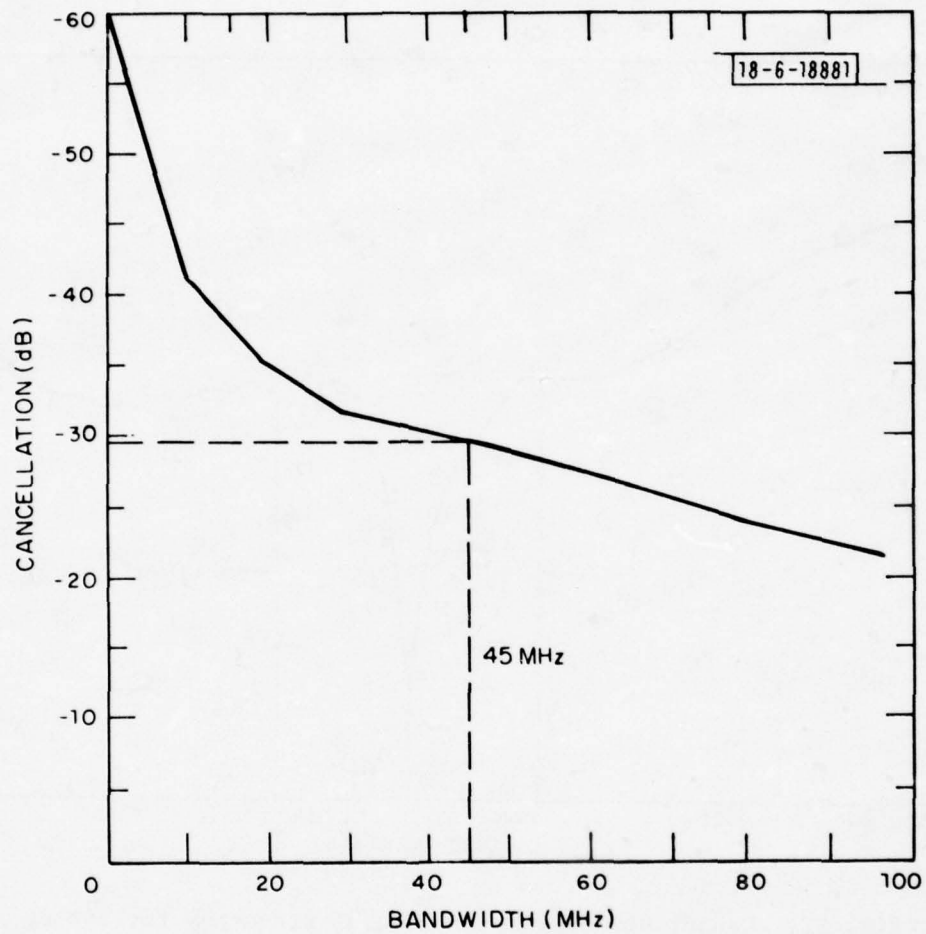


Fig. 23. Average cancellation as a function of bandwidth about 1550 MHz for the (4,2) null of Fig. 21.

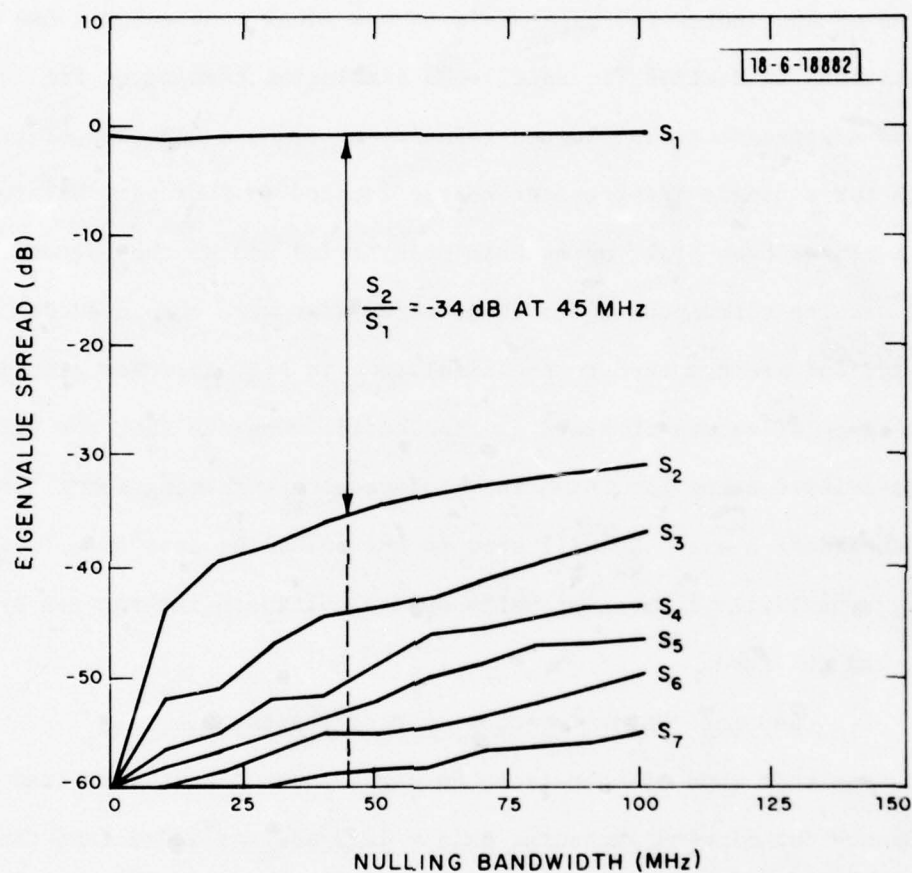


Fig. 24. Eigenspectrum of the measured correlation matrix as a function of bandwidth for the (4,2) null case of Fig. 21.

Before proceeding to the nulling performance obtained using a separate earth coverage reference antenna, it is interesting to compare the dispersion properties of the center-fed paraboloid to the ideal time-delayed MBA used in the simulations in Section V. Recall the simulation results of Fig. 9a, where the second eigenvalue s_2 is plotted relative to s_1 as a function of fractional bandwidth for a single interference source located in four particular locations: a center beam peak, outer beam peak, triad and at the edge of the FOV. Measured results corresponding to these same cases were obtained for the paraboloid, and are compared to the simulation in Fig. 25. For simplicity, only the range of values obtained is indicated. Observe that the paraboloid with time-delayed beams has increased dispersion averaging about 5 dB relative to the ideal beams. We will show in the following that this increased frequency sensitivity is most probably due to multipath interaction between the dish and the feed.

2. Separate Earth Coverage Reference Antenna

For this mode of operation, an eighth output port connected to the set of front-four dipoles (measured gain = 12.5 dB) was added (and time delay matched to the other channels) and used to obtain the quiescent radiation pattern. The beam steering vector \underline{w}_0 was then given by $\underline{w}_0 = \text{col}[0, \dots, 0, 1]$, where $\text{col}[\dots]$ denotes a column vector. Consider then forming a null at (4,2) for comparison with the composite-beams earth coverage mode treated above. Using the procedure outlined above, the resultant zero-bandwidth weights were set in and the measured contour pattern with null is illustrated

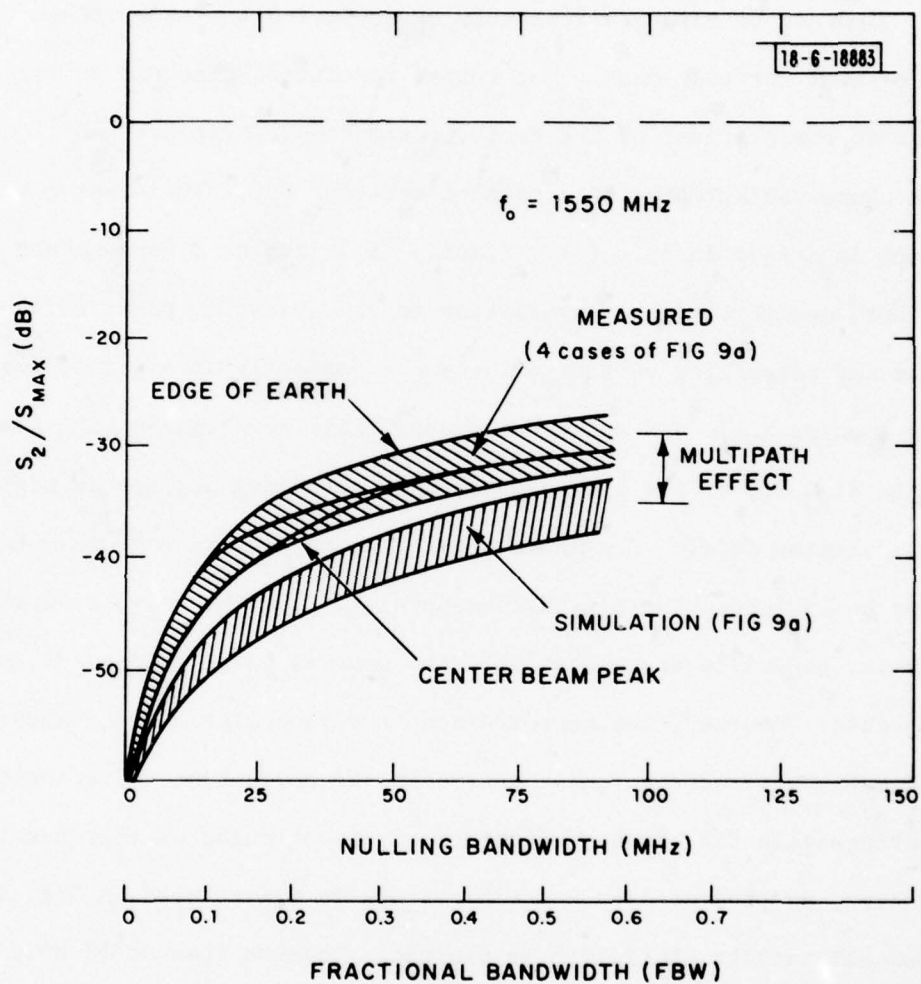


Fig. 25. Measured results for (S_2/S_{MAX}) vs bandwidth for the four single interference source locations used in the simulation of Fig. 9a.

in Fig. 26. Note in particular the better resolution obtained in this mode of operation compared to the seven-beam composite quiescent mode (compare Fig. 21 and 26; this can be seen qualitatively by comparing the area within the 20 dB contour level for each case). The better resolution obtained in Fig. 26 is due in part to the flatness of the earth coverage quiescent pattern⁽⁶⁾ and in part to the phase variation of this pattern over the FOV. This latter effect is examined in detail in Ref. (3). Briefly it arises as a consequence of the fact that, due to this phase variation in the quiescent pattern, the quiescent pattern and cancelling pattern only cancel perfectly at a single point, resulting in a point null, and not a "ring type" null as obtained with the seven beams in Fig. 21, or for a zero-phase type reference pattern as might be used in a simulation model. The maximum gain in the pattern with null has increased to 13.1 dB. The eigenvalues obtained from the measured correlation matrix vs. bandwidth are essentially the same as those of Fig. 24, as might be expected. However, the measured/computed cancellation vs. bandwidth is considerably more narrow-band compared to the seven-beam quiescent mode case, indicating again the strong dependence of cancellation on the quiescent steering vector, as predicted by Eq. (15). This is illustrated in Fig. 27 where the cancellation vs. bandwidth is plotted. Observe that at 45 MHz, only 25 dB cancellation is obtained. This narrowband behavior can be explained physically by examining the amplitude frequency response across the band for the earth coverage reference output port, as illustrated in Fig. 28. The sinusoidal behavior of the frequency response correlates well with multipath distances determined from the round trip distance between the dish and front four dipoles

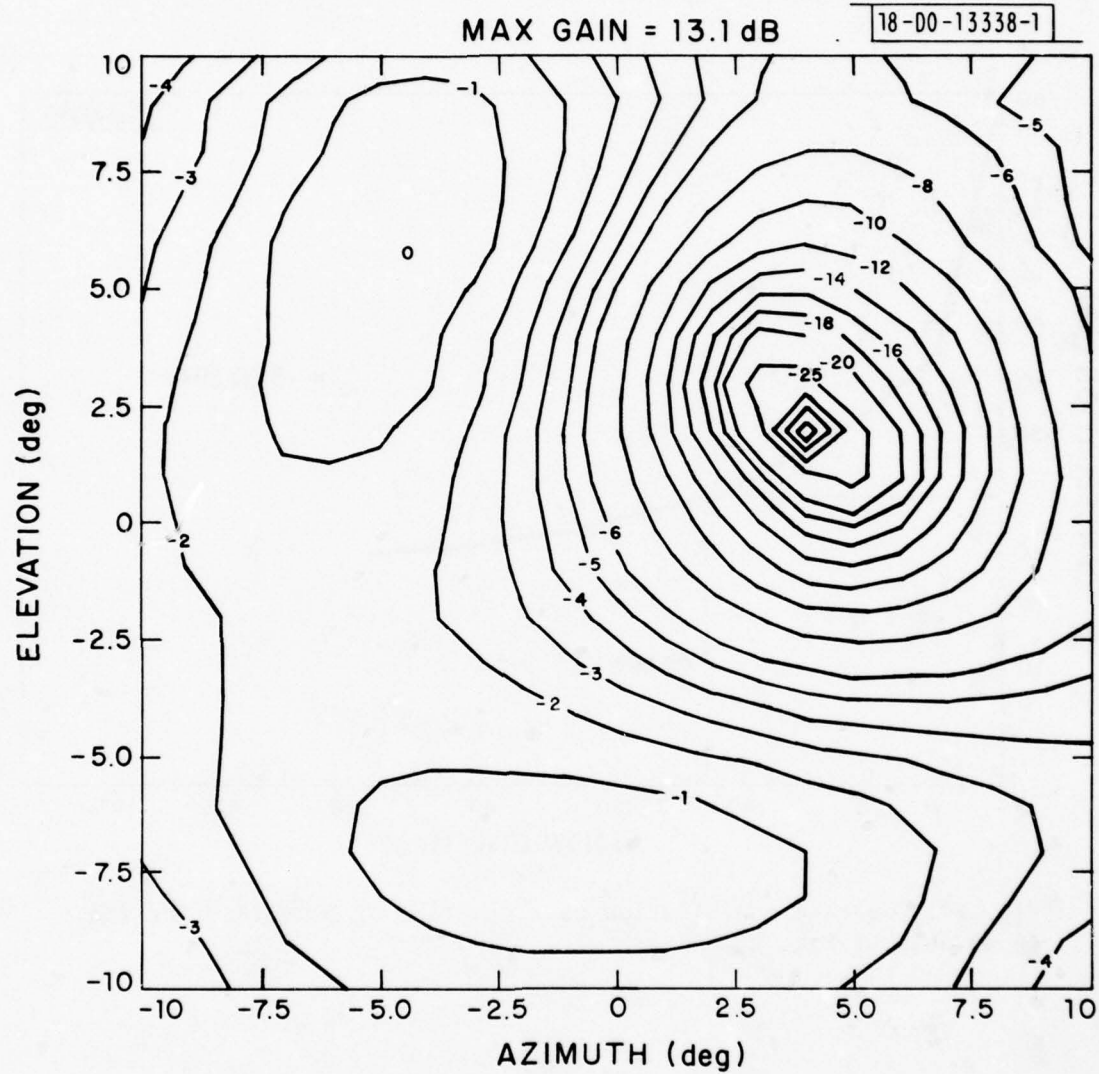


Fig. 26. Measured contour pattern with zero-bandwidth null at (4,2) using a separate earth coverage reference antenna.

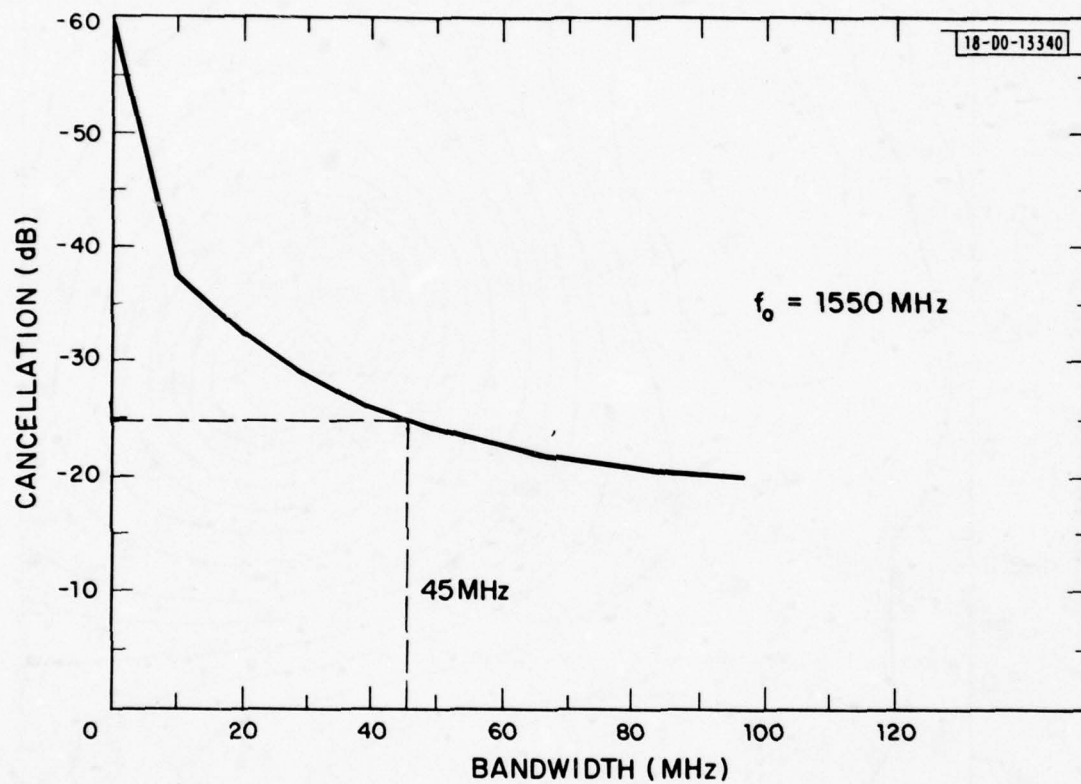


Fig. 27. Average cancellation as a function of bandwidth for the (4,2) null of Fig. 26.

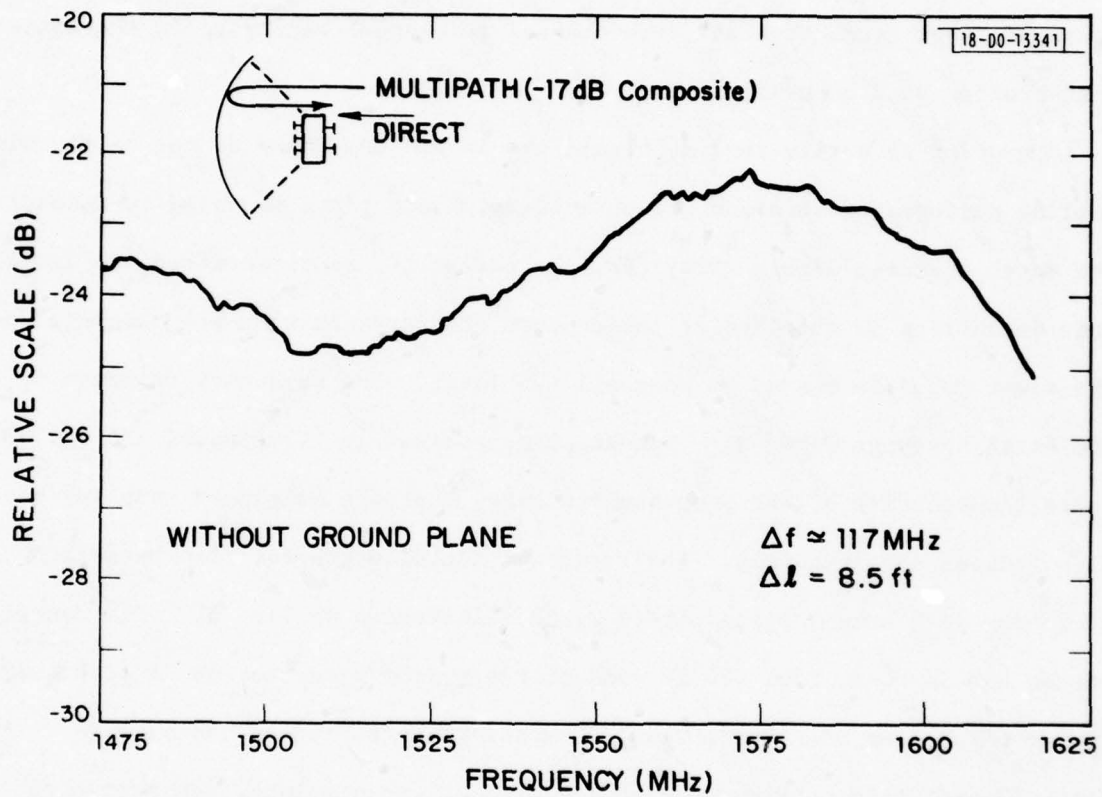


Fig. 28. Amplitude frequency response of the separate earth coverage antenna for the (4,2) null case.

as indicated in the figure. The magnitude of this multipath can be estimated from the ripple to be about -17 dB down from the incident wavefront. Of course, multipath between each of the seven MBA feeds is also present (and was measured), but tends to track from channel to channel resulting in the somewhat broader-band behavior of Fig. 23.

In order to verify that multipath was indeed the cause of the narrow band nulling performance observed above, a large ground plane was used to decouple the earth coverage dipole array from the reflector, as illustrated in Fig. 29. This decoupling is obtained at the expense of increased aperture blockage for the seven multiple beams, as we shall see later. The frequency response of the earth coverage array with ground plane present is illustrated in Fig. 30, where the flatness of the response indicates that the multipath coupling has been reduced significantly. The resultant cancellation for zero-bandwidth weighting with a null placed at (4,2) is illustrated in Fig. 31. The cancellation has improved from -25 dB without the ground plane to -36 dB with the ground plane over the 45 MHz band. Comparing the radiation contours in Figs. 32 and 26 for the cases with and without ground-plane, respectively, yields essentially the same nulling resolution. Thus the nulling resolution has remained essentially unchanged. This occurs because the multipath, to a first order, is not angle-of-arrival dependent, so that forming a more broad-band null in this case would not necessarily lead to poorer resolution. Finally, to illustrate the effects of the aperture blockage caused by the ground plane, the eigenvalue s_2 for the cases with and without ground plane

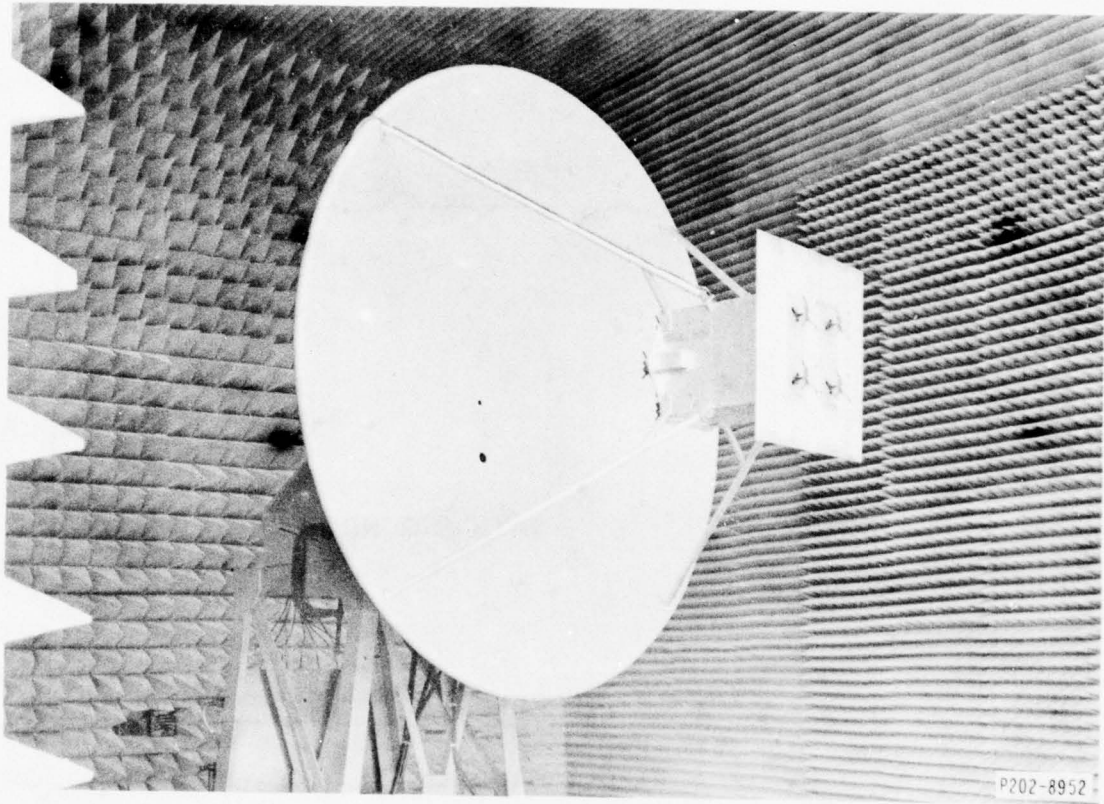


Fig. 29. Feed/reflector structure with ground plane used to isolate the earth coverage reference from the reflector.

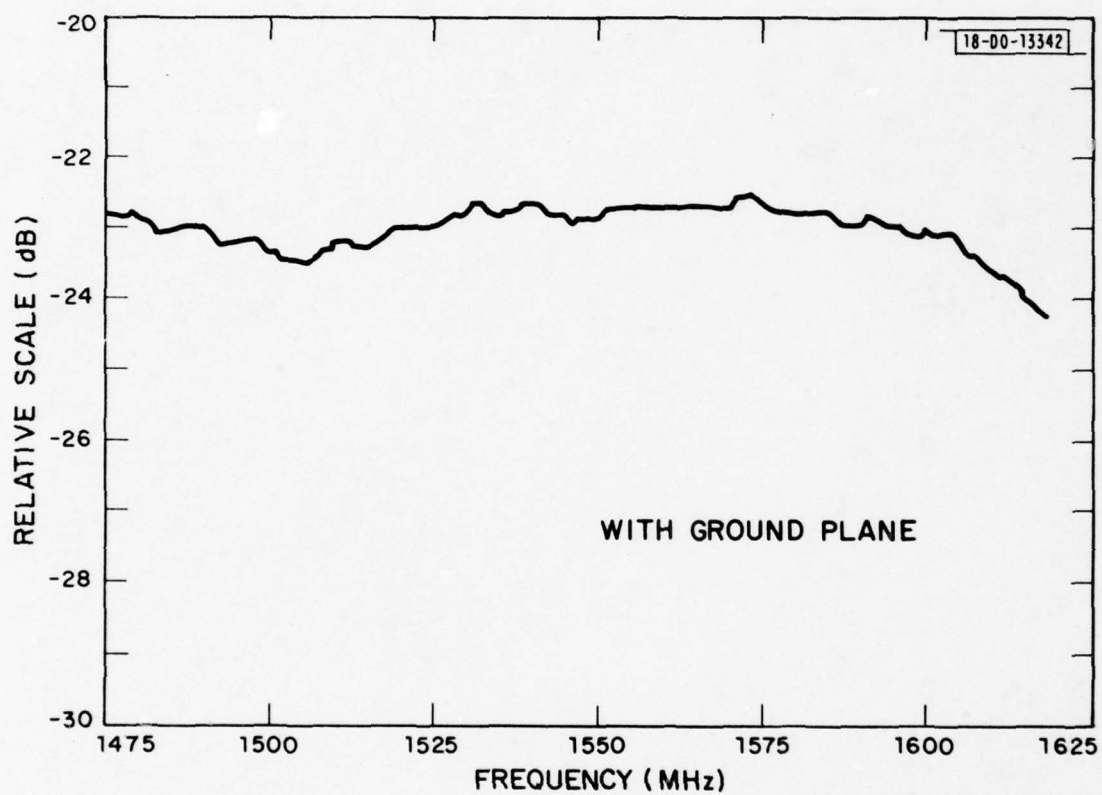


Fig. 30. Amplitude frequency response of the earth coverage reference channel with ground plane present.

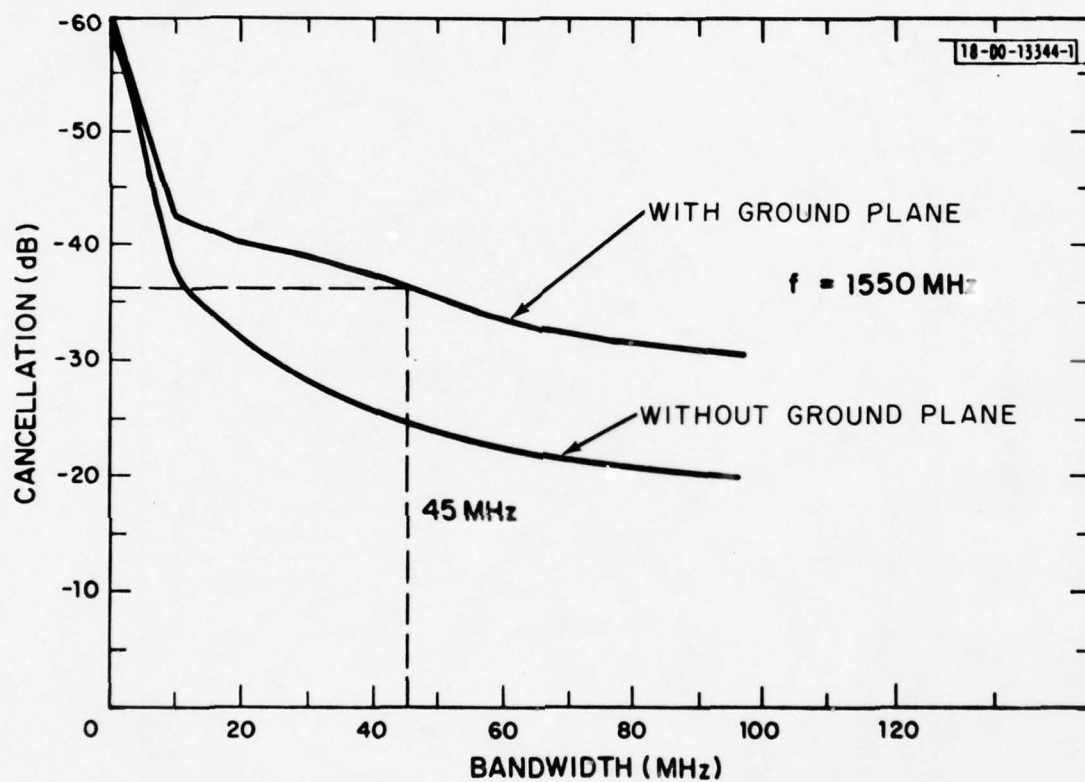


Fig. 31. Average cancellation as a function of bandwidth using the earth coverage reference antenna with and without the ground plane.

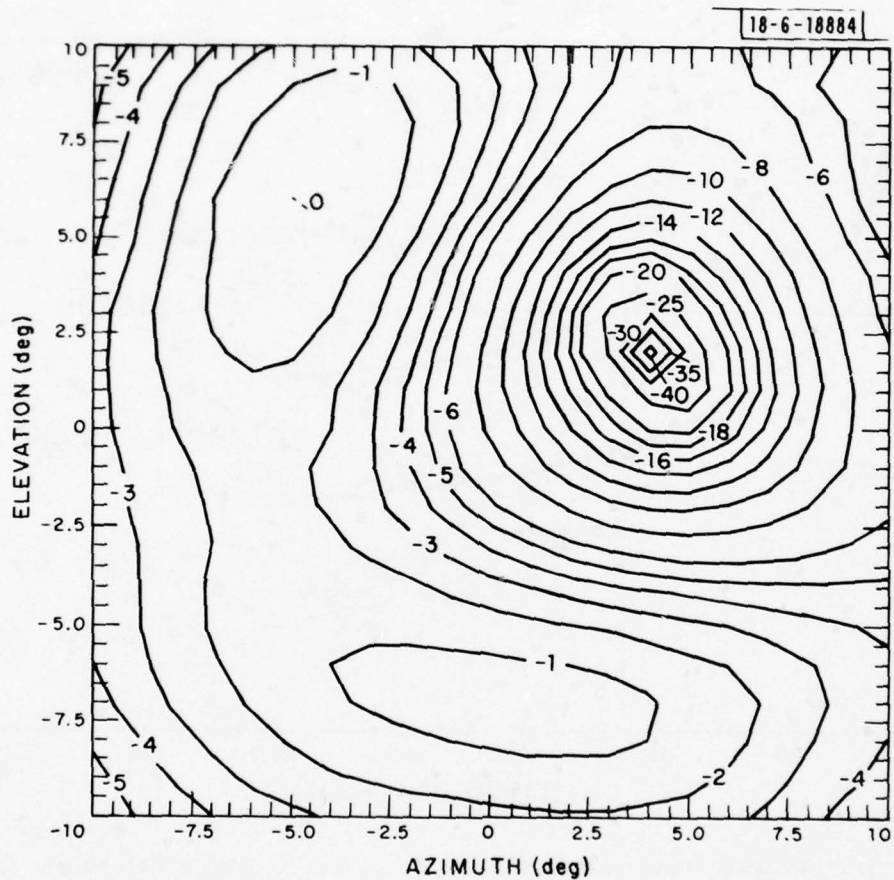


Fig. 32. Measured radiation contour with null at (4,2) using the earth coverage reference with ground plane.

is plotted in Fig. 33 relative to s_1 . Observe the increased dispersion caused by the ground plane is about 5 dB, indicating a generally poorer performance could be expected when operating with the ground plane for other quiescent weight vectors. Also indicated in Fig. 33 are the results obtained from a simulation using ideal time-delayed beams, indicating the poorer performance caused by the multipath effect. The eigenvalue spread due to the weight network above is also included for comparison to show that the measured dispersion is indeed resulting from the antenna structure.

Finally, for completeness, consider a four-null scenario, with and without the eighth port and with the ground plane removed. Simulations indicate that a "worst case" situation which could occur would be to place three sources at the triads between three beams, 120° apart in azimuth and a fourth source at the center beam peak. For ideal beams (either 0 or 180° phase) and a seven-beam composite earth coverage pattern (0 phase), this interference scenario will in fact defeat the system as the last three eigenvectors become orthogonal to \underline{w}_0 in this case. However, for the realistic case, due to the complicated phase present on each of the beam patterns, the scenario is handled reasonably well. The resultant radiation pattern, with nulls, for the seven-beam composite earth coverage quiescent pattern is illustrated in Fig. 34. Observe that a large connected null has been formed similar in shape to radial arms located 120 degrees apart, and connecting all the interference locations. Peak gain has increased significantly to 23.2 dB. The eigenvalue spread corresponding to this case is illustrated in Fig. 35. At 45 MHz, s_5/s_1 is

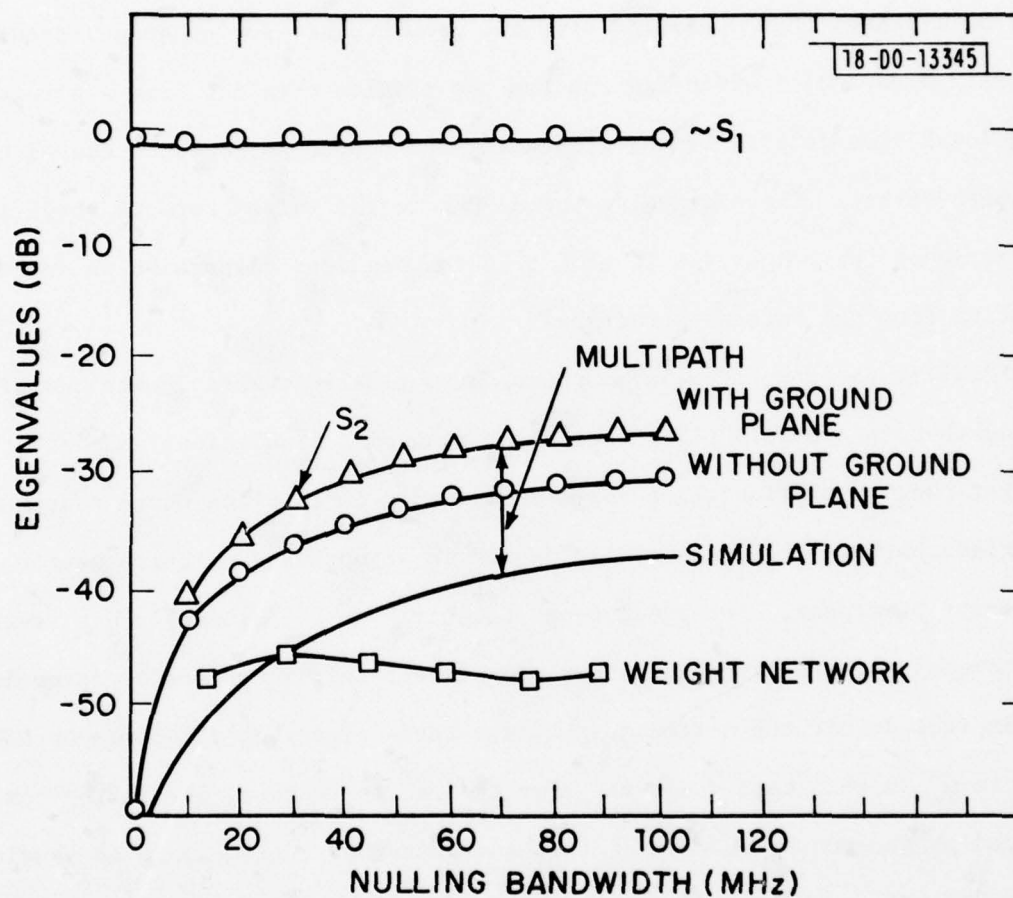


Fig. 33. Measured eigenvalue spread S_2/S_1 vs bandwidth with and without the ground plane for the (4,2) null case.

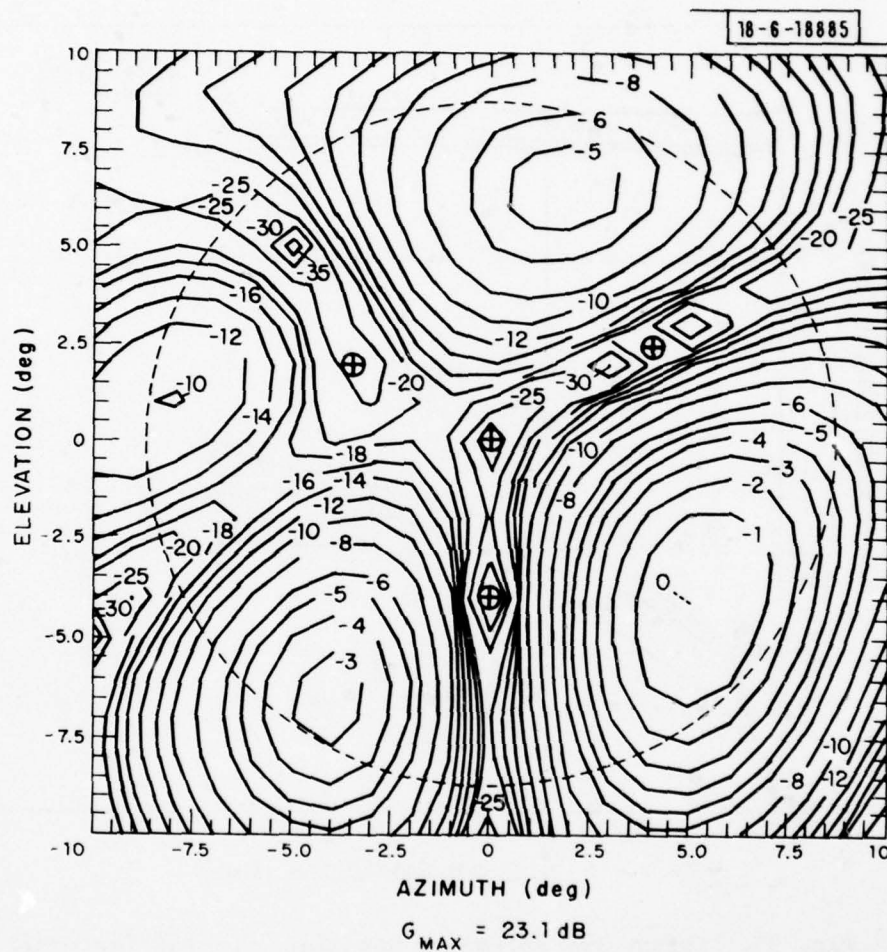


Fig. 34. Measured radiation contour with nulls produced at three 120° separated triad positions and the center beam peak. Seven-beam composite earth coverage quiescent pattern.

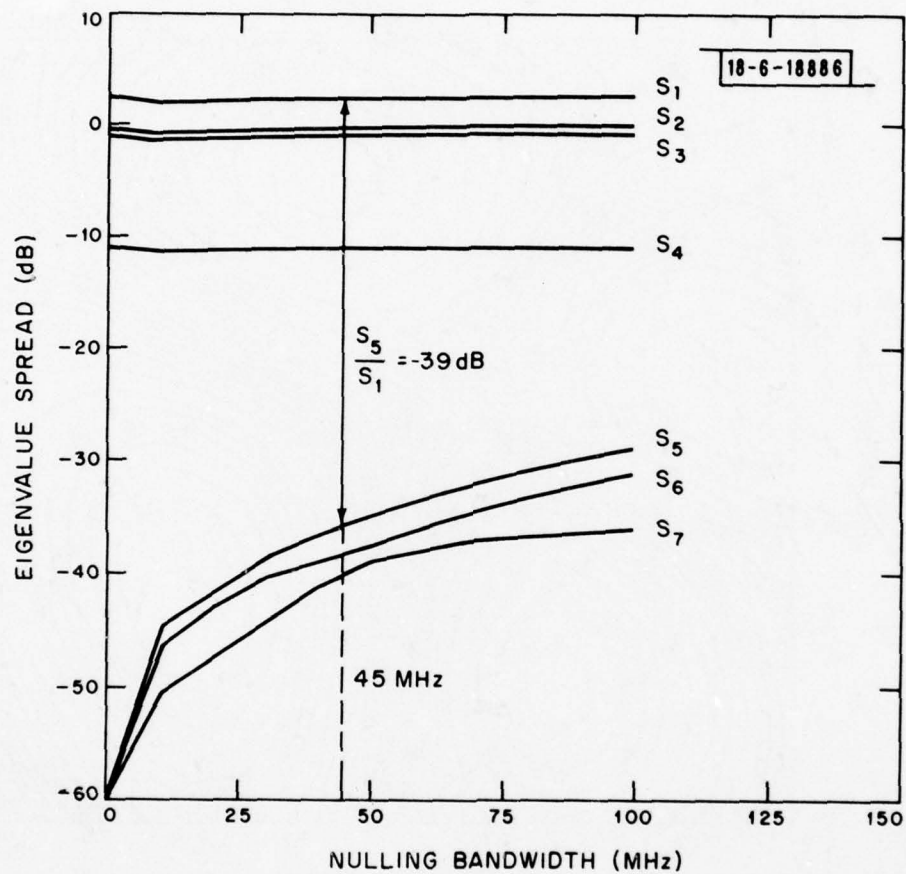


Fig. 35. Eigenvalue spread vs bandwidth for the four-null scenario of Fig. 34.

down some 39 dB, indicating a broadband null is achievable. Fig. 36 illustrates the cancellation obtained for this case, and also for the other modes of operation using the four-dipole array as an eighth port with and without the ground plane present. For these cases, the presence of the ground plane has negligible effect, and greatest cancellation is obtained with the seven-beam composite reference pattern. However, the coverage area available to the desired sources is considerably different for each case. Figure 37 illustrates the radiation pattern with nulls when the eighth port is used as reference. Note that in this case, the seven beams have formed a composite cancelling beam which combines with the reference pattern to form a broad null encompassing the entire center of the FOV. Clearly, Fig. 34 results in better resolution for desired sources in close proximity to the interferences.

B. Area Coverage

We consider now the case when maximum gain in the quiescent mode is dedicated to a particular user, or collective group of users. Consider then, for example, a quiescent radiation pattern having maximum gain allocated to a group of users at the center of the FOV, as illustrated in Fig. 38. Now assume a single interference source located 2° away from the beam maximum, having AZ,EL coordinates (2,0). Of particular interest then, is the effect on user-interference proximity of setting a weight over a non-zero bandwidth, similar to the results developed in Table 2 for the double-triangle geometry. To this end, we consider two possible weight setting bandwidths: narrowband (8 MHz, or 0.52%) and wideband (44 MHz or 2.8%), analogous to the simulations in Section IV. For these cases, the weights were computed using the measured

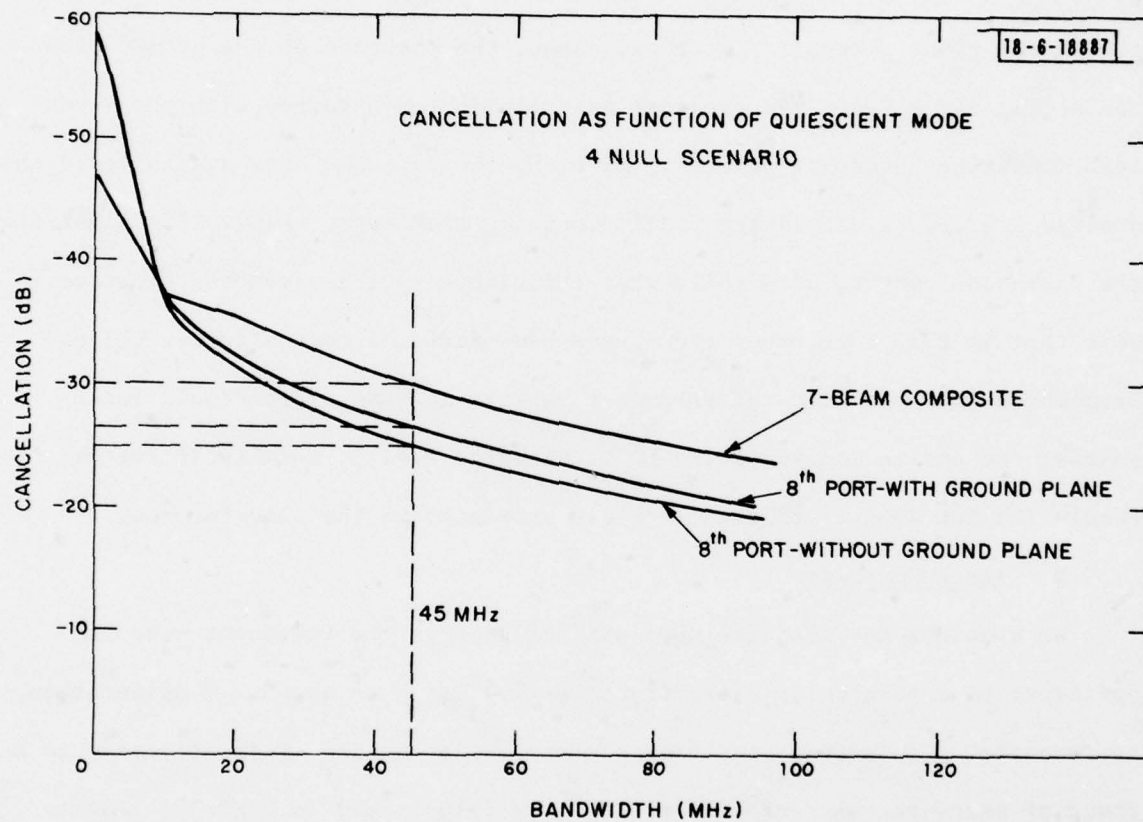


Fig. 36. Average cancellation as a function of bandwidth for the four-null scenario of Fig. 34, as a function of technique of realizing the earth coverage reference.

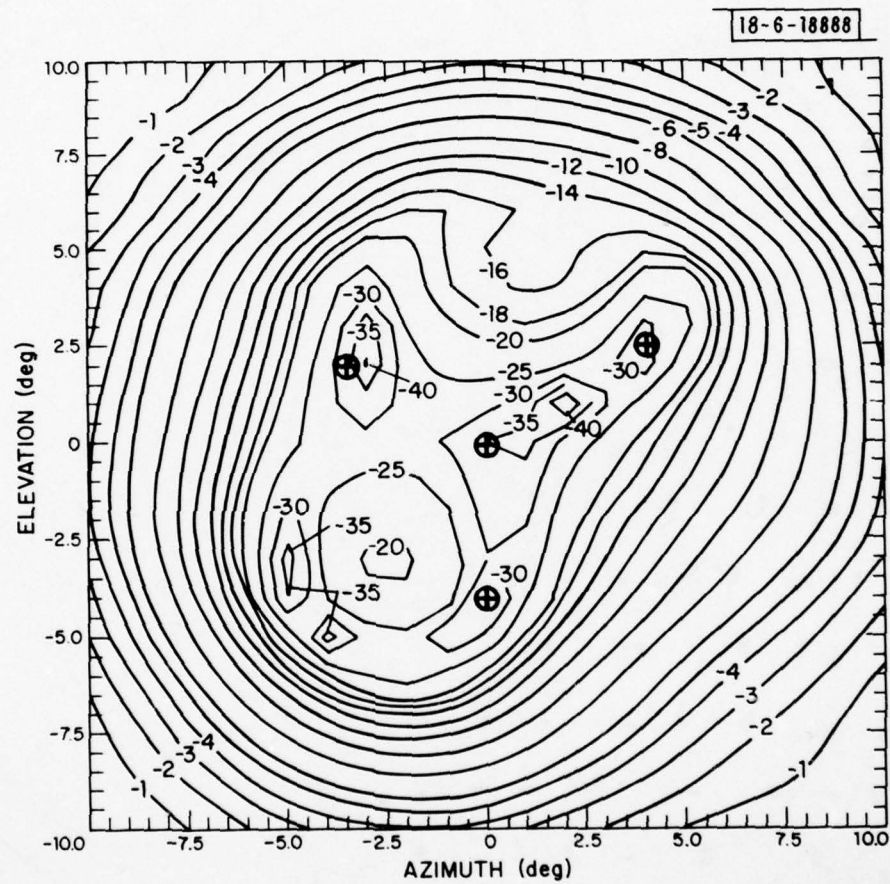


Fig. 37. Radiation contour with nulls for the scenario of Fig. 34 using the separate earth coverage reference (without ground plane).

18-6-18889

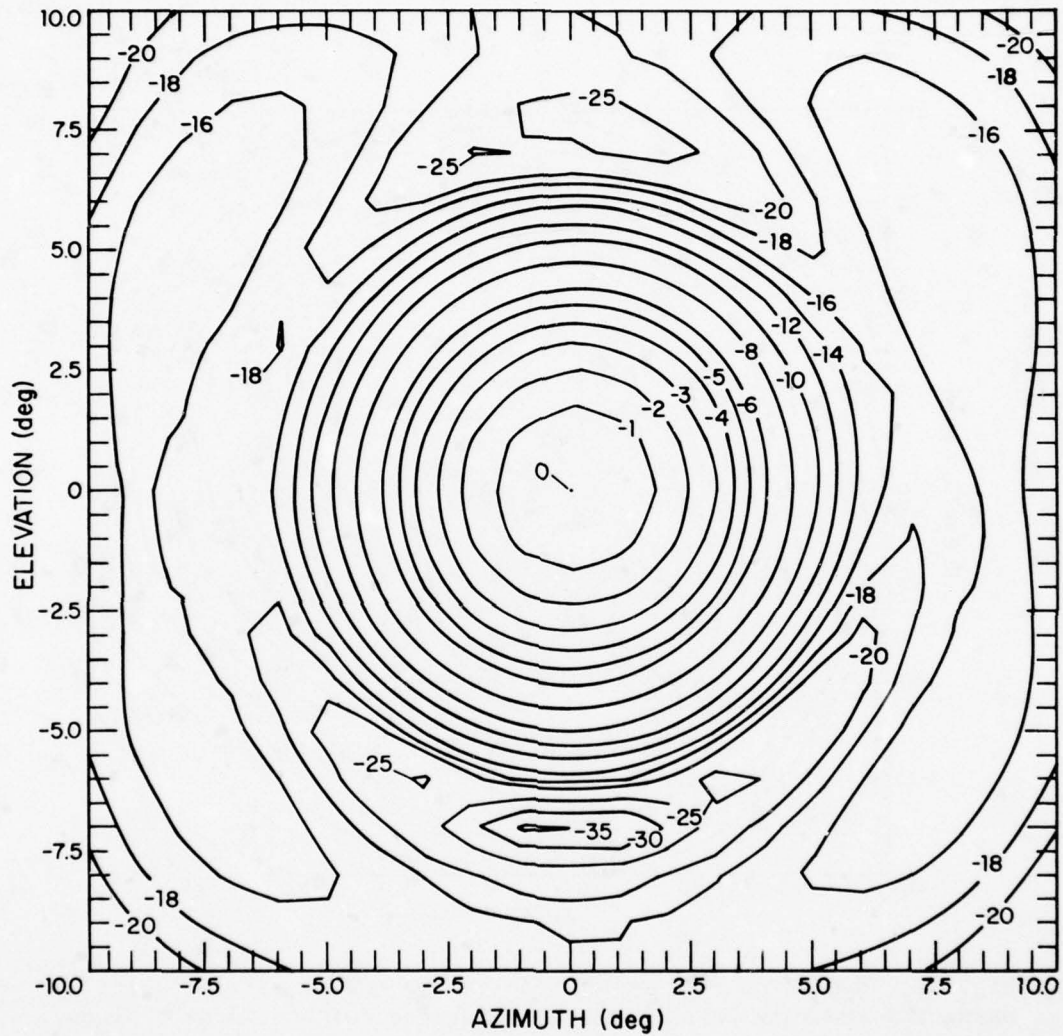


Fig. 38. Quiescent radiation pattern allocating maximum gain to users at the center of the FOV.

correlation matrix over the bandwidth under consideration, and then the radiation pattern was measured after setting these weights open-loop. Hence when the interference is in close proximity to the user direction, this open-loop setting leads to an inherent error in evaluating the actual directive gain to the signal. We estimate this gain is accurate so long as the gain in the user direction has not dropped more than 30 dB down from the peak value. The resultant measured contour radiation pattern, with null, for the 8 MHz weight setting bandwidth is illustrated in Fig. 39 and for the 44 MHz weight setting bandwidth in Fig. 40. The gain in the signal direction has dropped 9.2 dB for the 8 MHz weight setting bandwidth and 10.8 dB for the 44 MHz weight setting bandwidth. Furthermore, a wider-band null is evident in the 44 MHz null bandwidth contour, as can be seen by examining the average cancellation as a function of bandwidth for each case. This is illustrated in Fig. 41. Clearly as the bandwidth increases, the cancellation is as expected; i.e., a wider cancellation bandwidth is obtained for the 44 MHz weight setting bandwidth. The important parameter, however, is the average cancellation obtained over the signal bandwidth. Assume for example a 1 MHz collective user bandwidth at UHF, corresponding to approximately a 4 MHz bandwidth at 1550 MHz. Then it is interesting to note from Fig. 41 that over this bandwidth, the average cancellations for each weight setting bandwidth were both approximately equal to -50 dB. Thus, for this case, the main limitation imposed by using a wider nulling bandwidth is the loss in directive gain to the user. (This conclusion is valid for broadband noise type interference. Other types of interference open the possibility of null skewing off the signal band by more "intelligent" type interferers.)

18-6-18890

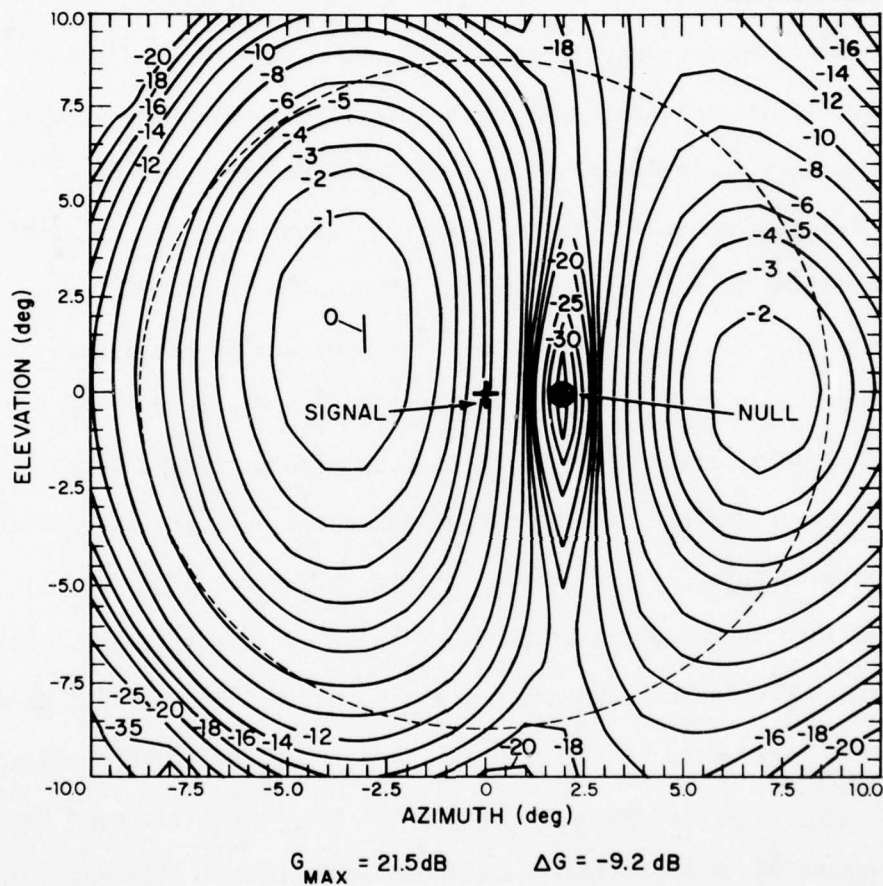


Fig. 39. Measured radiation pattern having null at (2,0) for quiescent radiation pattern of Fig. 38. 8 MHz weight setting bandwidth.

18-6-18891

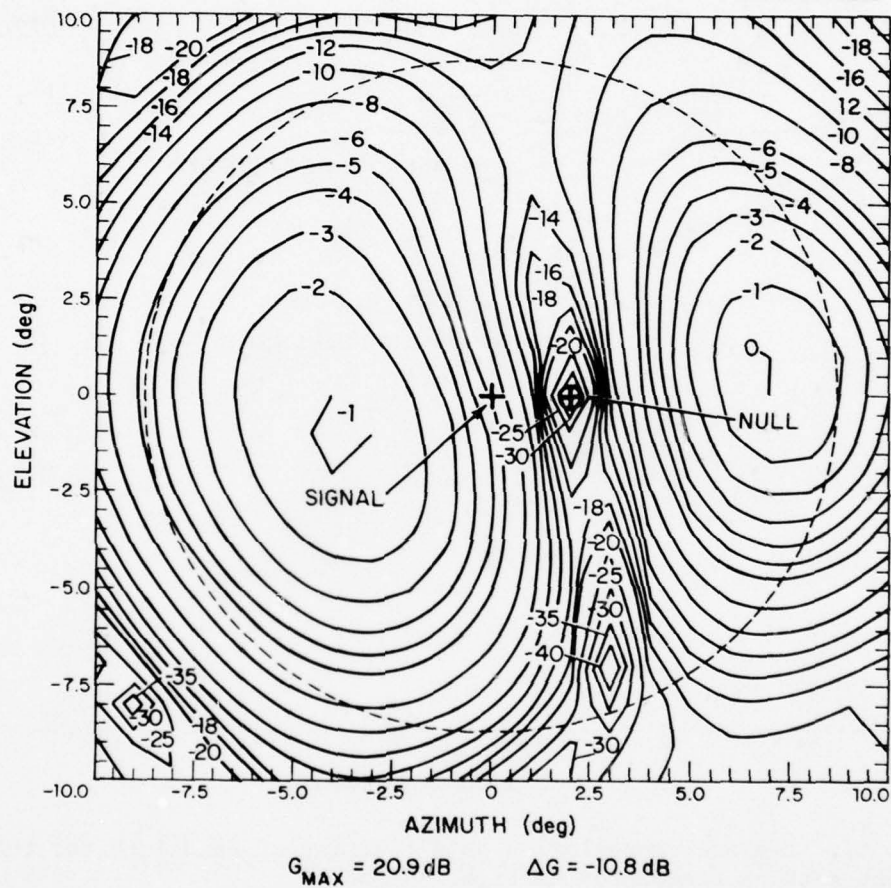


Fig. 40. Measured radiation pattern having null at (2,0) for quiescent radiation pattern of Fig. 38. 44 MHz weight setting bandwidth.

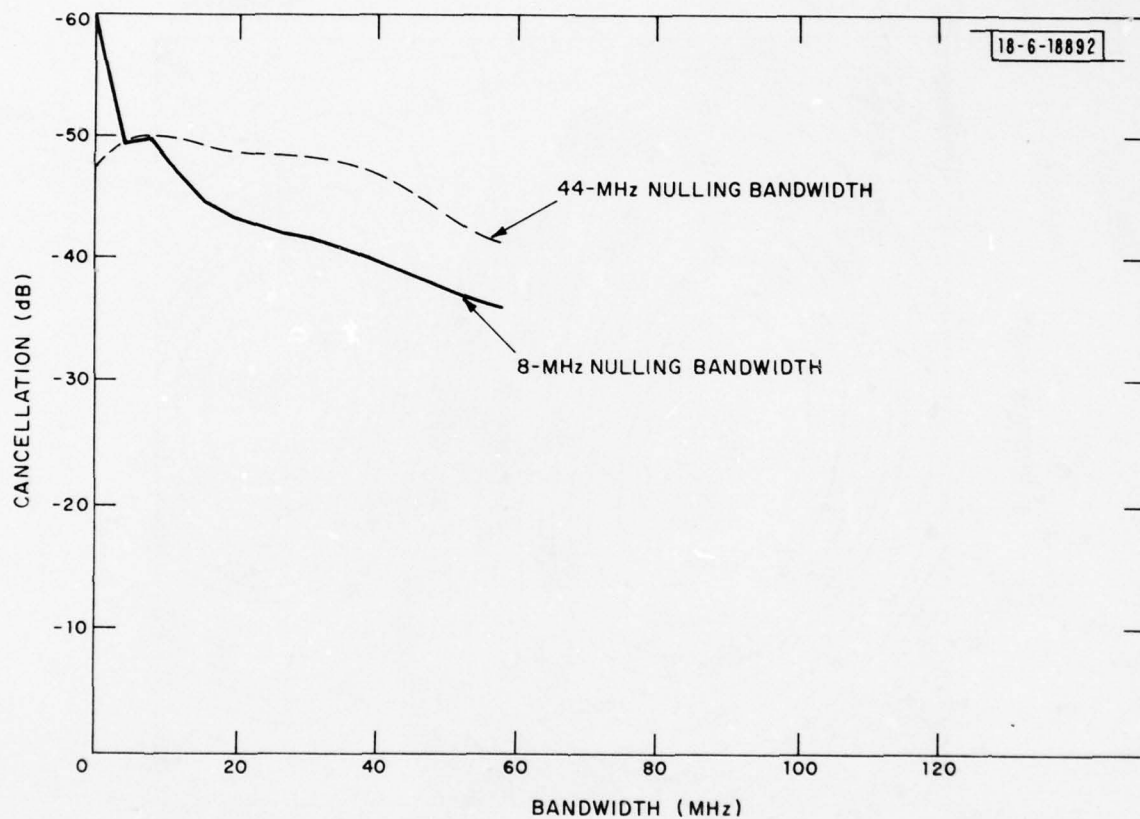


Fig. 41. Average cancellation as a function of bandwidth for the weight setting bandwidths of Figs. 39 and 40.

AD-A054 160

MASSACHUSETTS INST OF TECH LEXINGTON LINCOLN LAB
BANDWIDTH LIMITATIONS ON ACHIEVABLE CANCELLATION FOR ADAPTIVE N--ETC(U)
FEB 78 J T MAYHAN

F/G 9/5

UNCLASSIFIED

TN-1978-1

ESD-TR-78-25

NL

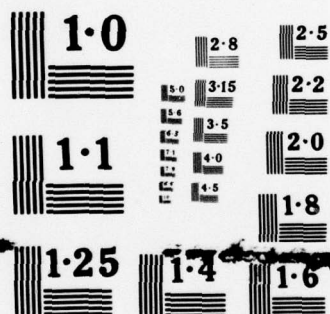
2 OF 2
ADA
054160



END
DATE
FILMED

6-78

DDC



NATIONAL BUREAU OF STANDARDS

In order to examine how the weight setting bandwidth affects the nulling resolution, results similar to the above were measured for several cases as the null position approached the user position in the $EL=0$ cut, similar to the simulation of Table 2 of Section IV. The results are tabulated in Table 4, where we determine the (S/I) improvement obtained for each weight setting bandwidth using the measured cancellation over an assumed 4 MHz composite user band, and also assuming that channel tracking errors limit the cancellation to 40 dB. The results are tabulated both vs. $\Delta\theta$ (degrees) and the normalized parameter $\Delta\theta/HPBW$. The differences between the loss in gain in the signal direction for the 44 MHz and 8 MHz bandwidths are not nearly as significant when compared to the results of Table 2 obtained with simulations. This is most probably due to the fact that multipath is still dominating the antenna performance even at the 8 MHz bandwidth. Note also that as $\Delta\theta \rightarrow 0$, the measured results for the decrease in directive gain (relative to $\Delta\theta/HPBW$) are worse for the test antenna when compared to the seven-element double triangle used in the simulation of Table 2. For example for $\Delta\theta/HPBW=0.15$, the loss in directive gain is only 15 dB for the double triangle array and 19 dB for the multiple beam reflector over the 44 MHz weight setting bandwidth. Whether or not this is due to the simplicity of the simulation modeling for the double triangle remains to be seen.

Some Practical Considerations

Finally, it is useful to consider the effects of a feed support structure which might be used with a reflector designed to "unfurl" in space. Such an unfurlable reflector was used on the ATS-6 satellite, and consisted of a metal

TABLE 4
(S/I) IMPROVEMENT AS NULL POSITION APPROACHES USER POSITION.
SIGNAL AT (0,0). NULL IN EL=0 PLANE. HPBW=5.75° (D/λ=10.7)

	Change in Gain as $\theta_J \rightarrow \theta_S$		Cancellation in 4 MHz		(S/I) IMP (Measurement)		(S/I) IMP Assum. <40 dB Cancell.	
	Wt. Setting Bandwidth							
	$\Delta\theta$ /HPBW	$\Delta\theta$	8 MHz	44 MHz	8 MHz	44 MHz	8 MHz	44 MHz
.17	1		-19.2	-18.7	35	34	21	21
.35	2		- 9.2	-10.8	40	39	31	29
.52	3		- 4.3	- 5.1	46	39	36	35
.70	4		- 1.6	- 1.8	42	38	38	38
.87	5		- 0.4	- 0.8	44	40	39	39
1.04	6		- 0.1	- 1.0	38	37	40	39

support structure extending outward from the center of the reflector to the feed. An L-band scale model of this feed support (hereafter designated as the truss) was constructed and the resultant antenna structure is illustrated in Fig. 42. The seven dipole feed array and reflector structure are the same as that used in the previous measurements. Only the outer support spars have been removed and replaced by the truss. Consider then a single null formed at coordinates (4,2) for comparison with previous results. The eigenvalue spread vs. bandwidth for the second two eigenvalues, s_2 and s_3 , is illustrated in Fig. 43 both for when the truss is present, and using the cross-over spars (Fig. 24). Additional multipath arising from the presence of the truss results in an increase of s_2/s_1 of 7 dB over that obtained using the spars. Although a detailed set of measurements was not obtained using the truss as a feed support, it is clear that a more suitable support structure would have to be designed if wideband nulling is desired.

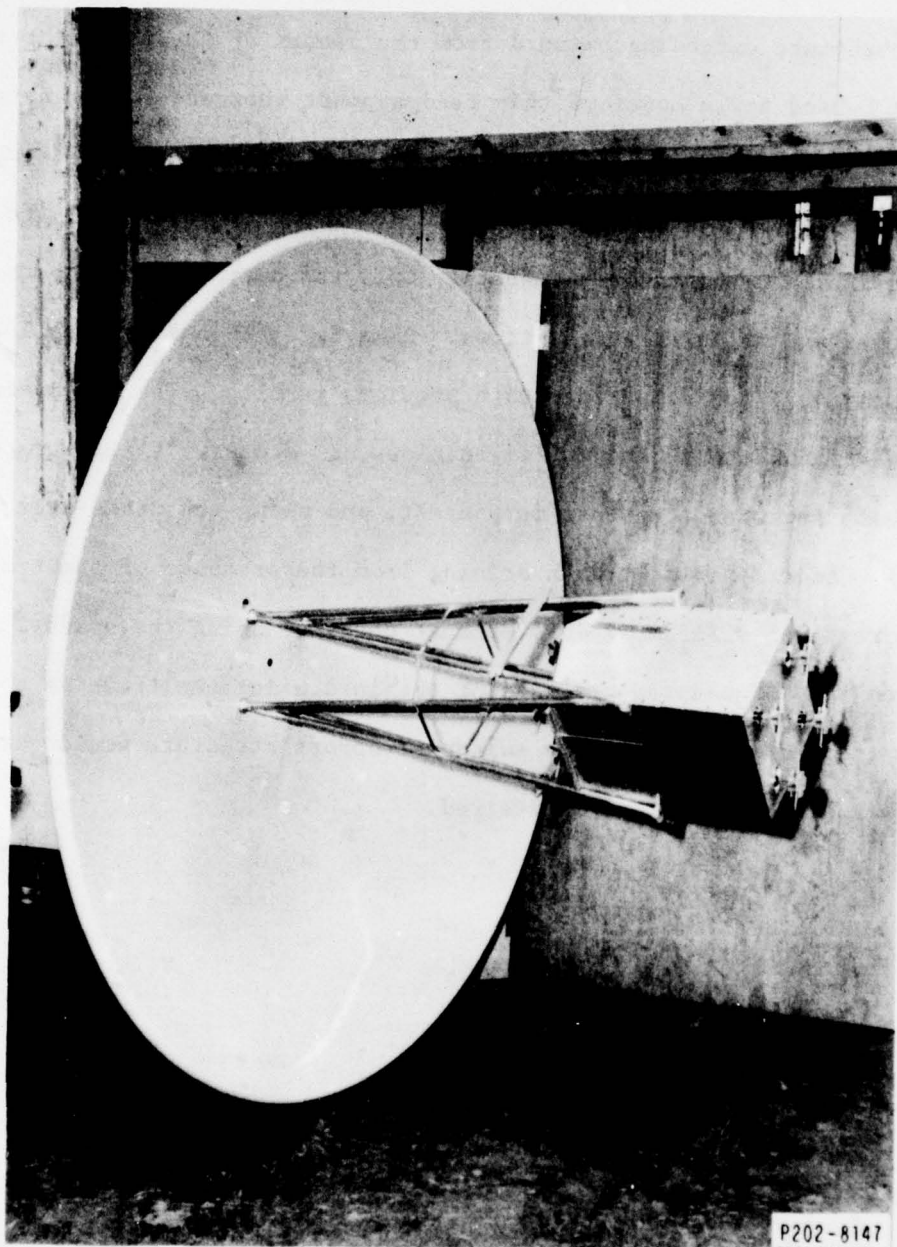


Fig. 42. Reflector-feed antenna structure using "space qualified" type feed support modeled after satellite ATS-6.

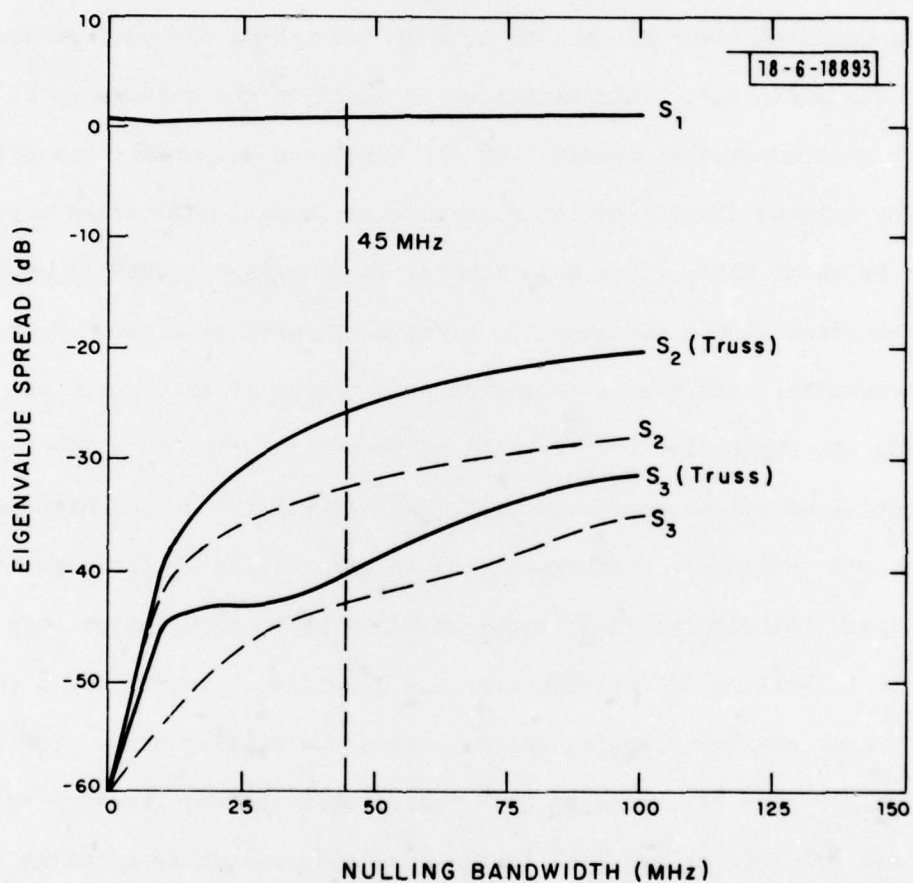


Fig. 43. Eigenvalue spread vs bandwidth with and without the "space qualified" feed support. (4,2) null position.

VI. Summary of Results

In the preceding sections we have examined in detail some of the limitations imposed by an adaptive nulling system operating over a non-zero bandwidth. In Sections I and II, a technique of evaluating the performance of the processor was presented. This technique is based on the dependence of the overall channel covariance matrix \underline{M} on the frequency dispersive properties both of the antenna itself and the post-antenna channel mismatches across the band. It is shown that, since \underline{M} is completely described by its eigenvalues and eigenvectors, if one examines the eigenvalues of \underline{M} as a parametric function of bandwidth, then the cancellation performance of the system can be determined. An expression for the achievable cancellation as a function of these eigenvalues and eigenvectors of \underline{M} , and also of the quiescent mode of operation, was obtained. Furthermore, by an examination of the eigenvalues vs. bandwidth, the various limitations on achievable cancellation were developed. In Section II, we examined this dependence strictly as a function of post-antenna channel-tracking errors across the nulling band. The eigenvalues of \underline{M} can then be expressed as a function of the rms tracking error σ^2 . A parametric tradeoff relating σ^2 to the amplitude and phase tracking errors required for a desired cancellation level was developed (Table 1, Fig. 6). In Section IV the eigenvalues of \underline{M} vs. bandwidth were examined for several classes of antennas which might be realized on a satellite for operation in the UHF band. The effects of a non-zero weight control bandwidth were examined, and shown to influence the nulling resolution (i.e., the allowable proximity of an interference source to a desired source). For all of the antenna configurations

considered, a nulling processor operating over a 3% bandwidth, and having a 40 dB dynamic range, would be significantly affected by the dispersive properties of the antenna, resulting in a wideband null being formed on the interference source. Finally, in Section V, we considered the effects caused by a real antenna structure in the form of a reflector-multiple feed MBA. It was demonstrated that multipath between the feed-reflector significantly limits the achievable nulling bandwidth one can obtain without using added degrees of freedom from the processor.

APPENDIX I CANCELLATION AS A FUNCTION OF EIGENVALUE SPREAD

In this appendix we derive Eq. (14) of Section II relating the cancellation C defined in Eq. (13) as a function of the spread in eigenvalues of the covariance matrix \underline{M} , assuming the weights are set for perfect cancellation at the center of the nulling band. The interference to noise ratio before adaption is given by (for $\underline{w}_0^\dagger \cdot \underline{w}_0 = 1$)

$$(I/N)_b = \underline{w}_0^\dagger \cdot \underline{M} \cdot \underline{w}_0 = \underline{w}_0 \cdot \sum_{k=1}^N s_k \underline{e}_k \underline{e}_k^\dagger \cdot \underline{w}_0 \quad (A1)$$

which can be approximated as

$$(I/N)_b \approx \sum_{j=1}^J s_j |\underline{e}_j^\dagger \cdot \underline{w}_0|^2 \quad (A2)$$

assuming some $\underline{e}_j^\dagger \cdot \underline{w}_0 \neq 0$ for the first J eigenvectors [if this were not true, then $(I/N)_b$ would be small and no nulling would be required]. The expression for $(I/N)_a$ is obtained using the adapted weight vector \underline{w} for zero bandwidth. This vector is essentially given by Eq. (10). Noting $\underline{e}_j^0 \simeq \underline{e}_j$, $j=1, \dots, J$, then \underline{w} takes the form

$$\underline{w} \simeq \sum_{j=1}^J [\underline{I} - \underline{e}_j \cdot \underline{e}_j^\dagger] \cdot \underline{w}_0 \quad (A3)$$

Then the expression for $(I/N)_a$ takes the form

$$(I/N)_a = \frac{\underline{w}_0^\dagger \cdot [\underline{I} - \sum_{j=1}^J \underline{e}_j \underline{e}_j^\dagger] \cdot \sum_{k=1}^N s_k \underline{e}_k \underline{e}_k^\dagger \cdot [\underline{I} - \sum_{j=1}^J \underline{e}_j \underline{e}_j^\dagger] \cdot \underline{w}_0}{\underline{w}_0^\dagger \cdot [\underline{I} - \sum_{j=1}^J \underline{e}_j \underline{e}_j^\dagger] \cdot [\underline{I} - \sum_{j=1}^J \underline{e}_j \underline{e}_j^\dagger] \cdot \underline{w}_0} \quad (A4)$$

Noting the orthogonality properties of the eigenvectors, i.e., $\underline{e}_j^\dagger \cdot \underline{e}_k = \delta_{j,k}$, where $\delta_{j,k}$ is the Kronecker delta function, then (A4) reduces to

$$(I/N)_a = \frac{\sum_{k=J+1}^N s_k |\underline{e}_k^\dagger \cdot \underline{w}_0|^2}{\underline{w}_0^\dagger \cdot \underline{w}_0 - \sum_{j=1}^J |\underline{e}_j^\dagger \cdot \underline{w}_0|^2} \quad (A5)$$

Using $\underline{w}_0^\dagger \cdot \underline{w}_0 = 1$, and dividing (A5) by (A4), we obtain Eq. (14) of Section II.

ACKNOWLEDGMENTS

It is a pleasure to acknowledge the support of numerous colleagues and friends who have contributed to this study. Particular thanks are due to Chris Slotta and Jeff Perry who performed the measurements reported in Section V; to Tim Turbett for programming the automated test system; to Leon Niro, Harold Lim and Harold Weiner for their programming support; to Charles Lindberg who designed the antenna and feed network used in the reflector measurements; to Chris Slotta who constructed the weight network illustrated in Fig. 18, and succeeded in matching the overall channel characteristics; to Alan Simmons, Michael Burrows and William Cummings for numerous discussions during the course of this study; to Dave Hodsdon for allowing the use of Fig. 6, which so clearly points out the relationship of channel tracking errors to achievable cancellation, to be published in this technical note; and finally, to Bob Burns for his attention to the many details required for the success of the measurements.

REFERENCES

1. B. Friedman, Principles and Techniques of Applied Mathematics (John Wiley and Sons, New York, 1966).
2. D. M. Hodsdon, Lincoln Laboratory, M.I.T., private communication.
3. M. L. Burrows and J. T. Mayhan, "Configuration Tradeoffs for Satellite Nulling Arrays," Technical Note 1978-5, Lincoln Laboratory, M.I.T. (to be published).
4. J. T. Mayhan, "Adaptive Nulling with Multiple-Beam Antennas," Technical Note 1976-18, Lincoln Laboratory, M.I.T. (30 September 1976), DDC AD-A034652/8, and IEEE Trans. Antennas Propag. AP-26 (to be published).
5. J. T. Mayhan and L. J. Ricardi, IEEE Trans. Antennas Propag. AP-23, 639 (1975).
6. J. T. Mayhan, IEEE Trans. Antennas Propag. AP-24, 769 (1976).

UNCLASSIFIED

SECURITY CLASSIFICATION OF THIS PAGE (When Data Entered)

REPORT DOCUMENTATION PAGE		READ INSTRUCTIONS BEFORE COMPLETING FORM
1. REPORT NUMBER 18 ESD-TR-78-25	2. GOVT ACCESSION NO.	3. RECIPIENT'S CATALOG NUMBER 14 TN-1978-1
4. TITLE (and Subtitle) 6 Bandwidth Limitations on Achievable Cancellation for Adaptive Nulling Systems		5. TYPE OF REPORT & PERIOD COVERED 9 Technical Note
7. AUTHOR(s) 14 Joseph T. Mayhan		6. PERFORMING ORG. REPORT NUMBER Technical Note 1978-1
9. PERFORMING ORGANIZATION NAME AND ADDRESS Lincoln Laboratory, M.I.T. ✓ P.O. Box 73 Lexington, MA 02173		8. CONTRACT OR GRANT NUMBER(s) 15 F19628-78-C-0002
11. CONTROLLING OFFICE NAME AND ADDRESS Defense Communications Agency 8th Street & So. Courthouse Road Arlington, VA 22204		10. PROGRAM ELEMENT, PROJECT, TASK AREA & WORK UNIT NUMBERS Program Element No. 35126K
14. MONITORING AGENCY NAME & ADDRESS (if different from Controlling Office) Electronic Systems Division Hanscom AFB Bedford, MA 01731		12. REPORT DATE 14 17 February 1978
		13. NUMBER OF PAGES 13 148 p.
		15. SECURITY CLASS. (of this report) Unclassified
16. DISTRIBUTION STATEMENT (of this Report) Approved for public release; distribution unlimited.		15a. DECLASSIFICATION DOWNGRADING SCHEDULE
17. DISTRIBUTION STATEMENT (of the abstract entered in Block 20, if different from Report)		
18. SUPPLEMENTARY NOTES None		
19. KEY WORDS (Continue on reverse side if necessary and identify by block number) bandwidth limitations multiple-beam antenna adaptive arrays closed-loop type antenna nulling interference cancellation adaptive nulling system		
20. ABSTRACT (Continue on reverse side if necessary and identify by block number) This technical note examines in detail the various limitations which influence the amount of cancellation achievable for a closed-loop type adaptive nulling system operating over a non-zero bandwidth. These limitations are categorized according to antenna limitations, and post-antenna channel tracking limitations. The former tend to be RF percentage bandwidth limited and the latter on the achievable component tolerances used to implement the channel (whether at RF or a lower IF). Both of these factors, and their influence on the nulling bandwidth, are examined in detail. Measured results are also presented for a seven-beam paraboloid-reflector type multiple-beam antenna (MBA), and the effects of feed-reflector multipath inherent in this geometry on the cancellation: bandwidth is evaluated in detail.		

DD FORM 1473 EDITION OF 1 NOV 65 IS OBSOLETE
1 JAN 73

UNCLASSIFIED

SECURITY CLASSIFICATION OF THIS PAGE (When Data Entered)

247 650

2